Dissertation

THE ROLE OF THE CALCIUM-ACTIVATED CHLORIDE CHANNEL TMEM16A IN THE LUNG

submitted by

Davor SKOFIC MAURER

for the Academic Degree of

Doctor of Philosophy (PhD)

at the

Medical University of Graz

Department of Physiology

under the Supervision of

Prof. Dr. Andrea OLSCHEWSKI

2020

Statutory Declaration

I hereby declare that this dissertation is my own original work and that I have fully acknowledged by name all of those individuals and organisations that have contributed to the research for this dissertation. Due acknowledgement has been made in the text to all other material used. Throughout this dissertation and in all related publications I followed the “Standards of Good Scientific Practice and Ombuds Committee at the Medical University of Graz”.

03.10.2020

Davor Skofic Maurer

Parts of this dissertation are published in the following peer-reviewed original research article, as well parts of the published work are being reproduced in this dissertation:

Cells, 2020, 9(9), 1984; **https://doi.org/10.3390/cells9091984**

Endothelial Dysfunction Following Enhanced TMEM16A Activity in Human Pulmonary Arteries (1)

Davor Skofic Maurer[1], Diana Zabini[1, 2], Chandran Nagaraj[2], Neha Sharma[3], Miklós Lengyel[4], Bence M. Nagy[2], Sasa Frank[5], Walter Klepetko[6], Elisabeth Gschwandtner[6], Péter Enyedi[4], Grazyna Kwapiszewska[1, 2], Horst Olschewski[2, 7], Andrea Olschewski[2, 3, *]

1 Otto Loewi Research Center, Medical University of Graz, Graz, Austria

2 Ludwig Boltzmann Institute for Lung Vascular Research, Graz, Austria

3 Experimental Anaesthesiology, Department of Anaesthesiology and Intensive Care Medicine, Medical University of Graz, Graz, Austria

4 Department of Physiology, Semmelweis University, Budapest, Hungary

5 Gottfried Schatz Research Center, Medical University of Graz, Graz, Austria

6 Department of Thoracic Surgery, Medical University of Vienna, Vienna, Austria

7 Department of Internal Medicine, Division of Pulmonology, Medical University of Graz, Graz, Austria

Presentations

TMEM16A in pulmonary hypertension

Davor Skofic Maurer

(Department of Physiology, Semmelweis University, Budapest, 2019)

Poster presentations

The role of the Ca^{2+}-activated Cl^- channel TMEM16A in the pulmonary vasculature

Davor Skofic Maurer, Chandran Nagaraj, Diana Zabini, Neha Sharma, Grazyna Kwapiszewska, Andrea Olschewski

(International Vascular Biology Meeting, Helsinki, Finland 2018)

The opposing effect of TMEM16A on the proliferation of pulmonary vascular cells

Davor Skofic Maurer, Chandran Nagaraj, Diana Zabini, Neha Sharma, Grazyna Kwapiszewska, Andrea Olschewski

(Ludwig Boltzmann Gesellschaft (LBG) meeting for health sciences, Vienna, Austria 2018)

Endothelial dysfunction following enhanced TMEM16A activity in human pulmonary arteries

Davor Skofic Maurer, Diana Zabini, Chandran Nagaraj, Neha Sharma, Miklós Lengyel, Bence M. Nagy, Saša Frank, Walter Klepetko, Elisabeth Gschwandtner, Péter Enyedi, Grazyna Kwapiszewska, Horst Olschewski, Andrea Olschewski

(Österreichischen Gesellschaft für Pneumologie (ÖGP), virtual conference, 2020)

Foreword

"I must not fear.

Fear is the mind-killer.

Fear is the little-death that brings total obliteration.

I will face my fear.

I will permit it to pass over me and through me.

And when it has gone past I will turn the inner eye to see its path.

Where the fear has gone there will be nothing. Only I will remain."

The litany against fear by Frank Herbert, Dune.

Doing a PhD is no easy task. Your whole mindset shifts and before you realize it, it is done. Learning how to be a researcher is not only a program of sharpening your skillset, I believe it is mostly about sharpening your mind. How you think, yes, but even more importantly how you feel, how you respond, how you filter – the people, the perceptions, the relationships, the emotions. While a big part falls upon the individual, just as important, if not more, is the time and care one receives from his mentor; a PhD in the end is a traineeship, a passing of the knowledge and experience from a “master of arts” to a “newbie” to help them become the best version of themselves. Special care and diligence should be taken and observed, so that the newbie gets the right tools in the right context in the right environment. This way, introducing a student into the wonderful world of science and research and raising them to be responsible, caring and accomplished scientists is a big responsibility but also an enormous honor; this student will grow up and carry a part of his mentor´s skillset, mindset and represent him wherever he will go. And most importantly - he will pass on what he learned and experienced to the next generation making the circle whole and complete. A self-sustaining legacy.

That I was able to go through a crash-course of obtaining these super-powers, I have to thank the Medical University of Graz and DK-MOLIN together with FWF. Without their financial support not all this would be possible. I would like to acknowledge the Otto Loewi Research Centre with the

Department of Physiology and Ludwig Boltzmann Institute for Lung Vascular Research. The latter provided the framework in which I was able to develop and build.

Budapest will forever stay in a special place for me. It is a beautiful city that enabled me to move out and rethink. Rethink myself, the project and the academic world. I would like to thank Miklós Lengyel, PhD Dr.med.univ. for not only the science but also for all the discussion. The politics seemed especially frequent and I admire his knowledge of history. A big thank you to Péter Enyedi, Prof. Dr.med.univ. for making me feel welcome and appreciated. Being a part of his group let me see research for what it could be and it let me grow. I will be forever grateful for the safe line.

I would like to thank specifically my group – Chandran, Bence, Neha and Diana. It is no easy (t)ask to be responsible for a newly hatched chick. They have done their part as best they could and I leaped the remaining gap. I would especially like to point-out the help of Diana for giving me a glimpse of what research could be and what research is not. It will serve as a compass in my future endeavors. Sabine and Liz are of course the sweethearts of our little group – thank you for mothering me through my drama outbursts. Thank you for accepting me for who I am.

I would like to acknowledge Prof. Dr. Andrea Olschewski. Because of her efforts, guidance and stability the project is today at the finish line. Thank you for giving me the opportunity to prove myself when challenged.

I have to mention the “holy trinity” as they called us once. Me, Neha Sharma and Helene Thekkekara Puthenparampil. Neha started a little bit before us but we were facing many problems and we faced them together. Doing a PhD is like a crash-course of growing-up in 4 years and I feel like we grew-up together. I see you as my childhood friends. And I liked making (intellectual) mud pies with you.

Thank you to Ayşe Ceren Mutgan and Tatjana Hirschmugl for making me feel loved and amazing when I felt the most alone. Finding friends and claiming friends in such a short time is truly rare and I am happy for the moments I have spent with each of you separately and crazy about the craziness we fostered when together. I am grateful and thankful for helping me and accepting me.

Moja prelepa Slovenija. Težko mi je bilo odditi in neverjetno se veselim prihoda nazaj. Prihajam kot popolnoma druga oseba ampak prihajam nazaj k „mojim ljudem“. Prijatelji so najpomembnejši proces v življenju. Zaradi njih rasteš, gradiš in ostajaš varen. Prijatelji so en izmed glavnih stebrov življenja. Selitev v tujino je neverjetno sito odnosov in hvaležen sem, da strahom navkljub, jih je

kar nekaj razumelo, ko enostavno ne gre. Pia Pužar Dominkuš, Alenka Bombač, Saška Polanc in Urška Slapšak, prašički kot se zagre. Nika Krivec, Lili Rozman. Vi ste ob meni od začetka. Hvala.

Ob koncu dneva sem le lupina brez ljubezni do mojih najbližjih. Urška, morda nisva v krvnem sorodu ampak brez tebe se ne bi zmogel čez preizkušnje, ki so me bombardirale zadnjih 12 let. V prvem tednu faksa sva se ujela in najin odnos je od takrat rastel, se razvijal in je danes v neverjetno lepih dimenzijah moje duše. Besede nikoli ne bodo zmogle izraziti ljubezni in hvaležnosti za vse, kar si mi dala in mi v tem norem svetu daješ še naprej.

Eva in Neža – veliko mene je v vama in veliko vaju je v meni. In za to sem neizmerno hvaležen.

Vanessa, Peter in Lanna. Želel bi si, da bi se videli več in delam na tem, da nam to tudi uspe. Ste nekaj tako lepega, četudi kaotičnega, ampak sem rad del vašega sveta. Takrat se počutim jaz zares jaz.

Mami. Jerma. Ni lahko gledati otroka, ko se muči in mu je težko. In si mislim, da tudi ni lahko gledati otroka in vedeti, da mu ne moreš pomagati. V eni točki otroka spustiš iz svojega objema in upaš, da leti dovolj dobro, da se izogne vsem stebrom. Malo sinov se lahko pohvali s tako utrganim odnosom s svojo materjo. Hvala za vse. Hvala za vzgojo, za podporo, hvala za sekiranje in nerazumevanje. Vse je del procesa, ki me je naredil takega kot sem danes. In v ogromno pogledih sem kar ok. Hvala atiju za svet priložnosti.

Simon. Počutim se kot da sva se prebila skozi vojno. Ti ranjen uspel pobegniti malo prej in sam se popolnoma razbit vračam par let kasneje, a srečen, ker je konec. Vojne je konec. Ta doktorat ni le uspeh mene, je uspeh naju in brez tebe mi nikoli ne bi uspelo. Hvala, ker si vztrajal z menoj skozi to dogodivščino. Zavedam se, da ni bilo težko le meni ampak da si se tudi sam odrekel mnogim rečem. Hvala, ker me podpiraš, ker te skrbi, ker vidiš moj potencial in me sprejemaš. Hvala, ker me imaš rad.

Biti ogenj, goreti in dogoreti!
Pepel ni ostanek ognja,
ostanek teme je.
Biti ogenj!
Svet je presvetljen,
tudi vesolje.
Ni strahu pred neskončnostjo,
ne pred večnostjo.

Vsak hip je večnost,
vsaka ura, vsak dan.
Svetla sem in plapolam.
Svetla sem in mirno gorim.
Tlim in sem svetla.
Kjer sem, je svetlo in toplo.

Biti ogenj –
do zadnjega zublja,
do zadnje iskre,
do zadnjega diha!

Neža Maurer, Ogenj do zadnjega diha

Acknowledgements

This work was conducted at the Ludwig Boltzmann Institute for Lung Vascular Research, the Department of Physiology and at the Center for Medical Research (ZMF I and II) of the Medical University of Graz. PhD study and stay abroad were supported by the Medical University of Graz through the FWF-funded PhD Program DK-MOLIN (grant number W1241).

I would like to thank my thesis committee consisting of Diana Zabini, PhD, Grazyna Kwapiszewska-Marsh, Priv.-Doz. Dr., Akos Heinemann, Univ.-Prof. Dr.med., Horst Olschewski, Univ.-Prof. Dr.med. and Andrea Olschewski, Univ.-Prof. Dr.med. for guiding me through the maze.

Additionally, I would like to thank in advance to my defense committee consisting of Andjelko Hrzenjak, Assoz. Prof. Priv.-Doz. Dr.rer.nat., Malgorzata Wygrecka Prof. PhD and Wolfgang Kübler, Prof. Dr.med. for going thoroughly through my thesis and I am looking forward to all the constructive suggestions.

Part of the patch-clamp experiments was performed by our collaboration partner from the group of Prof.Péter Enyedi, Semmelweis University, Budapest. Wire-Myography was performed with the help of Neha Sharma and Chandran Nagaraj, PhD from the Medical University of Graz and Ludwig Boltzmann Institute for Lung Vascular Research respectively. Live cell Ca^{2+} as well as precision-cut lung slice imaging was performed with the help of Diana Zabini, PhD from the Medical University of Graz and Ludwig Boltzmann Institute for Lung Vascular Research.

Table of Contents

Abbreviations and Definitions

5-HT	serotonin
ADMA	asymmetric dimethylarginine
Akt	Protein kinase B
AMPK	adenosine monophosphate-activated protein kinase
Ang-II	angiotensin-II
Ano1	Anoctamin-1
ATP	Adenosine triphosphate
BH4	Tetrahydrobiopterin
BKCa	large-conductance Ca^{2+}-activated potassium channels
BMPRII	Bone morphogenetic protein receptor type II
CaCC	Ca^{2+}-activated Cl^- channels
CaM	calmodulin
CaMKII	Calcium/calmodulin-dependent protein kinase II
Cav1	Caveolin-1
CFTR	cystic fibrosis transmembrane conductance regulator
cGMP	cyclic guanosine monophosphate
CICR	Ca^{2+}-induced Ca^{2+} release
DAG	diacylglycerol
EDCF	endothelium-derived contracting factors
EDHF	Endothelium-derived hyperpolarizing factors
EDRF	endothelium-derived relaxing factors

eNOS	Endothelial nitric oxide synthase
ER	Endoplasmic reticulum
ERK1/2	Extracellular signal-regulated protein kinases 1 and 2
Et-1	endothelin-1
FAD	flavin adenine dinucleotide
FMN	flavin mononucleotide
GA	Golgi Apparatus
GDP	Guanosine diphosphate
GPCR	guanine nucleotide-binding protein-coupled receptor
GTP	Guanosine triphosphate
H_2O_2	Hydrogen peroxide
HIF1α	Hypoxia-inducible factor 1-alpha
HIF2α	Hypoxia-inducible factor 2-alpha
HO-1	Heme Oxygenase-1
Hsp90	heat shock protein 90
IP_3	Inositol trisphosphate
IPAH	Idiopathic pulmonary arterial hypertension
MAPK	mitogen-activated protein kinase
mPAP	mean pulmonary pressure
NADPH	Reduced nicotinamide adenine dinucleotide phosphate
NO	nitric oxide
NOX	NADPH oxidase
$ONOO^-$	peroxynitrite

PA	pulmonary artery
PAECs	pulmonary arterial endothelial cells
PAH	pulmonary arterial hypertension
PASMCs	Pulmonary Artery Smooth Muscle Cells
PGI_2	prostacyclin
PI3K	Phosphoinositide 3-kinases
PIP2	Phosphatidylinositol 4,5-bisphosphate
PKA	Protein kinase A
PKC	Protein kinase C
PKG	Protein kinase G
PLC	phospholipase C
PVR	pulmonary vascular resistance
RMP	Resting membrane potential
ROC	receptor-operated Ca^{2+} channels
ROS	reactive oxygen species
RTKR	tyrosine kinase-linked receptor
RyR	ryanodine receptor
SERCA	sarco/endoplasmic reticulum Ca^{2+}-ATPase
sGC	Soluble guanylate cyclase
SIRT1	sirtuin 1
SOC	store-operated Ca^{2+} channels
SOCE	store-operated Ca^{2+} entry
SOD	Superoxide dismutase

STIM1	stromal interaction molecule 1
STIM2	stromal interaction molecule 2
TGFβ	Transforming growth factor beta
TMEM16A	Transmembrane member 16A
TRPC	Transient receptor potential channels
VEGF	Vascular endothelial growth factor
VEGFR	Vascular endothelial growth factor receptor
VGCC	Voltage-gated Ca^{2+} channels
VRAC	volume-regulated anion channel
vWF	Von Willebrand Factor

List of Figures

List of Supplementary Tables

Abstract in German

Pulmonalarterielle Endothelzellen (PAEC) sind unentbehrlich für die Homeostase der pulmonalen Blutgefäße. Dementsprechend führen fehlgeleitete Signalwege zur Entwicklung von pulmonal-arterieller Erkrankungen. Störungen in Ionenkanalfunktionen können dabei entscheidende Rolle spielen. Die idiopathische pulmonalarterielle Hypertonie (IPAH) ist eine fortschreitende Erkrankung, die durch u.a. Dysfunktion der Endothelzellen gekennzeichnet ist. In der Vergangenheit wurden in dieser Hinsicht vor allem K^+ Ionenkanäle erforscht. Neuerdings haben sich Cl^- Ionenkanäle ebenfalls als ein weiterer pathologisch relevanter Faktor erwiesen. Ein wichtiger Teil der Cl^--Leitfähigkeit ist der Ca^{2+}-aktivierte Cl^--Strom (CaCC). Dieser wird hauptsächlich durch TMEM16A Ionenkanäle vermittelt, einem Kanal, der mit der Aufrechterhaltung unterschiedlicher physiologischer Prozesse in diversen Zellen verbunden ist. TMEM16A wurde bereits auch mit verschiedenen pathologischen Vorgänge in den Gefäßen in Zusammenhang gebracht, sowohl in der systemischen als auch in der Lungenzirkulation.

Die Rolle von TMEM16A für die endotheliale Dysfunktion war bisher nur wenig erforscht. Im Rahmen dieser Studie konnten wir das Profil von TMEM16A erweitern und seine Bedeutung für die Störung verschiedener Signalwege demonstrieren. Dabei fokussierten wir uns an Prozesse, die für die Identität der Endothelzellen wesentlich sind. In dieser Arbeit berichten wir über eine gesteigerte TMEM16A-Aktivität in IPAH-PAEC. Durch TMEM16A Überexpression in gesunden primären humanen PAEC *in vitro*, als auch durch *ex vivo* Überexpression in isolierten humanen Lungenarterien zeigen wir die funktionellen Konsequenzen der erhöhten TMEM16A-Aktivität. Diese äußerten sich durch Änderungen in der Ca^{2+} Dynamik und der eNOS-Aktivität, sowie durch eine verminderte NO-Produktion, Proliferation, Wundheilung, Gefäßneubildung und eine abgeschwächte Acetylcholin-vermittelte Relaxation menschlicher Lungenarterien. Unsere Ergebnisse zeigen, dass die erhöhte Aktivität der TMEM16A Kanäle in gesunden Lungenarterien schwere Mängel verursacht, die den pathologischen Veränderungen der pulmonalarteriellen Hypertonie ähneln.

Abstract in English

Pulmonary arterial endothelial cells (PAECs) are an important source of factors maintaining homeostasis within the pulmonary vasculature. However, when dysfunctional they are also a perfectly-positioned driver of pathological development. Ion-channelome represents an essential part in this balancing act, regulating many features that maintain endothelial cell identity and their progression towards endothelial dysfunction. Idiopathic pulmonary arterial hypertension (IPAH) is a progressive disease hallmarked by dysbalanced ion-channelome and endothelial dysfunction. Traditionally K^+ channels were featured in understanding the detrimental role of dysbalanced ion conductance. More recently, Cl^- channels have proven to be another pathologically-relevant factor and an intriguing target. An important part of Cl^- conductivity is Ca^{2+}-activated Cl^- current (CaCC), which is mainly mediated by TMEM16A, a channel associated with the maintenance of different physiological processes, however its pathological footprint has been emphasized in several pathologies, including of systemic and pulmonary vasculature.

The effect of TMEM16A in the homeostasis and pathological development of endothelial dysfunction has been so far underrepresented. Within the scope of this study, we were able to extend the pathological footprint of TMEM16A demonstrating its role in the fundamental disruption of downstream signalling pathways otherwise essential to the identity of an endothelial cell. Here we report enhanced TMEM16A activity in IPAH PAECs. Upon TMEM16A overexpression in healthy primary human PAECs *in vitro* and in human pulmonary arteries *ex vivo*, we demonstrate the functional consequences of the augmented TMEM16A activity with alterations of Ca^{2+} dynamics and eNOS activity as well as decreased NO production, proliferation, wound-healing, tube-formation and attenuated acetylcholine-mediated relaxation of human pulmonary arteries.

Thus, our results indicate that disease-associated TMEM16A activity pathologically primes healthy pulmonary arteries and ultimately causes severe deficiencies resembling of that found in pulmonary arterial hypertension.

1. Introduction

1.1. Pulmonary circulation

The pulmonary circulation is a high-flow, low-resistance and low-pressure system able to adapt cardiac output with minimal changes to mean pulmonary pressure (mPAP) ranging in a healthy individual around 14 +- 3 mmHg (2). Endothelial cells play an important part connecting the bloodstream with the surrounding lung tissue, mediating a plethora of ultimately very different functions; they optimize gas exchange, control barrier integrity, regulate vascular tone and respond to different chemical, physical and mechanical stimuli by dynamically adjusting not only their receptor-effector signalling but also their secretome. Pulmonary arterial endothelial cells (PAECs) are thus established as metabolically highly active population within the pulmonary locality (3). In healthy pulmonary vascular bed, the arterial endothelium holds the balance of vasodilation and vasoconstriction by synthesizing a variety of paracrine and endocrine factors. While some favour relaxation, i.e nitric oxide (NO), prostacyclin (PGI2) other favour constriction, i.e. serotonin (5-HT), endothelin-1 (Et-1), angiotensin (Ang-II) etc in response to different stimuli. Background NO production is an important mediator of low vascular tone in normoxic conditions, yet when impaired this leads to a state of prolonged and excessive pulmonary vasoconstriction going side by side with affected proliferatory response in different locally present cell types (4). As a vital part of the respiratory system, PAECs therefore also represent a perfectly-positioned mediator of pathological manifestations. Endothelial dysfunction has become a definition for alterations ranging from barrier dysfunction leading to vascular leakage; altered vasoconstriction and/or vasodilation mechanisms; acquisition of proinflammatory phenotype; dysbalanced proliferative and apoptotic pathways and miscommunication within and without the neighboring cells (3).

1.1.1. Pulmonary hypertension

Pulmonary hypertension is a progressive condition diagnosed by an elevation in resting mean pulmonary arterial pressure (mPAP) > 20 mmHg with a pulmonary vascular resistance (PVR) >= 3 WU as assessed by right-heart catheterisation (5). The condition can have different origins and is therefore classified in 5 WHO groups as defined by the last World Symposium on Pulmonary

Hypertension (5). Group 1 or pulmonary arterial hypertension (PAH) includes several conditions characterized by progressive narrowing of small pulmonary arteries (PAs) ultimately leading to increased PVR and mPAP. Major factors in the observed vascular occlusion is sustained vasoconstriction and vascular remodelling (6–8). Even though there is an extensive structural reconstruction of the vascular wall, where histologically all layers of the wall are involved, the hallmark of the vascular response remains increased muscularization of previously non-muscularized distal arterioles (6,7,9). Consequently, increased right ventricular afterload and pulmonary vascular resistance (PVR) contribute to right ventricle strain causing cardiac hypertrophy, however with persistent elevated pulmonary resistance this leads to progressive contractile dysfunction, decompensation, dilatation and in severe cases to right heart failure (10–12).

With the current pharmacological targeting of vasoconstriction, the patients with PAH still face poor prognosis with estimated 3-year survival of 54,9 % (95 % CI, 41.8 to 68.0) for incident cases and 58.2 % (95 % CI, 49.0 to 69.3) for prevalent cases (13). Positively associated with survival are female gender, greater 6-minute walk distance, lower right atrial pressure, New York Heart Association function class I/II and higher cardiac output (13). Whether pulmonary vasoconstriction, remodelling followed by the obstruction of the vascular lumen or markedly increased vascular stiffness (14,15), it is clear that long term pharmacological efforts for hackling pulmonary hypertension and its high mortality are not only towards preventing vasoconstriction but also towards addressing its aberrant structural malformations. Therefore, a better understanding of the aetiology, progression and molecular pathobiology paving the way towards not only new but also more adapted treatment options are of upmost importance (16–19).

1.1.1.1. Endothelial dysfunction

The exact molecular mechanisms of PAH are multifaceted yet still largely unknown. One of the common driving factor of vascular remodelling present across all pulmonary hypertension WHO groups is endothelial dysfunction (20). The most commonly mentioned hypothesis of the role of endothelial dysfunction in the pathogenesis of PAH defines several stages in PAEC pathological transformation enabling apoptosis-resistant pro-proliferative endothelial cell expansion, thus vascular remodelling (21–24). PAH endothelial cells present with other pathological phenotypic shifts as well; (i) acquisition of a pro-proliferative and anti-apoptotic phenotype, (ii) a transition

from a quiescent-to-activated state, (iii) acquisition of a pro-inflammatory phenotype, (iv) endothelial cells also start producing and secreting immoderate amounts of growth factors affecting not only other types of cells in the locality but also systemically via the blood circulation and (v) the communication between endothelial cells and the rest takes key position in understanding the pathological changes seen in pulmonary hypertension (3,19).

It has been described that BMPRII mutations contribute significantly in the development of familial PAH (25,26), while mutations can be found in 6-40 % of patients with IPAH (27–30). Even though loss-of-function or reduction in BMPRII remains an important factor in IPAH (31), it is nevertheless not the main contributing factor, since it is evident that the change in genetic footprint of these patients is changed not only in comparison to healthy individuals but also in comparison to patients with familial PAH (32).

Another important aspect of molecular dysfunction in PAH is the apparent endothelial nitric oxide synthase (eNOS)-nitric oxide (NO)-soluble guanylate cyclase (sGC)-protein kinase G (PKG) pathway dysbalance (33–35) and when additionally connected to oxidative stress the rise of detrimental reactive nitrogen species (RNS), specifically peroxynitrite ($ONOO^-$) (36,37). IPAH patients have disrupted eNOS pathways. (38–45) Persistent eNOS activation induces PH in mice and humans through PKG nitration causing the vasodilation defect (35). Moreover, hypoxic mice and monocrotaline rat models of PH have impaired ACh-mediated vasorelaxation (46). Interestingly, to some extent underlying BMPRII and eNOS pathways, is reduced caveolin-1 in PAH patients (30,35,47). Caveolin-1 is a membrane protein localized in caveolae, where it regulates eNOS activation on the one hand (48) and has a role in BMPRII membrane localization on the other (49). A decrease in caveolin-1 is present in remodelled PAs of PAH patients (30), causing persistent eNOS activity and PKG dysfunction by extension in PAECs (35) and reduced BMP-dependent Smad signalling in PASMCs (49,50).

1.2. Ion channels and ion homeostasis in endothelial cells

Vascular endothelium is a multifunctional system capable of different responses to mechanical, chemical and neuronal signals coming from the luminal or abluminal side (51,52). All of the vascular endothelial functions together with their capability of sensing and rapidly responding relies extensively on the ion-channel landscape of these cells and their activity patterns. The role

of ion channels in the transduction of these signals is either (i) in managing quick cellular responses, e.g. synthesis or release of different factors in response to a variety of transmitters and on the other hand (ii) in managing slower cellular responses, e.g. the expression of several surface and adhesion molecules, cytoskeletal changes, remodelling and angiogenesis (51). This signal transduction is impaired during vessel disease and injury, inflammation, and hemodynamic disturbances, e.g. hypertension (51,53).

Ion-channelome represents a finely tuned network within a functioning entity with vast differences among not only different cell types but also within the same, e.g. endothelial cells of different organs systems or based on their localization in the vessel tree. The complexity is further extended by the ions they preferably bind, their electrophysiological properties and by the factors that are able to modulate their activity. This staggering diversity acts as a coordinated mechanism, defining cell physiological state, dynamically adapting to the surrounding cues and when dysbalanced, provides the basis for a pathological development (51,53). The contribution of a dysfunctional endothelium to the pathophysiological progression of different diseases is being more and more apparent, ranging from cardiovascular diseases, diabetes and hypercholesterolemia. The basis of a dysfunctional endothelial cell can be connected to their ion channelome interconnected with abnormal resting membrane potential (RMP) dynamics (51). The membrane potential of endothelial cells is tightly connected to the activity of its ion channel activity. Resting membrane depolarization results in a steep rise in intracellular concentration of Ca^{2+}, an essential second messenger regulating all key systems that are defining cell identity (54). The main ion species maintaining the RMP are K^+, Na^+ and Cl^- through a variety of functionally diverse ion-channels (55–57), i.e. Ca^{2+}-activated K^+ channels, inwardly rectifying K^+ channels and voltage-dependent K^+ channels, volume-regulated anion channel (VRAC), Ca^{2+}-activated Cl^- channels (CaCC) and possibly cystic fibrosis transmembrane conductance regulator (CFTR) channel.

The main determinant of RMP in endothelial cells is the activity of K^+ channels. However, the expression of these channels has been reported to vary among different types and states of endothelial cells (51). Consequently, a bimodal distribution of RMP has been defined; the first group have a RMP between -70 and -60 mV, controlled mainly by K^+, and the second between -40 to -10 mV controlled by Cl^- (56,58). The relative contributions of K^+, Na^+ and Cl^- to RMP are 27 to 95 %, 3 to 30 % and 9 to 35 % respectively (51). In rats, small PAECs gain an additional expression of a Cl^- conductance in the first few weeks of postnatal development moving away from predominantly K^+-determined RMP of -70 mV to -45 mV. The increase in Cl^- conductance

was proposed to be associated with increase in pulmonary blood flow, cell depolarization, Ca^{2+} influx and resulting NO production (59). Moreover the RMP of rat (60,61) and bovine (56,62) PAECs was likewise determined at -38,3±2,2 or -35±1.52 and -26±3 or -56±3,5 mV respectively, with the reduction of extracellular Cl^- concentration further depolarizing the membrane potential thus confirming the efflux of Cl^-. Furthermore, the described current was blocked by an inhibitor of CaCC 5-nitro-2-(3-phenylpropylamino)-benzoate (NPPB) (56,63). All these reports indicate that the Cl^- conductance significantly influences the RMP of PAECs and consequently determines its function. While the RMP of PAH PASMC is well defined and shown to be depolarized (57,64), it is not well described for PAECs. IPAH PAECs have an upregulation of the calcium-activated chloride channel TMEM16A (65) and increased TMEM16A activity causes the cell membrane depolarization (57,66). It is possible that IPAH PAECs are similarly depolarized, as in the case of PAECs isolated from monocrotaline rat model of PH (61).

1.2.1. Calcium

Cytosolic Ca^{2+} is one of the most important second messengers, regulating from gene expression and cellular secretion to contraction and cellular metabolism in practically every electrically excitable and non-excitable cell. The distinct patterns of Ca^{2+} dynamics can be achieved by a plethora of different pathways that fine-tune the ability of agonists to modulate Ca^{2+} any by doing so define the observed endothelial cell heterogeneity (67). Most of the EC intracellular Ca^{2+} is sequestered within the ER, with estimations as high as 75 %, while the rest 25 % represents the mitochondrial pool (68). In general ER contains large amounts of Ca^{2+}-binding proteins, e.g. GRP 94 and 78, RP 60 and calreticulin and together they sequester enough Ca^{2+} for it to reach a milimolar range (69). On the other hand, mitochondria likewise sequester Ca^{2+}, yet their role is not in holding Ca^{2+} upon impending overload but they rather display a capability of conveying Ca^{2+} signals of their own (70). Mitochondria appear in close proximity to IP_3R-enriched parts of ER and mitochondrial Ca^{2+} uptake sites face multiple IP_3R. In this manner the mitochondrial Ca^{2+}-activated Ca^{2+} release, secondary to IP_3-activated ER release, can enhance the primarily ER emptying Ca^{2+} signal. On the other hand, the mitochondrial Ca^{2+} uptake could suppress the local positive feedback of Ca^{2+} on IP_3R. Mitochondrial Ca^{2+} activity is therefore critical in the overall Ca^{2+} oscillation patterns (71,72) and together with ER enables subcellular hubs of differential Ca^{2+} dynamics based on IP_3R sensitivity and excitability (73,74). The cooperation between the ER and

the mitochondria is further emphasized by a trans-mitochondria flux enabling refilling of the Ca^{2+} in the presence of IP_3-generating agonist (75). Both ER and mitochondria cooperate in creating the intracellular Ca^{2+} landscape, e.g. ER stress is tightly connected to the metabolic changes resulting from disturbed ER-mitochondria communication in PAH PASMCs and PAECs (76,77). ER-mediated Ca^{2+} leak leads to increased mitochondrial sequestration, promoting energy production in the early stages but inducing apoptosis chronically (78).

1.2.1.1. Calcium dynamics

Ca^{2+} dynamics is tightly connected to the activity of different types of ion-channels, thus having an important functional consequence. Depending on the concentration of a Ca^{2+} rise-inducing agonists, two different types of Ca^{2+} behaviour constitute a typical response; the first are Ca^{2+} oscillations presumably caused by frequent discharges of intracellular calcium stores, while the second represents a biphasic increase with a fast rise followed by a long-lasting plateau (51,79). While the fast transient peak consists of IP_3-sensitive release from Ca^{2+} stores, the plateau represents extracellular Ca^{2+} entry, activated by store depletion. The latter is significantly modified not only by channels active in plasma membrane but also by the buffering of cytosolic Ca^{2+} by mitochondria and ER (79).

In response to various hormonal and chemical substances, as well as physical stimuli endothelial cells respond with elevation in cytosolic Ca^{2+} concentration. There are multiple pathways of intracellular Ca^{2+} modulation: (i) entry through voltage-dependent Ca^{2+} channels, receptor-operated and store-operated Ca^{2+} channels (ROC and SOC respectively); (ii) Ca^{2+} release and uptake from the ER or mitochondria; (iii) activity of Ca^{2+}-Mg^{2+} ATPase pumps or Na^{+}-Ca^{2+} exchangers, (iv) release and uptake from other intracellular Ca^{2+} stores (e.g. nicotinic acid-adenine dinucleotide phosphate (NAADP)-sensitive lysosome-like acidic compartments) (80,81). The mobilized Ca^{2+} gets quickly removed either by plasma membrane Ca^{2+} ATPases (PMCA) and Na^{+}-Ca^{2+} exchangers or by sarco/endoplasmic reticulum Ca^{2+}-ATPase (SERCA) extruding Ca^{2+} into the extracellular space or the ER respectively (82).

Moreover, there is a continuous leak of ER Ca^{2+} into the cytosol. While the process itself does not affect the overall homeostasis under healthy conditions, it usually manifests whenever other Ca^{2+}-modulating mechanisms are pathologically defective. Even though the molecular entities responsible for the leak have yet to be identified, ER Ca^{2+} sensors STIM1 and STIM2 (83,84) have

been implicated in SOCE-associated Ca^{2+} disruptions across different conditions, including IPAH (85–87). With ER stress being an important part of PAH endothelial dysfunction (77,88) and Ca^{2+} leak being an essential part of ER stress (89), STIM1 and 2 could be of interest in delineating mechanism of IPAH endothelial dysfunction (90).

1.2.1.2. Mechanisms of intracellular calcium rise

Endogenous calcium release

The most commonly referred mechanism of intracellular Ca^{2+} release begins with the activation of guanine nucleotide-binding protein-coupled receptors (GPCRs). Ligand-binding to the α subunit of a G protein q subtype ($G_{\alpha q}$) causes a switch from GDP-bound to a GTP-bound state and a $G_{\alpha q}$ disassociates from a $G_{\beta\gamma}$ activating phosphoinositide phospholipase C (PLC)-β in the process (91–93). In this way ligands such as bradykinin, angiotensin II, serotonin and acetylcholine all cause a series of events ultimately hydrolysing phosphatidylinositol-4,5-bisphosphate (PIP_2) to yield IP_3 and diacylglycerol (DAG) (94). Furthermore, binding of VEGF, PDGF or EGF to tyrosine kinase-linked receptors (RTKs) (95,96) or mechanical stimuli (97) can likewise result in increased levels of IP_3. Diffused IP_3 binds to the ER IP_3R and triggers the release of Ca^{2+} store (94,98). Alternatively Ca^{2+} release can be enhanced via activation of ryanodine receptors (RyRs) through a process known as Ca^{2+}-induced Ca^{2+} release (CICR) (99,100). The depletion of Ca^{2+} stores on the other hand activates the replenishment by oligomerization of ER-transmembrane protein stromal interaction molecule 1 (STIM1), redistribution towards the interface between the ER and cell membrane. This activates membrane store-operated Ca^{2+} channels, including Orai1 and TRP channels triggering the capacitive Ca^{2+} entry (51,101–103). Both capacitive and Ca^{2+}-induced Ca^{2+} release maintain an increase in intracellular Ca^{2+} concentration. While lower to moderate concentrations of Ca^{2+} ranging from 50-200 nmol/L and 1-10 µmol/L activate IP_3 and RyR receptors respectively, higher concentrations inhibit their activation via an inhibitory feedback mechanism. In this way increased amounts of Ca^{2+} are taken up by the SR Ca^{2+} ATP-ase and mitochondrial Ca^{2+} uniporter. The uptake in the latter activates the Na^+/Ca^{2+} exchanger causing oscillatory Ca^{2+} release with the effect of more controlled Ca^{2+} activation of eNOS on the one hand and further activation of IP_3 and RyR receptors on the other, spreading the Ca^{2+} signal (72).

Voltage-gated calcium channels (VGCC)

Voltage-gated Ca^{2+} channels (VGCC) are responsible for sensing the electrical state of the cell and mediate depolarisation-based extracellular Ca^{2+} influx. Based on their physiological and pharmacological characteristics, there are 10 groups of VGCC based on subunit composition grouped into 5 larger groups based on characteristics of Ca^{2+} current; L, N, P/Q, R and T-type VGCC (104). Among the Ca^{2+} channels that are present in the lung vasculature, L-type and in recent years T-type channels are most commonly described. L-type VGCC can be found in conduit and resistance PAs, yet their density is as twice large in the PASMCs of resistance PAs (105). On the other hand vascular endothelial cells have long been considered electrically non-excitable, yet besides voltage-gated Na^+ and K^+ channels, they nevertheless express also T-type Ca^{2+} channels (106–108). T-type VGCC have lower conductance and deactivate faster (109) and recent reports hint there might a spatial component to endothelial distribution of these channel as well (110). Moreover, during a long-lasting depolarization, R-type VGCC could be responsible for a sustained Ca^{2+} influx (111).

Transient receptor potential (TRP) channels

TRP channels are voltage-independent non-selective cation channels, permeable to Na^+, K^+, Cs^+, Li^+, Ca^{2+} and Mg^{2+}. There are more than 30 channels stratified into several families and subfamilies based on functional and structural similarities. Of these TRPC have been shown especially important for maintaining endothelial cell and smooth muscle cell homeostasis on the one hand and driving pathophysiological changes on the other (112–115). All TRPC members are activated by stimulation of GPCRs or RTKs leading to PLCβ or γ activation respectively, and to PIP_2 hydrolysis (116). The following increase in cytosolic DAG and IP_3 either activates some members of TRPC family directly, while others activate after Ca^{2+} store emptying caused by IP_3 binding to ER IP_3R. TRPC channels therefore represent vascular representatives of receptor-operated channels (ROC) and store-operated channels (SOC) respectively (116). It has been shown that all of the members, i.e. TRPC1-7 are expressed in healthy lung tissue and within vasculature, specifically PAs and PAECs (114,115). In a healthy lung TRPC1, 4 and 6 are especially enriched, while PASMCs express high levels of TRPC1, 4 and especially 6 with low levels of TRPC5 and 7, PAECs express high levels of TRPC1, 3 and 4 with low levels of TRPC5, 6 and 7 (114). ROC TRPC6 seems to be a predominant isoform in PASMCs, while SOC TRPC4 is predominantly

present in the vascular endothelium, where it mediates various physiological effects including the lung microvascular permeability (117) and vasodilatory effect of acetylcholine on isolated mouse aortic rings (118). TRPC1 and 6 on the other hand are thought of being the main components of agonist- and hypoxia-induced vasoconstriction of pulmonary arteries (119,120). TRPC channels therefore establish marked differences between cell types given that (i) cells have different TRPC composition, (ii) TRPC channels have different pathways of activation and that (iii) some TRPC channels additionally form heteromultimers of different characteristics (121).

TRPC have been strongly implicated in the pathogenesis of PH. TRPC3 and 6 are upregulated in PASMCs of IPAH patients (114), TRPC1 and 6 are both increased in PASMCs maintained in sustained hypoxia (119), and in PASMCs of mouse and rat models of PH (122). Manipulation of these two channels decreases SOCE and PASMCs proliferation (114,123). On the other hand, TRPC1 and 4 seem to be important determinants of PAEC physiology affecting SOCE and barrier integrity (117,124–126).

1.2.1.3. The functional role of calcium in endothelium

Ca^{2+} dynamics regulates several crucial endothelial functions, including (i) the release of vasoactive and growth factors, cytokines and coagulation factors, (ii) the barrier maintenance and (iii) angiogenesis (127).

Secretion

Endothelial cells are key players in the synthesis and secretions of different molecules acting locally and systemically. Additionally to vasoactive compounds, also compounds important for haemostasis and thrombolysis, growth modulators and inflammatory agents are being produced and secreted as a response to different cues. The former and the latter both are regulated by changes in the intracellular Ca^{2+} dynamics, mediated by the release of Ca^{2+} stores via activation of IP_3R and the extracellular Ca^{2+} influx (51).

The effect of an increase in intracellular Ca^{2+} concentration favours the release of pro-vasodilatory factors, such as NO, EDHF and prostacyclins (20,51,128). The production of the latter also includes the activation of ERK1/2, which phosphorylates phospholipase A2, a step needed for the

synthesis of PGI_2 (129). Vasoconstrictor responses of endothelial cells are mostly mediated by endothelin-1, yet the reports on its Ca^{2+}-mediated release are contradictory, e.g. thrombin and bradykinin both increase intracellular Ca^{2+} concentration, yet only thrombin causes increased secretion of Et-1 (51,130). In contrast, the effect of endothelial cell Ca^{2+} concentration increase is unclear on balance between haemostasis and thrombolysis. While the Ca^{2+} increase favours the production and release of procoagulants, e.g. platelet activator factor, vWF, it also promotes the release of activators of fibrinolysis and thrombolysis, e.g. tPA, TFPI, PAI-1 and protein S (51).

Even though the most important role of NO is promoting vasodilation, it can also act as an anticoagulant, EC growth and inflammatory inhibitor. However, in the case of the increased $ONOO^-$ transformation, it can act oppositely. A similar ambiguity can be shown for PGI_2. It seems likely that the overall effect of all these factors combined is either reflective of an additional regulation of their secretion and/or by the balance of their activity when combined. The latter is especially important, since these factors have different potencies and their activity is usually limited to the locality of their secretion.

Permeability

Increase in intracellular Ca^{2+} concentration by different agonists enhances the permeability of microvessels allowing the exchange across blood and tissue. The increased permeability goes hand in hand with changes in intracellular junctions, cytoskeletal reorganization and cellular contraction (131). An important aspect of microvascular permeability is also its contact with the underlying extracellular matrix, where Ca^{2+} influx is needed for the endothelial cell spreading and contact with basement membrane (132). On the other hand a Ca^{2+} increase in larger vessels is more complex and dependant on the agonist, e.g. ionomycin-mediated increases and a comparable ATP-mediated Ca^{2+} rise reduces the permeability (133).

An important determinant of endothelial cell permeability is the endothelial cell-specific myosin light-chain kinase (MLCK) activity. The increase of Ca^{2+} influx and binding of Ca^{2+}/CaM complex, MLCK interacts with myosin and actin causing cell shrinkage, increased permeability and transendothelial leukocyte migration (134). Since the induced increase of intracellular Ca^{2+} levels not only increases cell permeability (135) but also upregulates endothelial adhesion molecules, Ca^{2+} dynamics importantly regulates also inflammatory response (136).

Growth and angiogenesis

Aerobic glycolysis is the predominant bioenergetic pathway in endothelial cells generating up to 85 % of total cellular ATP (137–140). Though highly inefficient, aerobic glycolysis represents a mechanism of fast ATP production thus supporting rapidly changing sprouting behavior and vascularization into oxygen-deprived tissues. Moreover, glycolysis represents an important biosynthetic pathway of macromolecules supporting e.g. mass duplication before cell-division (139,141). Thus, manipulating glycolysis severely disrupts several processes supporting angiogenesis, while manipulation of respiration has no effect (139), establishing mitochondria of endothelial cells function more as signaling hubs (142).

A rise in endothelial Ca^{2+} is an important pro-angiogenic event (90). In response to several growth factors and chemokines the Ca^{2+} change stimulates endothelial cell proliferation, migration, adhesion and tube formation *in vitro* and *in vivo* (143). Ca^{2+} signals are mediated mainly by endogenous IP_3R-stimulated Ca^{2+} release and extracellular Ca^{2+} influx mediated by SOCE, mostly through STIM1, Orai1 and TRPC1, 4 and 6 (90,144). Furthermore, the role of anion channels was likewise established in angiogenic processes. Their inhibition disturbs the tube formation *in vitro*, *ex vivo* and *in vivo* making them therapeutically interesting targets in conditions with pathological angiogenesis (51,145).

The VEGF superfamily of growth factors in connection to VEGFR are master regulators of angiogenesis (146). In the vascular endothelium mainly VEGFR1 and 2 are mainly expressed, however angiogenic signalling runs primarily through VEGF-A-VEGFR2, even though VEGF-A displays higher binding affinity for VEGFR1. Consequently, it is assumed that in some cases VEGFR1 functions as a decoy receptor in regulating VEGF-A signalling, though in others VEGFR1 seems to play a unique role in tissue-specific release of growth factors (146). Following the dimerization and auto/trans phosphorylation of the VEGFR2, the receptor affects downstream pathways important for regulating angiogenesis; (i) PLCγ1 and RAS/RAF/ERK/MAPK promoting the vascular development and arteriogenesis, (ii) eNOS stimulating proliferation and migration, (iii) SRC and small GTPases regulating endothelial junctions, permeability, shape, migration and polarization (146–150). A crucial part of the VEGF-stimulated proliferation, migration and tube-formation is the increase in intracellular Ca^{2+} (147,151). Typically VEGF-A-mediated Ca^{2+} response is biphasic, consisting of IP_3-dependent ER release followed by a prolonged extracellular SOCE-mediated influx, however some reports show an additional level of regulation through the

type of Ca^{2+} signalling patterns triggered by exposure to different concentrations of VEGF-A (151–154). Other growth factors are tightly connected to angiogenic processes as well; FGF-1 and -2, IGF-I, EGF and PDGF all play a part in promoting angiogenesis through regulation of intracellular Ca^{2+} concentration, whether it is through stimulation of endogenous store release or influx of extracellular Ca^{2+} (90).

Several pathways connect the Ca^{2+} signal to its angiogenic effect, among other ERK1/2 (155–158), PI3K/Akt (81,159) and eNOS (81,160) pathways. A rise in intracellular Ca^{2+} concentration is a known MAPK activator, including the ERK1/2 pathway (156–158). ERK1/2 represents one of the main signalling pathways promoting endothelial cell proliferation, migration, survival and angiogenesis (147,150,161–166). It is an important mediator connecting endothelial cell metabolism with growth factor signalling (161–166). VEGF-associated IP_3-mediated Ca^{2+} release and Ca^{2+} influx through TRPC3-4 and the SOCE maintain its activity (90,155,167). Some reports also hint at VEGF-stimulated endothelial cells boost of glycolysis goes through ERK1/2 stabilization of a transcription factor MYC, a known driver of cell growth, proliferation and anabolic metabolism (139,141,168–170). Moreover, ERK1/2 is also an essential part of eNOS activation, another important regulator of angiogenesis (156,171–178). eNOS activity together with NO production is an essential pro-angiogenic factor, stimulating proliferation, migration and tube formation (179,180). eNOS activity is connected to cell Ca^{2+} levels. Besides CaM/Ca^{2+}-mediated activation through association and substituting the inhibitory cav-1. Additionally, Ca^{2+}-associated activation of eNOS goes also through kinase activity phosphorylating Ser615, Ser633 and Ser1177 located within the inhibitory reductase domain preventing the activation of eNOS in the absence of Ca^{2+} rise (156,176,181). IP_3-mediated ER emptying is assumed as the main pathway responsible for eNOS activation, yet the activation can also go through SOCE (160,176).

1.2.2. Chloride

Traditionally, the expression of K^+ channels have been shown to importantly influence the RMP and by extension the cell physiology. More recently, chloride channels have been established as important contributors in the maintenance of a polarized cell membrane (54,57,59,182,183), hinting at important roles for volume-regulated anion channel (VRAC), cystic fibrosis transmembrane conductance regulator (CFTR) and Ca^{2+}-activated Cl^- channels (CaCC). Cl^- channels are distributed throughout the cell and can be found in the plasma membrane, ER, Golgi

apparatus, mitochondria, nucleus, endosomes, lysosomes and cell vesicles (184–186). Therefore they do not only affect the cell membrane potential but are also emerging as important signalling effectors, regulating various cell functions from gene and protein expression, post-translational modifications to cell volume, cycle, proliferation, differentiation, ROS levels in spatio-temporal manner (184). Cl^- is capable of regulating the activity of ion channels (187,188) and enzymes (184,189,190).

Cl^- anion plays an important role in regulating cell cycle and proliferation (184,191–193). Reports suggest that CaCC TMEM16A can promote and decrease cell proliferation. Though it is not yet exactly known what contributes to the opposite effects, some reports show that its effect could be supported by the additional activity of cell-specific factors (194,195). TMEM16A activity is directly connected to the activation of ERK1/2 and cyclin D1, possibly through Cl^- level modulation, thus promoting cell proliferation (196). On the other hand, cell shrinkage from Cl^- efflux is an important apoptotic event. TMEM16 proteins are known to affect the cell death pathways through still unresolved means. It is possible that in these cases, Cl^- assumes the role of a signalling effector (184). TMEM16A was recently implied to promote apoptosis of rat lung microvascular EC through increased in mitochondrial ROS and p38 activation (65).

1.2.2.1. Volume-regulated anion channel (VRAC)

VRAC is partially activated in a resting non-stimulated endothelial cell, suggesting that its activity contributes to the setting of the RMP. Its inhibition causes a general hyperpolarization of depolarized PAECs because of a dominating inward-rectifier potassium current and the same is true vice-versa (197). While a decrease in the intracellular ionic strength and not an increase in the cell volume has been mainly shown to activate the channel´s outward conductance, other less obvious pathways have been pointed out in recent years (198). VRAC conductance is mainly carried by Cl^-, yet also amino acids and organic osmolytes cross the pore; the anion permeability sequence for VRAC is $SCN^- > I^- > NO_3^- > Br^- > Cl^- > HCO_3^- > F^-$ > gluconate > glycine > taurine > aspartate, glutamate (198–200).

1.2.2.2. Cystic fibrosis transmembrane conductance regulator (CFTR)

CFTR is low-conductance, cAMP-activated outward rectifying channel (201). Most commonly the channel is referred to as a major determinant of epithelial cell homeostasis and its driving role in the development of cystic fibrosis (202), yet its expression and importance is of equal importance in the endothelium (201,203,204). Interestingly, in epithelium there seems to be a need of both TMEM16A and CFTR expression in order for a functional CFTR (205,206), hinting at a possible communication between the two. Furthermore, an increased activation of CFTR has been connected to the downregulation of VRAC as well as CaCC channels (207,208). It seems that TMEM16A can also be functionally suppressed by CFTR (209), and CFTR on the other hand can be suppressed by HIF-1α (210,211), thus hypoxia possibly enhancing Ca^{2+}-activated Cl^- secretion (212). It is therefore possible that hypoxia and the stabilization of HIF-1α with suppression of CFTR might lead to a shift from cAMP-dependent towards Ca^{2+}-activated Cl^- secretion (213).

1.2.2.3. Calcium-activated chloride channels (CaCC)

The first observation of the Ca^{2+}-activated Cl^- current has been in the 1980s (214), yet it took until 2008 for the identification of the TMEM16 protein family and its most prominent member TMEM16A determined as a key molecular part of the Ca^{2+}-activated Cl^- conductance (215–217). TMEM16A is activated by an increase in intracellular Ca^{2+} concentration in combination with RMP depolarization (218,219). Its current demonstrates voltage-dependent activation, strong outward rectification and a deactivating tail current on depolarization (220). Half-maximal intracellular Ca^{2+} concentration for activation is voltage-dependent; 2,6 µM at -60 mV, 0.3 µM at +60 mV and the anion permeability ratio is NO_3^- (2.20) > I^- (1.85) > Br^- (1.74) > Cl^- (1.0) > F^- (0.43) (217). The activity of TMEM16A was reported to be regulated by calmodulin, cholesterol, phosphoinositides and by various stimuli, e.g. thermal and mechanical (221). Moreover, TMEM16A also tethers ER to plasma membrane. It interacts with IP_3R type 1 and is activated by IP_3R-mediated Ca^{2+} store release, yet not by extracellular Ca^{2+} influx (222). TMEM16A activation has further been connected to ORAI1-mediated SOCE (223), TRPC6 (224) and CFTR as well (209).

The functional channel is a homodimer with each monomer consisting of 10 transmembrane domains. Each monomer contains one pore and two Ca^{2+}-binding sites (225). When only one site is occupied, the channel remains closed until depolarization causes it to open. On the other hand,

with both sites occupied, TMEM16A opens in a voltage-independent manner followed by a channel rundown (226). The voltage and Ca^{2+} gating of TMEM16A is conferred by a series of acidic amino acid residues in the first intracellular loop (227) and two intracellularly-facing glutamates E702 and E705 that mediate an additional level of Ca^{2+} sensitivity (228).

Alternative splicing of TMEM16A seems to be extensive and it contributes to the structural and functional diversity of the channel (216,229,230). At first, different combinations of four variants were described, termed a-d, corresponding to alternative transcription start sites, exons 6b, 13 and 15; segments a and b are located in the N-terminus while segments c and d in the first intracellular loop (216,227,229). Later, variant 0 was described (231), then a variant lacking a dimerization domain (232), a variant with lacking exons 1-2 and a part of exon 3 (233). Additionally the region between exons 6-16 undergoes extensive alternative splicing (230). All mentioned variants represent functional TMEM16A channels, yet (i) demonstrate different activity characteristics, (ii) are localizing to specific tissues or (iii) are hallmarking pathological states. In any case, this highlights the heterogeneity of Cl^- current and its importance in the homeostasis of healthy tissues on the one hand and in the pathogenesis of diseased on the other.

TMEM16A has been shown to be a key part in maintaining homeostasis of several cellular systems, including the gut (234,235), airway epithelium (235–237), kidney (238) and brain (239). On the other hand its dysfunction has been undoubtedly placed in the pathophysiology of several heterogenous diseases such as cancer, hypertension, gastrointestinal motility disorders and cystic fibrosis (233,240–242). In addition, TMEM16A regulates the functionality of systemic and pulmonary vascular network, indicating the important contribution of Cl^- current in maintaining the electrophysiological homeostasis of the vascular cells, including PASMCs and PAECs (57,65). Indeed, the RMP of vascular endothelial cells being closer to the Cl^- equilibrium indicates the important contribution of Cl^- channels in maintaining its RMP and that small changes in the activity of these channels could potentially have important downstream repercussions (51,56,59–62). Consequently, TMEM16A has been established in several vasculopathies in different tissue and organ systems, emphasizing its role in the regulation of vascular tone and remodelling (57,65,243–245).

1.3. Endothelial NO synthase (eNOS)

Endothelial cells are an important source of nitric oxide (NO) as a regulator of vascular tone (246–250). Endothelial NOS (eNOS) is a predominant source of NO in the pulmonary blood vessels, since the knockout of eNOS but not the inducible NOS impairs endothelium-dependent vasorelaxation and promotes increased pulmonary artery pressure and hypoxic vasoconstriction (251,252). NO has a short half-life; within seconds, its reaction with superoxide anions, oxygen or thiol groups (acting as a storage pool) removes NO from the locality with the biotransformation of NO and its N-oxides taking place within different metabolic routes of the body (253). As complex as the activation of eNOS as complex the possibilities causing its dysfunction. If the ability of endothelial cells to produce NO is blunted, the onset of vascular dysfunction paves the way to cardiovascular disease (254).

Since the half-life of produced NO is short, the subcellular localization of eNOS is relevant for its physiological effects (255). Within the microvascular endothelial cells, the majority of eNOS is localized to plasma membrane, where it is targeted to cholesterol-rich calveolae, together with a few other eNOS regulatory proteins (256,257). In addition, eNOS can also be localized in the membrane of the Golgi apparatus (GA), mitochondria, perinuclear regions and the actin cytoskeleton but the majority of NO is being produced by the eNOS in the outer cell membrane and the membrane of the GA (255,258,259). GA-associated and caveolae-associated eNOS have different mechanisms of activation, where the former is more sensitive to Akt phosphorylation, the latter is to Ca^{2+} influx (255). Moreover, subcellular localization of eNOS achieves spreading of its functionality with plasma membrane-associated having an important role in NO production, while the GA-associated in the S-nitrosylation of proteins (260,261).

Having eNOS localized in caveolae keeps the enzyme in close proximity to a milieu of different signalling molecules, e.g. GPCRs, ion channels, protein kinases and RTKs therefore keeping it in an optimal position for activation. Allosteric inhibitor caveolin-1 (Cav1) keeps eNOS inactive until sufficient increase in intracellular Ca^{2+}. Ca^{2+}/calmodulin (CaM) complex displaces Cav1 and eNOS translocates to the cytosol where further cofactors and substrate are in sufficient quantity to enable its activation (262–264).

The binding and processing of L-arginine into NO requires the combination of eNOS dimerization with binding of several cofactors. The N-terminal haeme-binding oxygenase domain of the enzyme contains binding sites for BH_4, heme, L-arginine and Zn^{2+}, while the C-terminal cytochrome P450-

binding reductase domain binds flavin mononucleotide (FMN), flavin adenine dinucleotide (FAD), NADPH and contains an autoinhibitory domain. The domains are linked by a region binding Ca^{2+}/CaM and the catalytic activity of eNOS depends on the rate of electron transfer from the reductase to the oxygenase domain, oxidizing L-arginine to produce NO in the process (265). The role of the autoinhibitory domain is in regulation of the electron transfer between the domains ultimately regulating eNOS activity (266). In the case of eNOS dysregulation where the ability of dimerization is affected, the oxygenase domain takes over with generating superoxide anions (267,268). The catalytic activity of eNOS is regulated by numerous posttranscriptional and posttranslational modifications, protein-protein interactions as well as inter- and intra- domain electron transfer mechanisms within eNOS (269–272).

1.3.1. Calcium-dependent activation

The activation of eNOS can be both Ca^{2+}-dependent as well as -independent. Ca^{2+} dynamics within the cell is a potent regulator of eNOS activity. Not only the increase but also the frequency, amplitude, duration and the spread of Ca^{2+} ions affects its activity (273). The activation pathway starts from the respective membrane receptor and travels downstream via coupling with G proteins (91–93). The following activation of PLC, production of IP_3 ultimately activates ER IP_3R causing Ca^{2+} release (94,98). Moreover, the increased intracellular Ca^{2+} is taken up by the SERCA and the mitochondrial Ca^{2+} uniporter. Mitochondria mediate oscillatory Ca^{2+} release achieving a more controlled Ca^{2+} activation of eNOS (72). While the basal activity of eNOS is caused by Ca^{2+} leak from the ER and mitochondria, the exaggeration of Ca^{2+} oscillations leads to an ineffective activation of eNOS altogether.

SOCE is responsible for a steady increase in intracellular Ca^{2+} concentration of approximately 250 nM. Even with the comparable increase with direct extracellular influx of Ca^{2+} achieved with ionomycin, the SOCE-mediated increase causes 10-times greater NO production than ionomycin. This demonstrates SOCE as an essential part of eNOS activation (274). Optimally, phosphorylated eNOS requires above 80-100 nM of intracellular Ca^{2+} concentration for activation and up to 200 nM for maximal activation (275). The absence of sustained synchronous intracellular Ca^{2+} concentration bursting of this range results in decreased NO output even when eNOS itself remains functional (276). Even though sustained-phase Ca^{2+} response is important for eNOS activation (274), if constant Ca^{2+} bursting fails to reach the threshold or the time above the

threshold needed to maintain periodic eNOS activation, the resulting reduction in NO output will cause endothelial dysfunction (275). Thus, the rise in NO production is sustained over a longer period in healthy endothelial cells, while the rise in dysfunctional endothelial cells is slower and quicker to plateau back to baseline (276).

1.3.2. Post-translational modulation of eNOS activity

An important aspect of eNOS activation are also posttranslational modifications that follow the early Ca^{2+}/CaM-dependent activation. Thiopalmitoylation, myristoilation, S-nitrosylation, acetylation, glycosylation and others lead the enzyme through a complex activation dynamics, (277–281), yet most potent one by far is eNOS phosphorylation. The activity of Ca^{2+}-dependent or -independent CaMKII, PKC, Akt, PKA, AMPK and ERK1/2 determines the state of numerous activatory and inhibitory eNOS sites. While some of these sites are kinase-specific, others can be promiscuous (264,282–285).

Of all the sites, the best characterized are the activatory Ser1177 (or Ser1179 depending on the species) and inhibitory Thr495 sites. Ser1177 is a common target of PKA, Akt, AMPK, Ca^{2+}/CaM-dependent PK II and ERK1/2, the complexity of each pathway further layered by the staggering amount of different stimuli activating these effectors through different mechanisms. Thr495 is a target of Rho-kinase, PKC and by some reports also ERK1/2. Activation of eNOS by phosphorylation of Ser1177 usually goes hand in hand with simultaneous dephosphorylation of Thr495. Other reported sites are activatory Tyr81, Ser615, Ser633, Ser1177, and inhibitory Ser114, Thr495 and Tyr657 (286). Other reported ERK1/2 target sites are also Ser114, Ser602 (287) and Ser635 (156). Interestingly phosphorylation of Ser635 (bovine) could be responsible for the prolonged activation of eNOS that persists beyond peak activation at approximately 5 minutes after stimulation (288). Ser615 and 633 are located in the putative CaM autoinhibitory sequence within the FMN binding domain of eNOS; phosphorylation of Ser617 makes eNOS more susceptible to activation by Ca^{2+}/CaM and subsequent Ser637 phosphorylation increases its maximal activity to the level of Ser1179 phosphorylation in BAEC (288).

1.3.3. Autoinhibitory domain

Phosphorylation sites Ser615, Ser633 and Ser1177 all lie within two autoinhibitory domains (289). The first two sites lie within a 43-45 amino acid long section in the FMN-binding domain which prevents the binding of CaM and therefore the activation of eNOS (290). The third lies within a 14 amino acid autoinhibitory domain located in a C-terminal tail interacting with flavin domain and in doing so interferes with Ca^{2+} sensitivity. Deletion of the first leads to an increase in CaM-dependence, deletion of the second improves Ca^{2+} sensitivity, while the enzyme with both domains deleted results in a constant Ca^{2+}-insensitive eNOS. A third, less described, peptide sequence has also been reported to interfere with CaM binding (289,291). It has been postulated that the autoinhibitory domain interacts with FMN-binding domain, ultimately regulating the electron flow. There are contradicting reports showing that various synthetic fragments of autoinhibitory domain, including an 11 amino acid potent fragment AAF, diminished the activity of eNOS in isolated samples, while on the other hand it activated it in intact PAECs, PAs and whole lung (266,292). It is therefore possible that the mechanism of action depends on the structural integrity of eNOS as well as the accessibility of other binding factors.

1.3.4. The role of NO in vascular homeostasis

1.3.4.1. NO and vascular tone

Even though the production of NO affects several different processes e.g. inhibition of platelet aggregation and endothelial surface adhesion molecules, biogenesis of mitochondria, ultimately it remains a powerful regulator of the vascular tone by (i) activating the sGC-cGMP-PKG pathway and (ii) by modulation of other endothelium-derived hyperpolarizing factors (EDHF) and vasoconstrictors (293).

Endothelial-derived NO targets sGC in the smooth muscle cell layer. The consequent production of cGMP leads to the activation of cGMP-dependent protein kinase (protein kinase G; PKG). PKG-mediated cellular effects include (i) inhibition of the ER Ca^{2+} release by IP_3R phosphorylation, (ii) inhibition of extracellular Ca^{2+} influx by large-conductance Ca^{2+}-activated potassium channels-mediated (BKCa), (iii) plasma membrane hyperpolarization preventing L-type Ca^{2+} channels from opening, (iv) indirect promotion of SERCA-mediated Ca^{2+} uptake and (v) stimulation of PMCA-

mediated Ca^{2+} extrusion. All these effects combined achieve the reduction in intracellular Ca^{2+} level rendering the MLCK (294–298).

Moreover, NO interacts and modulates other endothelium-derived relaxing factors (EDRF), namely prostacyclin and endothelial-derived hyperpolarisation factors (EDHF), where the physiological balance between both maintains cardiovascular homeostasis distinct of the the vessel size (299–301). Furthermore NO prevents the production and action of endothelium-derived contracting factors (EDCF) and endothelin-1 (293,302).

1.3.4.2. NO in angiogenesis

Angiogenesis is a coordinated multi-step process that includes degradation of the basement membrane, endothelial cell proliferation and migration, ultimately leading to organization into a network, supporting tube-formation, fusion and pruning with pericyte stabilization (141). Modulation of NOS-derived NO regulates organization of endothelial cells into capillary-like structures, meaning NO represents an essential part of vessel homeostasis and new vessel formation *in vitro* (179,303,304), *ex vivo* (305) and *in vivo* (306–308). Even though it is not clear how NO promotes angiogenesis, it has been shown that it inhibits apoptosis on the one hand (309) and enhances proliferation and migration on the other (304,310). Pathways implicated in these processes range from expression levels of growth factors (311,312), to regulation of podokinesis (313), integrin expression (314), extracellular matrix dissolution (311) and production of angiostatin, an endogenous antagonist of endothelial cell angiogenesis (315). Since eNOS-deficient mice exhibit abnormal lung morphological and vascular development and failure to upregulate several key pro-angiogenic genes, such as VEGF/Flk1, Ang-1/TIE2, FGF2/FGF-R and TGFβ1/2, it has been suggested that NO may additionally modulate HIF1α and HIF2α activity (316). NO production is severely impaired in IPAH PAECs (45). Together with defective tube formation (21) this indicates that NO dysregulation is at the base of defined IPAH vascular malformations.

1.3.5. Dysfunction of endothelial NO production

Disturbances in eNOS function can be found across different diseases connected to aging, deleterious environmental factors, obesity, endocrinologic disorders, atherosclerosis and hypertension (176). The observed reduction in NO-dependent relaxation can result from a dysfunction of numerous limiting factors: (i) decreased eNOS activation, (ii) limiting substrate availability, (iii) reduced bioavailability of NO, disturbed (iv) eNOS dimerization, (v) arginase activity, (vi) cofactor and endogenous inhibitor levels, (viii) eNOS coupling and (ix) the transfer of vasodilatory cues to smooth muscle cell layer (176).

The concentrations of L-arginine or its *de novo* synthetisation substrate L-citruline in the human body are rarely a limiting factor (317,318). On the other hand the substrate competition can be responsible for limiting eNOS activation. Increased activity of iNOS due to inflammation or increased arginase activity can successfully compete for the same substrate that eNOS needs to produce NO (319,320). With age or with the development of diseases, e.g. hypertension, the activity of arginases within the vascular endothelium increases due to the negative effect of ROS and Rho-kinase stimulating its expression, translocation and activity (319,320). On the other hand increased and continuous production of NO by iNOS also promotes S-nitrosylation of the cysteine residues important for the dimerization of eNOS (321) thus its inactivation (322). Interestingly, in the same manner iNOS is also capable of reducing the activity of arginase (323). Furthermore, the oxidative stress importantly affects NO homeostasis; dysbalanced ROS can lower the bioavailability of NO, the activity of eNOS and by extension also modulate various signalling pathways across many different cell types. Moreover, ROS together with other mechanisms can render the transfer of NO-mediated vasodilatory cues to the smooth muscle layer ineffective by reducing sGC responsiveness (176,324).

1.3.5.1. Dimerization

The dimerization of eNOS is necessary for the enzyme to bind BH4 and L-arginine needed to produce NO. With age, diabetes mellitus, increased ROS or hypoxia the process can be disrupted increasing the monomerization of the enzyme. While reduced L-arginine or BH4 levels significantly affect the enzyme activity (325,326), the dimeric structure can be further destabilized by increased

NO levels, iNOS-mediated S-nitrosylation and ROS, as well as decreased levels of Hsp90 and Caveolin-1 (176).

1.3.5.2. Oxidative stress and bioavailability

The effect of oxidative stress and H_2O_2 on eNOS activation is hard to predict; H_2O_2 can act as a secondary messenger (327) and can inhibit (328) or stimulate (329–331) eNOS. The effect of H_2O_2 seems to be concentration dependant, whereas low levels stimulate the activitiy by Ser1177 phosphorylation and high levels disrupt the dimerization of the protein via destabilizing ZnS_4 (321,332,333). The increase in oxidative stress affects ZnS_4 cluster which is higly sensitive to NO, $ONOO^-$ and H_2O_2 and its oxidation results not only in the monomerization of the enzyme but also, owing to the close proximity to the catalytic centre, in the inhibition of the catalytic activity by translocation of the flexible arm to block the substrate accessing the catalytic site (289). With this, the flexible arm prevents the access of haeme to molecular oxygen, thus enhanced superoxide generation that ZnS_4 cluster would otherwise produce. Since the oxidation of Zn is reversible, when the physiological redox levels are restored, the ZnS_4 is restored to its normal state and the flexible arm regains its open conformation (289).

Moreover increased presence of superoxide anions additionally favours the formation of a highly reactive $ONOO^-$ which represents a significant way of NO bioavailability reduction (334–336). Not only that $ONOO^-$ decreases the vasodilatory activity of NO but acts as a signalling molecule in its own right, impacting various different signalling pathways across a plethora of different cell types (324). $ONOO^-$ is a strong oxidant that reacts with haeme- or thiol- containing proteins, lipids and nucleic acids. Furthermore, nitrogen dioxide can nitrate tyrosine residues of proteins. Together the effects of dysbalanced nitrogen oxidative species production, oxidative and nitrative, in excess can disrupt several different pathways ultimately leading to dysfunction and apoptosis (324,337).

There are several possibilities of oxidative species increase in endothelial cells: (i) increased endogenous substances capable of increasing ROS to pathophysiological levels, e.g. aldosterone, angiotensin II, hydrogen sulphide, leptin, resistin, testosterone and (ii) varied expression of antioxidant enzymes, e.g. SOD, catalase and HO-1, dysregulation in NOX and cyclooxygenase-2 on the one hand and (iii) endothelial enzymes capable of producing superoxide anions, e.g. NOX, xanthine oxidase, cyclooxygenases, members of the mitochondrial electron

transport chain and eNOS itself on the other. Dysbalanced ROS and consequently NO homeostasis has been described in several conditions and diseases, from smoking, intoxications with arsenic and mercury, exposure to air pollution but also in obesity, diabetes mellitus and hypertension, including PAH demonstrating increased ROS, decreased ROS-neutralizing mechanisms and tyrosine nitration (36,37,324).

An additional level of eNOS modulation by ROS is via its endogenous inhibitor asymmetrical dimethyl arginine (ADMA), which can be increased by oxidative stress (338,339). The production of ADMA can be reduced by SIRT1 (340). PAH patients have increased ADMA and decreased activation of SIRT1 (341–343).

1.3.5.3. Reduced vasodilatory response

The reduction of NO-mediated vascular relaxation can be a direct result of a reduced sGC responsiveness as a consequence of (i) differential expression of sGC subunits and disturbed dimerization or desensitization by e.g. oxidative stress and $ONOO^-$ targeted mostly at the NO-binding sGC subunit β and (ii) differential expression or activity of sGC modulating proteins, such as HO-1, phosphodiesterases or BKCa on the other (344,345). Hypoxia prevents the dimerization of the subunits ameliorating NO-meditated vasorelaxation (346). Since up to 40 % of adult patients with PH do not respond to therapy with inhaled NO and the responders further complicated by the short duration of NO-mediated vasorelaxation and even rebound pulmonary vasoconstriction, most likely the underlying cause is either the altered sGC expression or alteration in the dimerization of the enzyme affecting its activity. Since sGC levels are elevated in IPAH patients, the discrepancies in the dimerization are the likely cause with an extension of elevated PDE5 as seen in PAH (33,34,347,348). Furthermore, IPAH patients have disrupted eNOS pathways with different reports on the protein level of eNOS, yet a decreased exhaled NO (38–45). It is assumed that eNOS is dysregulated either by disruption in post-translational modification or increased formation of ROS, namely $ONOO^-$ (349). Moreover, persistent eNOS activation induces pulmonary hypertension in mice and humans through PKG nitration causing the vasodilatory defect (35) and hypoxic mice and monocrotaline rat models of PH have impaired ACh-mediated vasorelaxation (46).

2. Hypothesis and Aims

PAECs isolated from patients with IPAH express higher level of Ca^{2+}-activated Cl^- channel TMEM16A, yet the functional consequences have been lacking. Since the physiology of vascular endothelium is importantly shaped by the activity of Cl^- channels, I hypothesized that **increased TMEM16A-associated ion conductivity in pulmonary endothelium provides basis for endothelial dysfunction as defined in IPAH endothelial phenotype.**

To connect how increased TMEM16A activity would lead to endothelial dysfunction my aims were:

- To establish the role of endothelial TMEM16A in pulmonary arterial tone.
- To define electrophysiological characteristics of IPAH PAECs as defined by TMEM16A conductivity.
- To look into TMEM16A overexpression-associated PAEC phenotype and establish the importance of previously reported MAPK in TMEM16A-primed PAECs.
- To investigate acetylcholine responsiveness of TMEM16A-overexpressing endothelium especially in connection to nitric oxide production.

3. Materials and Methods

3.1. Human lung samples

Human lung tissue samples were obtained from patients with IPAH who underwent lung transplantation at the Department of Surgery, Division of Thoracic Surgery, Medical University of Vienna, Austria. The protocol and tissue usage were approved by the institutional ethics committee (976/2010) and patient consent was obtained before lung transplantation. The patient characteristics included: age at the time of transplantation, weight, height, sex, mean pulmonary arterial pressure (mPAP) measured by right heart catheterization, pulmonary function test, as well as oxygen and medication before transplantation. The chest computed tomography (CT) scans were reviewed and the diagnoses were verified by an independent board including experienced pathologists, radiologists, and pulmonologists. Healthy donor lung tissue was obtained from the same source. Detailed patient characteristics can be found in Table S1.

3.2. Cell isolation and culture

Donor and IPAH PAECs:

For the isolation of donor and IPAH pulmonary artery endothelial cells (PAECs), pulmonary arteries (< 2 mm in diameter) were isolated and the endothelium incubated with an enzymatic mixture of collagenase, DNAse and dispaze in HBSS at room temperature (RT). Cell suspension was collected, resuspended in VascuLife Complete SMC Medium and cultured in gelatine-coated T25 flasks at 37 °C and 5 % CO_2. After reaching 70-80 % confluency, cells were trypsinized, enriched by 3 consecutive steps of CD31-selective magnetic-activated cell sorting technology and verified via morphological and marker confirmation (smooth muscle actin, fibronectin, vimentin, von Willebrand Factor, smooth muscle myosin heavy chain and CD31). Surplus PAECs were frozen (endothelial cell complete medium containing 12 % FCS and 10 % DMSO) and stored in liquid nitrogen until further use. Passages 3-9 were used for the experiments.

Human PAECs purchased (Lonza, Switzerland) or isolated as described above, were cultured in gelatine (0.1 % gelatine solution in PBS) coated cell culture flasks in Lonza endothelial cell growth medium (EBM™-2 supplemented with EGM™-2 containing growth factors, cytokines and other

supplements, with final 2 % FCS concentration), here referred to as complete medium. Whenever the starvation medium was used, EBM™-2 was supplemented with 0.5 % FCS and 0.2 % antibiotics. Detailed patient characteristics of isolated and purchased PAECs can be found in Table S1 Table S2respectively.

PASMCs:

The isolation and culture of human PASMC has been performed according to Stulnig et al (350). After the removal of the endothelial cell layer, the media was peeled away from the underlying adventitial layer and cut into approximately 1-2 mm^2 sections, centrifuged and resuspended in VascuLife Complete SMC Medium supplemented with 20 % FCS and 0.2 % antibiotics, then transferred to T75 flasks and cultured at 37 °C and 5 % CO_2. After a confluent monolayer of PASMC had formed, the cells were trypsinized and either cultured in VascuLife Complete SMC medium supplemented with 10 % FCS and 0.2 % antibotics, or frozen (VascuLife Complete SMC Medium containing 15 % FCS and 10 % DMSO) and stored in liquid nitrogen until further use. Passages 4-8 were used for the experiments. Detailed patient characteristics of isolated PASMCs can be found in Table S1.

3.3. Precision-cut lung slices (PCLS)

Donor lung cuts were filled with 3 % low melting agarose and let to solidify at 4 °C for 15 min. Cylindrical cores of 8 mm in diameter were cut and sliced in cutting solution to sections of 250 µm thickness using a Krumdieck live tissue microtome. Freshly cut slices were then transferred to the incubation medium and kept at 37 °C and 5 % CO_2 in the incubator. Incubation medium was changed 4 times separated by 30 min wash steps and finally left overnight. On the following day the slices were either fixed in 4 % formaldehyde for 1 h or kept for further use in culture. Further information regarding solutions and materials can be found in Table S5 and Table S6 respectively.

3.4. Overexpression of TMEM16A

Cells:

For TMEM16A overexpression, human PAECs or PASMCs were seeded on gelatine-coated chamber slides or in 6-well plates and left to settle in fully supplemented medium overnight. On the next day the medium was replaced by fresh complete medium containing either TMEM16A-encoding adenoviruses $Ano1^{Ad}$ or control $Ctrl^{Ad}$ (Cyagen Biosciences, USA) at multiplicity of infection 50 (MOI 50). After 24 h the medium was replaced by fresh complete medium. For further assays, cells were collected either 48 or 72 h after the start of infection.

Measurements of Ani9 efficacy were performed by our collaborators at the group of Prof. Dr. Péter Enyedi, Semmelweis University, Budapest. HEK293T cells were seeded at a density of 20.000-50.000 cells per 35 mm dish 48 h prior to transfection in complete DMEM. The vector used was constructed at the University of Münster, by cloning the TMEM16A gene from a human podocyte cDNA library into a pQCXIP expression plasmid. Cells were transfected using LipofectAMINE2000 transfection reagent and UltraMEM Reduced Serum Medium according to the manufacturer's instructions (2 µL Lipofectamine2000 in 1 mL medium per 35 mm dish). Cells were transfected with 0.8 µg TMEM16A-overexpressing and 0.2 µg CD8-overexpressing plasmid per 35 mm dish and used for experiments 24-48 h after transfection. Transfected cells were identified by using anti-CD8 magnetic beads.

Isolated pulmonary arteries and precision-cut lung slices (PCLS):

In the case of isolated human pulmonary arteries or PCLS, the vessels or PCLS slices were incubated with the adenovirus in basal VascuLife Medium for 24 h followed by exchange of the viral solution and incubation for further 24 h. After 48 h the vessels were either used for isometric tension measurements, immunofluorescence imaging or collected for protein assessment followed by western blot.

Further information regarding solutions and materials can be found in Table S5 and Table S6 respectively.

3.5. Immunofluorescence staining

Human lung sections

Formalin-fixed paraffin-embedded human lung tissue blocks were cut to 3.5 µm thick slices. Sections were deparaffinised at 60 °C overnight and antigen retrieval was performed with Dako Target Retrieval Solution pH 9.0 at 95 °C. Lung sections were blocked with 10 % BSA for 1 h at RT and immunolabelled with antibodies against Von Willebrand factor (vWF) and TMEM16A at 4 °C overnight. On the following day, the sections were washed, then labelled with Alexa Fluor 555 a-rabbit and Alexa Fluor 647 a-mouse secondary antibodies for 1 h at RT. Finally, the slides were preserved using a mounting medium containing 4′,6-diamidino-2-phenylindole dihydrochloride (DAPI) and imaged with Zeiss LSM 510 META laser scanning confocal system. Duplicates were processed either without the primary antibody or with the primary antibody against TMEM16A pre-incubated with the immunogen peptide as negative controls.

Precision-cut lung slices (PCLS)

Formalin-fixed pieces were blocked at 4 °C overnight in PBS containing 5 % BSA and 0.5 % Triton X-100. On the next day, the slices were transferred to primary antibodies against vWF and TMEM16A prepared in the same solution and incubated for 24 h at 4 °C. On the following day, the pieces were washed, then labelled with a mixture of AlexaFluor 555 a-rabbit secondary antibody and DAPI prepared in PBS with 3 % BSA and incubated for another 24 h at 4 °C. The pieces were preserved using a DAKO mounting medium and imaged with Nikon's A1+ confocal laser microscope system.

In the case of TMEM16A overexpression, the staining procedure was similar to the one described above; the pieces were incubated with a mixture of AlexaFluor 488 a-rabbit secondary antibody and DAPI.

vWF antibodies were labelled with Mix-n-Stain™ CF™ 633 Antibody Labeling Kit according to the manufacturer's instructions.

Human PAECs

Cells were seeded onto gelatine-coated chamber slides and formalin-fixed. After blocking with 5 % BSA, the cells were incubated overnight at 4 °C with antibodies against Von Willebrand factor and TMEM16A. On the following day, the cells were washed, then labelled with Alexa Fluor 555 a-rabbit and Alexa Fluor 647 a-mouse secondary antibodies for 1 h at RT. Finally, the slides were preserved using a mounting medium containing DAPI and imaged with Nikon's A1+ confocal laser microscope system. Duplicates were processed either without the primary antibody or with the primary antibody against TMEM16A pre-incubated with the immunogen peptide as negative controls.

For the labelling of TMEM16A-overexpressing human PAECs, cells were infected with a MOI 50 as described above. 72 h after adenoviral infection, the cells were fixed with 4 % paraformaldehyde. The following staining protocol was similar as described above; the slides were incubated with Alexa Fluor 647 a-rabbit secondary antibody and imaged with Nikon's A1+ confocal laser microscope system.

Further information regarding antibodies and materials can be found in Table S4 and Table S6 respectively.

3.6. Analysis of protein expression

For the analysis of total protein, cells were lysed in CHAPS[2] buffer and analysed with Western blot. Alternatively, pieces of healthy human lung tissue were collected in CHAPS[2] buffer followed by homogenization with beads and MagNA Lyser instrument or sonication respectively. After centrifugation (13.000 g, 10 min), the protein concentration of the supernatant was determined with Pierce BCA Protein Assay Kit according to the manufacturer's instruction. A specific amount of protein from each sample was mixed with 10x Loading buffer and run on 8 or 15 % SDS-polyacrylamide gels, followed by electro transfer to a nitrocellulose membrane. After blocking the membrane with 5 % BSA in TBS-T, the membrane was probed with one of the following antibodies: TMEM16A, pp38, p38, pERK, ERK, pAkt,, pAkt, tAKT, pSAPK/JNK, SAPK/JNK, PCNA, Cl. PARP, Cyclin D1, eNOS, LC3B, pSer1177 eNOS or pThr495 eNOS. Afterwards the membrane was incubated with horseradish peroxidase conjugated secondary antibody and the final detection of the proteins was performed using a SuperSignal West Femto, ECL prime or ECL

Start Kit and a ChemiDocTM Touch Imaging System. As housekeeping genes B-Actin or Vinculin were used.

For testing the effect of TMEM16A-overexpression on eNOS phosphorylation, 48 h after adenoviral infection, the cells were 2 h serum-starved and stimulated with 5 µM acetylcholine (ACh). Protein was collected at 0, 5, 15, 30 and 60 min post stimulation.

For testing the effect of reduced Cl^- on eNOS phosphorylation, the cells were incubated for 24 h with either Ringer´s solution containing physiological [Cl^-] or solution with KCl and NaCl exchanged with potassium and sodium gluconate to half the amount respectively (([Cl^-] was reduced from 129.5 to 67.25 mM). After 2 h serum starvation, the rest of the protocol was performed as described above.

Further information regarding used antibodies, solutions and materials can be found in Table S4Table S5Table S6 respectively.

3.7. Measurement of whole-cell Ca^{2+}-activated Cl^- current (I_{ClCa})

Whole cell Ca^{2+}-activated Cl^- current was measured as reported previously. (57) Briefly, donor or IPAH PAECs grown on gelatine-coated dishes were harvested with StemPro Accutase, centrifuged (300 g, 10 min), resuspended in complete medium and incubated at 37 °C for 15 min to allow them to attach before measurements. In the case of adenoviral manipulation of TMEM16A expression, cells were incubated with $Ano1^{Ad}$ or its control $Ctrl^{Ad}$ at MOI 50 as described above (see Overexpression of TMEM16A) and used after 48 h.

The cells were incubated in bath solution I until the formation of whole-cell configuration. Once the amplitude of TMEM16A current was stable, the cells were perfused with bath solution II, containing TEA-Cl to minimize K^+ current contamination, and vehicle or benzbromarone (Bbr). In order to measure I_{ClCa}, the command potential was stepped from a 0 mV holding potential to -40, 0, +40, +80 and +120 mV for 1.5 s, allowing 0.5 s recovery time at the holding potential between each step. The average current measured between 1000 and 1500 ms of each voltage step was plotted against the holding potential. Due to the almost symmetrical Cl^- concentration of the bath and pipette solutions, the reversal potential (E_{rev}) for Cl^- was expected to be around zero.

Measurements of Ani9 efficacy were performed by our collaborators at the group of Prof. Dr. Péter Enyedi, Semmelweis University, Budapest. HEK293T cells were kept at a holding potential of -60 mV. TMEM16A currents were measured at the end of 600 ms voltage steps (applied every 4 s) to -100, -60, -20, +20, +60 and +100 mV. Once the amplitude of the TMEM16A current was stable (the TMEM16A current gradually increased after the whole cell configuration was achieved due to the diffusion of the calcium from the pipette solution to the cytoplasm), 1 μM Ani9 was applied to bath solution.

Patch pipettes were pulled from thick-walled borosilicate glass by a P-87 puller (Sutter Instrument Co., Novato, CA, USA) and fire polished. Pipettes were filled with pipette solution (pipette resistance was between 3-5 MΩ) and connected to the headstage of an Axopatch-1D patch clamp amplifier (Axon Instruments, Inc., Foster City, CA, USA). Cut-off frequency of the eight-pole Bessel filter was adjusted to 200 Hz, data were acquired at 2 kHz. Experiments were carried out at RT (21 °C). Solutions were applied using a gravity-driven perfusion system. Data were digitally sampled by Digidata 1550B (Axon Instruments, Inc.) and analysed by pCLAMP 10 software.

Further information regarding used solutions and materials can be found in Tables Table S5 and Table S6 respectively.

3.8. Live cell Ca^{2+} imaging

Live cell Ca^{2+}-imaging was done as previously reported (351). Human PAECs or PASMCs were seeded on 25 mm glass coverslips and infected with a viral solution of $Ano1^{Ad}$ or $Ctrl^{Ad}$ at MOI 50. 48 h after adenoviral infection, the cells were loaded with 2 μM Fura-2-acetoxymethyl ester (Fura-2AM) for 45 min at 37 °C. The single glass cover slip was mounted on the stage of a Zeiss 200 M inverted epifluorescence microscope coupled to a PolyChrome V monochromator (Till Photonics, Germany) light source in a sealed temperature-controlled RC-21B imaging chamber (Warner Instruments, USA). Fluorescence images were obtained every 3 s with alternate excitation at 340 and 380 nm and the emitted light collected at 510 nm by an air-cooled Andor Ixon camera (Andor Technology, Ireland). Background fluorescence was recorded from each cover slip and subtracted before calculation. The acquired images were stored and processed offline with TillVision software (Till Photonics, Germany).

All solutions were prewarmed to 30 °C and cells were stimulated with a 15 µM selective SERCA blocker 2,5-Di-t-butyl-1,4-benzohydroquinone (BHQ) in the presence and absence of extracellular Ca^{2+}. Maximal and minimal ratio values were determined at the end of each experiment by treating the cells with 5 µM ionomycin (maximal ratio) followed by 20 mM EGTA-mediated chelation of all free Ca^{2+} (minimal ratio). Cells that did not respond to ionomycin were discarded. The basal Ca^{2+} levels were determined as an average of initial 50 s and $[Ca^{2+}]_i$ was calculated as previously described (352). BHQ-induced Ca^{2+} peak and Ca^{2+} response following Ca^{2+} readmission were calculated as the maximal peak height subtracting the baseline.

Further information regarding solutions and materials can be found in Table S5 and Table S6 respectively.

3.9. DAF-DM mediated nitric oxide measurement

PAECs were seeded in gelatine-coated dark 96-well plates and treated either with TMEM16A-overexpressing adenovirus or Ringer´s solution with reduced Cl^-.

In the case of adenovirus, following infection at MOI 50 and 48 h of overexpression, the cells were starved for 2 h with Ringer´s solution and loaded with 10 µM 4-Amino-5-Methylamino-2',7'-Difluorofluorescein Diacetate (DAF-FM) for 30 min at 37 °C. The cells were stimulated with 5 µM ACh for 20 min followed by measurement on CLARIOstar Plus (BMG Labtech, Germany) at Ex/Em = 495/515 nm. All the assays were performed in quadruplicate and normalized to protein content.

Further information regarding solutions and materials can be found in Table S5 and Table S6 respectively.

3.10. Wound healing assay

Human PAECs or PASMCs were seeded in 2 well culture-inserts (Ibidi, Germany) and infected with either $Ano1^{Ad}$ or $Ctrl^{Ad}$ at MOI 50. Following overnight starvation and altogether 48 h of TMEM16A overexpression, the inserts were removed to create a gap of approximately 500 µm and the cells were immersed in a complete medium. The closing gaps were photographed at 4x

magnification (Olympus CKX41) at 0, 12, 24, 36 and 48 h after removal of the inserts and the photos quantitatively assessed comparing the initial gap with the area of the healing wound using image analysing software (ImageJ 1.46r).

Further information regarding solutions and materials can be found in Table S6.

3.11. Pulmonary arterial isometric tension measurements

All animal studies were approved by the Austrian Ministry of Education, Science and Culture under the license number BMWFW-66.010/0043-WF/V/3b/2016. 10-12 week-old wild-type male mice were sacrificed by cervical dislocation and lungs collected for pulmonary artery (PA) isolation. Using stereo zoom microscope SZX7 (Olympus, Tokyo, Japan) second order PAs of 4 mm in length were isolated and cut in half. One half was always used for a vehicle control. Alternatively, human PAs (4 mm), isolated from human lung tissue obtained from Vienna (976/2010), were isolated, cut in half and incubated with either $Ano1^{Ad}$ or $Ctrl^{Ad}$ for 24 h, after which the solution was exchanged for VascuLife SMC medium without any growth factors or FCS (LifeLine Cell Technology) for a further 24 h.

In both cases the isolated PAs were mounted on the wire myography system (Danish Myo Technology 620M, Aarhus, Denmark) with the help of tungsten wires. Afterwards the PAs were equilibrated for 30 min in physiological salt solution (PSS; pH 7.4, 100 % oxygen, 37 °C) followed by an increase of basal tension to 2 mN and stabilization for further 30 min. The vessel viability was tested with 3 sequential steps of depolarization, PSS with 120 mM KCl (KPSS; isotonic replacement of NaCl by KCl) each lasting 15 min. The vessels with mean KPSS response below 2 mN were discarded. The effect of vasoactive agents (high potassium chloride, thromboxane analog U44619 (300 nM), L-NAME (300 µM), benzbromarone Bbr (0.1-30 µM) or acetylcholineACh (0.1-30 µM)) was tested by directly adding the agents into the chamber and the differences were measured between the vessels incubated with the substances or vehicle, or in the case of human PAs between TMEM16A-overexpressing Ano1Ad or CtrlAd expressing vessels.

The myography chambers were connected to force transducer units for isometric measurements (PowerLab, ADInstrument, Oxford, UK). The vasorelaxation was calculated as percentage (% relaxation) of the contraction induced by 300 nM U46619.

Further information regarding solutions and materials can be found in Tables Table S5 and Table S6 respectively.

3.12. Measuring cell metabolic state

The Agilent Seahorse XFp setup (Agilent, USA) was used to assess the mitochondrial and glycolytic function of primary human PAECs or PASMCs. 20.000 cells were seeded into 8-well plates and infected with either Ano^{Ad} or $Ctrl^{Ad}$ and incubated for 24 h. 48 h after adenoviral infection, Seahorse XFp Cell Mito Stress and Glycolysis Stress Test Kits were used according to the manufacturer´s instructions. Briefly, with the use of Oligomycin, Rotenone and Rotenone/Antimycin A, the mitochondrial state can be assessed. Altermatively, with the use of Glucose, Oligomycin and 2-Deoxy-D-glucose glycolytic function can be assessed. All the assays were performed in triplicate and normalized to protein content.

Further information regarding materials can be found in Table S6.

3.13. Matrigel tube-formation assay

To test endothelial cell angiogenic potential, Matrigel tube formation assay was used (Merck Millipore). 200.000 cells were seeded in a gelatine-covered 6-well plate and infected with either $Ano1^{Ad}$ or $Ctrl^{Ad}$ at MOI 50 and incubated for 24 h. Following overnight starvation and 48 h after adenoviral infection, the cells were trypsinized, counted and 50.000 cells per 96-well plate were seeded onto prepared matrigel in triplicate according to the manufacturer’s instructions. After 6 h of incubation period at 37 °C, the tubular networks were photographed at 4x magnification (Olympus CKX41) and photos quantitatively assessed comparing the number of branching points using image analysing software (ImageJ 1.46r).

Further information regarding materials can be found in Table S6.

3.14. Assessment of cell proliferation *in vitro*

To study the influence of TMEM16A on human PAEC proliferation, 10.000 cells per well were seeded in 96-well plates and infected with either $Ano1^{Ad}$ or $Ctrl^{Ad}$ at MOI 50. After 24 h the medium was replaced by fresh complete medium and the cells serum-starved overnight. On the following day the cell medium was replaced by fresh starvation medium with added ^{3}H-thymidine. The proliferation was determined after 24 h [^{3}H]-thymidine incorporation (BIOTREND Chemikalien GmbH, Cologne, Germany) and altogether 72 h after adenoviral infection as an index of DNA synthesis, and detected with a scintillation counter (Wallac 1450 MicroBeta TriLux Liquid Scintillation Counter & Luminometer, PerkinElmer, Waltham MA, USA). Each independent experiment was performed in quintuplicate.

Further information regarding materials can be found in Table S6.

3.15. Assessment of cell resting membrane potential *in vitro*

To study the influence of TMEM16A on human PAEC resting membrane potential, 80.000 cells per well in a 6-well plate were seeded and transfected with either $Ctrl^{Ad}$ or $Ano1^{Ad}$ at MOI 50. After 24 h the medium was replaced by fresh complete medium and the cells were serum-starved overnight. 48 h after adenoviral infection, the medium was replaced with starvation medium supplemented with 10 µM $DiBAC_4(3)$ dye for 30 min at 37 °C after which the cells were collected with cell-scratcher in PSS. Fluorescence Signal Intensity was measured on CytoFLEX S flow cytometer (Beckman Coulter, USA) at Ex/Em=490/516 nm.

Further information regarding solutions and materials can be found in Table S5 and Table S6 respectively.

3.16. Assessment of cell Cas3/Cas7 activation *in vitro*

To study the influence of TMEM16A on Cas3/Cas7 activation, we seeded 150.000 PAECs or PASMCs per well in a 6-well plate and transfected the next day with either $Ctrl^{Ad}$ or $Ano1^{Ad}$ at MOI 50. After 24 h the medium was replaced by fresh complete medium and the cells serum-starved overnight. The next day the medium was exchanged by fresh starvation medium. As a positive

control, we incubated the cells with 10 µM Staurosporin (STS) for 24 h. 72 h after adenoviral infection, CellEvent™ Caspase-3/7 Green Detection Reagent was used according to the manufacturer's instruction. The fluorescent signal shift was measured with CytoFLEX S flow cytometer (Beckman Coulter, USA) at Ex/Em = 503/530 nm.

Further information regarding solutions and materials can be found in Table S6.

3.17. Cell-cycle analysis

To study the effect of TMEM16A overexpression on cell cycle progression of primary human PAECs or PASMCs we seeded 200.000 cells per well in a 6-well plate and transfected with either $Ctrl^{Ad}$ or $Ano1^{Ad}$ at MOI 50. After 24 h the medium was replaced by fresh complete medium and the cells serum-starved overnight. The next day the medium was exchanged by fresh starvation medium for further 24 h. 72 h after adenoviral infection, the cells were trypsinized, resuspended in PBS, then transferred into cold EtOH under continuous vortexing and incubated at 4 °C for at least 30 min. After washing using PBS supplemented with 0,5 % FCS, the cell pellet was resuspended in a solution containing 1 µg/mL DAPI and 0,1 % Triton x-100 in PBS and incubated at RT for 10 min, then transferred on ice until measurements were done. Fluorescence Signal Intensity was measured on CytoFLEX LX flow cytometer (Beckman Coulter, USA) at Ex/Em = 3 55/461 (bandpass filter 450/45). The data was analysed using ModFit software.

Further information regarding solutions and materials can be found in Table S6.

3.18. qRT-PCR

qRT-PCR was performed as described previously. (57) Briefly, PAECs were grown until confluence and serum-starved overnight. RNA was collected using the PeqGOLD Total RNA kit (PeqLab, Erlangen, Germany) and transcribed into cDNA with the iScript reagent mix (Bio-Rad, Hercules CA, USA). To assess *ANO1* expression, exon-exon junction spanning primers targeting the boundaries of exons 1 and 2 were acquired from Eurofins, Graz, Austria (see supplementary table S3). The primers covered the region without reported alternative splicing, therefore they amplified all splice variants. qRT-PCR was performed using Blue S'Green qPCR Kit.

Further information regarding primer sequences and materials can be found in Table S3 and Table S6 respectively.

3.19. Isolated perfused and ventilated rat lung (IPL)

Male Sprague-Dewley rats weighing 200-300 g were anesthetized with intraperitoneal injection of Ketamine/Xylazine followed by 600 µL of a 5000 U/mL heparin stock 5 min after narcosis. A tracheotomy was performed and mechanical ventilation was applied at a tidal volume of approximatey 12.4 ml/kg b.w., an end-expiratory pressure of -2 cm H2O and a respiratory rate of 60 breaths/min. Hyperinflation (-20 cmH2O) was performed at 1 min intervals. After a sternotomy, right ventricle was used to catheterize the pulmonary artery and another catheter was inserted into the left atrium through the left ventricle and both fixed with a ligature. The lungs were perfused with 37 °C sterile Krebs-Henseleit buffer supplemented with 2 % bovine serum albumin and mean pulmonary arterial pressure (PAP) was continuously monitored and expressed in cmH2O. After an initial steady-state of 20 min with the flow of 10 mL/min, we preconstricted the pulmonary vasculature with 20 nM U46619, followed by the increasing concentrations of Ani9. Results were summarized as % vasorelaxation compared to the baseline obtained after U46619 pre-constriction.

Further information regarding primer sequences and materials can be found in Table S6.

3.20. Statistical analysis

Data is shown either as individual data plots with median, as mean ± s.e.m or as floating bars plot (min-to-max). In all cases, n numbers are representing number of replicates, N numbers are representing number of patients. Numbers are given in the corresponding figure legend. Statistical analyses were performed using Prism 8.0 (GraphPad Software, La Jolla, CA, USA) and are identified in the corresponding figure legend. All datasets met the assumptions of the statistical test used, statistical analyses were two-sided and p values < 0.05 were considered significant.

4. Results

4.1. TMEM16A maintains pulmonary endothelial homeostasis

To understand how Cl^- conductivity would be placed in the pathological cascade defining IPAH endothelium, I aimed to look at Ca^{2+}-activated Cl^-channel TMEM16A in the pulmonary arteries. As a first step I investigated TMEM16A levels in various pulmonary compartments, i.e. in human lung homogenate (hLH), primary human pulmonary arterial endothelial cells (PAECs) and primary human pulmonary arterial smooth muscle cells (PASMCs). By using western blot analysis, I could show that TMEM16A is expressed in the human lung tissue and is enriched in the pulmonary vascular bed (**Figure 1a**). Similarly I used quantitative PCR to look at mRNA level of TMEM16A in PAECs and PASMCs and could show an enrichment in PAECs (**Figure 1b**).

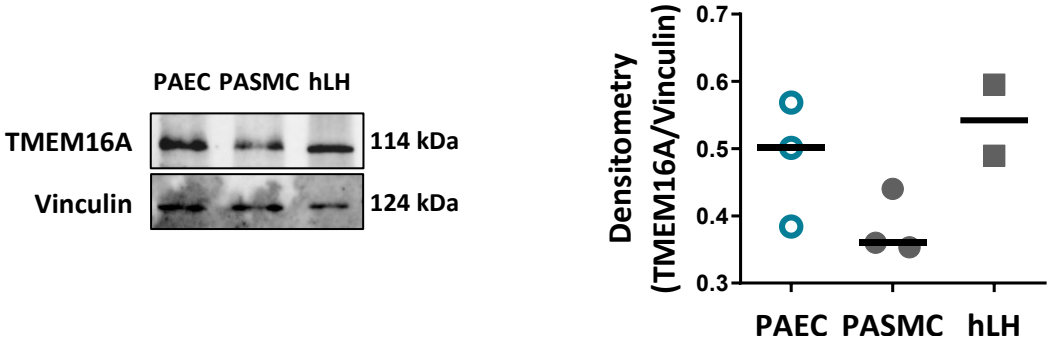

(**a**)

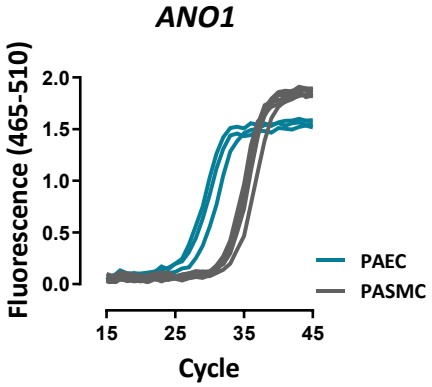

(**b**)

Figure 1. TMEM16A expression in donor PAECs, PASMCs and human lung homogenate. (a) Western blot showing TMEM16A expression in donor PAECs, pulmonary arterial smooth muscle cells (PASMCs) and human lung homogenate (hLH) (N = 2-3 patients). Vinculin served as loading control. (b) Gene expression of ANO1 in donor PAECs and PASMCs. (Reproduced from (1) in accordance with the MDPI and the CC BY 4.0 license).

In continuation, I looked for a specific TMEM16A inhibitor that would enable me to specify TMEM16A-associated I_{ClCa} and its effect on physiology. Several inhibitors of TMEM16A have been described before. Among others, Ani9 was reported as a selective TMEM16A inhibitor of submicromolar potency with no modulation of intracellular Ca^{2+} signalling nor CFTR activity. I introduced Ani9 was implemented into several investigations assessing its efficacy in inhibiting TMEM16A-associated Ca^{2+}-activated Cl^- current, mitigating vasodilation of *ex vivo* mouse pulmonary arteries (PAs) and by following its effect on mPAP of *ex vivo* isolated and perfused rat lung (IPL). First, to investigate the inhibitory potential of Ani9, TMEM16A-overexpressing plasmid was introduced into HEK293T cells and highly increased Ca^{2+}-activated Cl^- current (I_{ClCa}) was observed. Ani9 successfully reduced the current by approximately 87 % showing much promise for the following investigations (**Figure 2**).

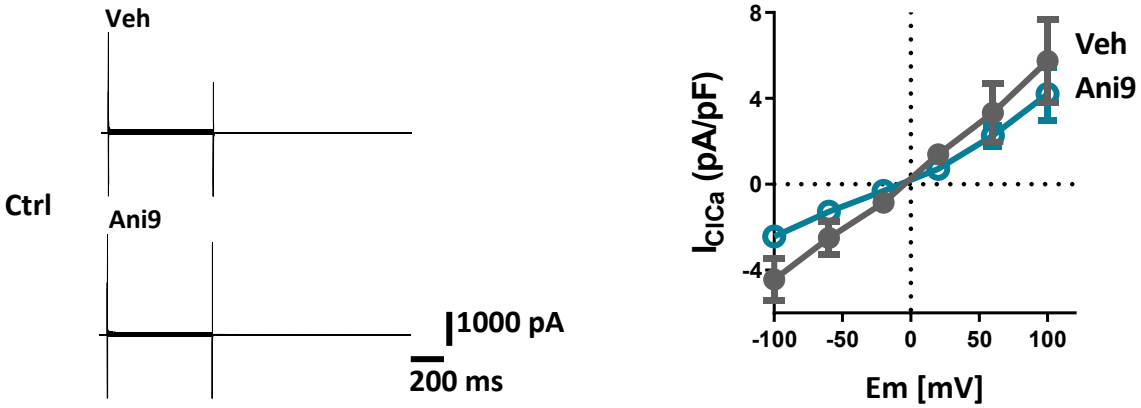

(**a**)

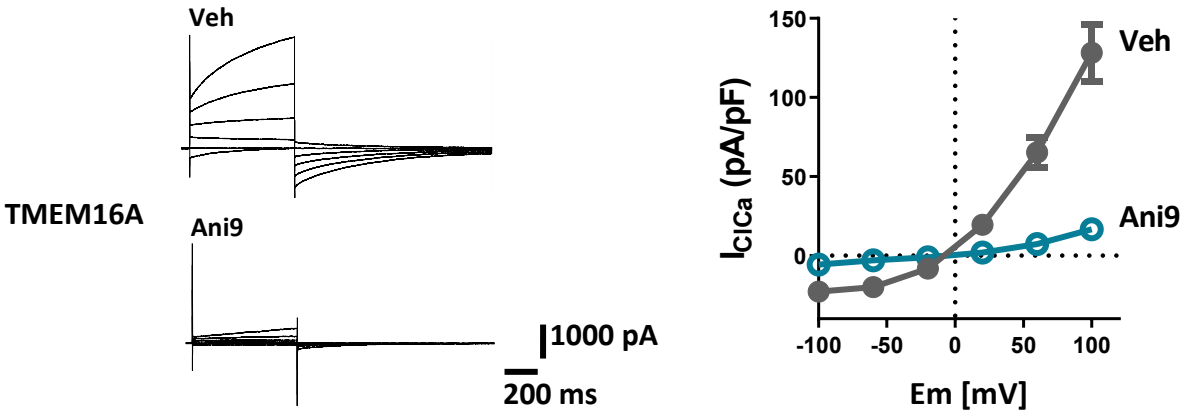

(**b**)

Figure 2. The efficacy of Ani9 in inhibition of TMEM16A-associated I_{ClCa}. Representative whole-cell Ca^{2+}-activated Cl^- current (I_{ClCa}) traces (left) and normalized current-voltage (I-V) relationships measured with voltage clamp in TMEM16A-overexpressing HEK293T cells showing the effect of 1 μM Ani9 (right). Figure was generated with n = 5 cells. (The patch-clamp investigations were carried out with the support from the group of Prof. Péter Enyedi, Semmelweis University, Budapest).

To explore the physiological relevance of Ani9 *ex vivo*, I used two separate models (**Figure 3a-b**). First, using isometric tone measurements the effect of Ani9 was investigated. Increasing dose of Ani9 led to a step step-wise relaxation of U46619 pre-constricted rat PAs up to approximately 40 % (**Figure 3a**). In the *ex vivo* rat IPL model, increasing dose of Ani9 resulted in a step-wise mPAP reduction in U46619 pre-constricted lung up to approximately 50 % (**Figure 3b**). Even though Ani9 proved to be a potent inhibitor of I_{ClCa}, it ultimately did not reach the *ex vivo* efficacy of another previously reported other strong inhibitor of TMEM16A benzbromarone (Bbr).

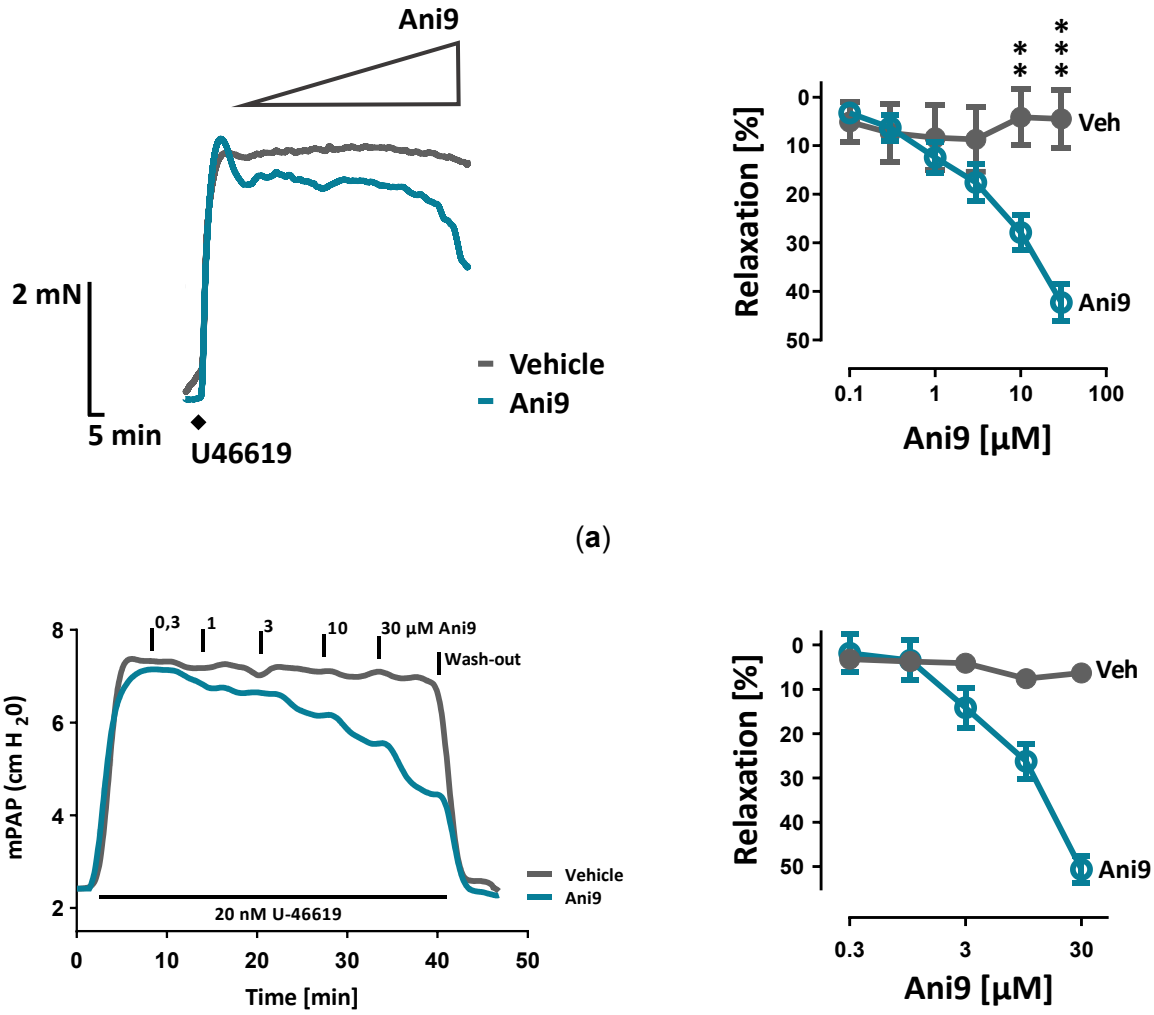

Figure 3. Ani9-mediated vasorelaxation. (a) Ani9-induced vasorelaxation of U46619 pre-constricted rat pulmonary arteries. Figure was generated with 5-9 vessels in each group taken from 3 rats. ** $p < 0.01$, *** $p < 0.001$, two-way ANOVA with Bonferroni post-hoc test. (b) Representative graph showing the effect of Ani9 on mPAP of isolated and perfused rat lung preconstricted with U46619 (left) and the quantification plotted as % of relaxation (right). Figure was generated with n = 3 rats in the groups perfused with Ani9 and n = 1 in the group perfused with vehicle (DMSO). ((a) was performed by Neha Sharma, Medical University of Graz)

Thus, in continuation of the project I used Bbr as a tool in dissecting TMEM16A-conducted I_{ClCa}. By employing whole-cell voltage clamp, I isolated Ca^{2+}-activated Cl^- current in primary human PAECs and primary human PASMCs (**Figure 4a-b**). In PAECs I could define higher I_{ClCa} which was further supported by significantly increased Bbr-mediated inhibition (**Figure 4c**). These data suggests that TMEM16A activity is bigger in pulmonary vascular endothelium in comparison to the vascular smooth muscle cell layer and that Bbr is a potent inhibitor of TMEM16A in the pulmonary vascular compartment.

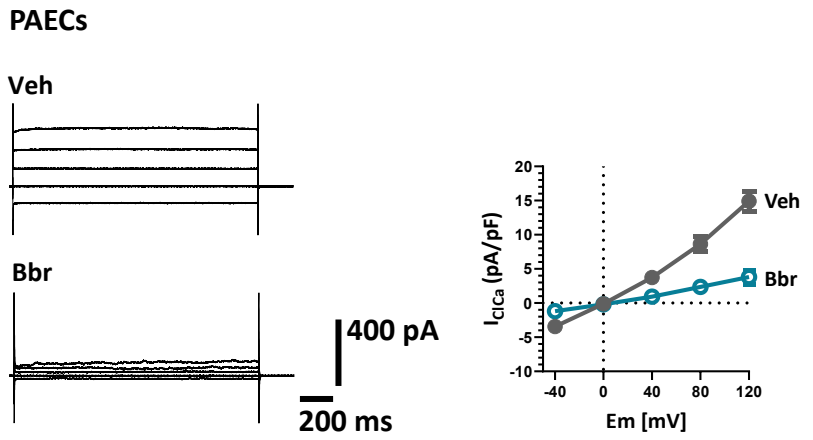

(**a**)

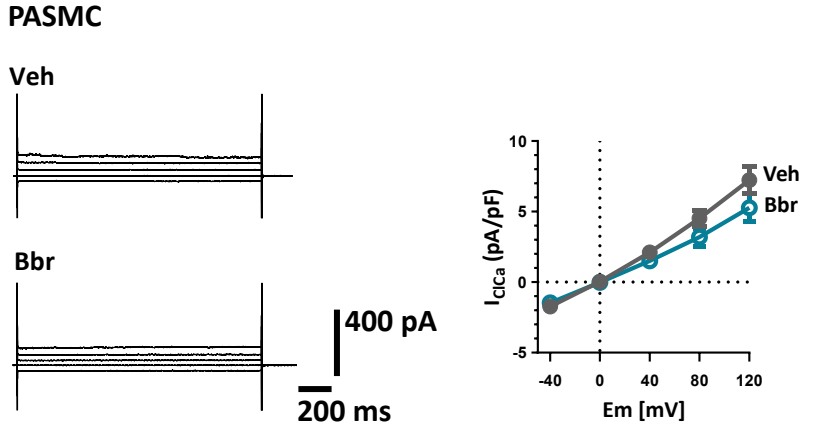

(**b**)

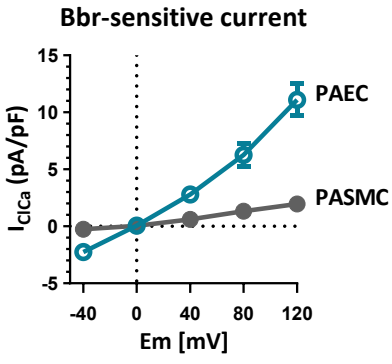

(**c**)

Figure 4. TMEM16A defines calcium-activated chloride current in pulmonary arterial endothelial cells. (a-b) Representative whole-cell Ca^{2+}-activated Cl^- current (I_{ClCa}) traces (left) and normalized current-voltage (I-V) relationships measured with voltage clamp in PAECs (a) and PASMCs (b) showing the effect of benzbromarone (Bbr) (right). c) Calculated Bbr-sensitive current in donor PAECs and PASMCs. Figures were generated with n = 5-13 cells from healthy donors. (Reproduced from (1) in accordance with the MDPI and the CC BY 4.0 license).

To further establish the importance of endothelial TMEM16A in maintaining vascular tone, isometric tension measurements of isolated mouse PAs were used and the effect of Bbr on the vascular tone *ex vivo was* investigated. In comparison to Ani9, Bbr mediated step-wise relaxation of U46619 pre-constricted PAs up to approximately 87 % (**Figure 5a-b**). Upon deliberate removal of the endothelial layer, I could observe a slight yet significant shift in the relaxation (**Figure 5a**), demonstrating that PA endothelium might play a role in mediating TMEM16A-associated relaxation through Bbr activity. Furthermore, by incubating PAs in Nω-Nitro-L-arginine methyl ester hydrochloride (L-NAME), a potent and specific inhibitor of eNOS, the measured relaxation of PAs was shifted even further (**Figure 5b**), demonstrating that TMEM16A modulation of pulmonary vascular tone goes, at least to some degree, through eNOS and therefore endothelial NO production.

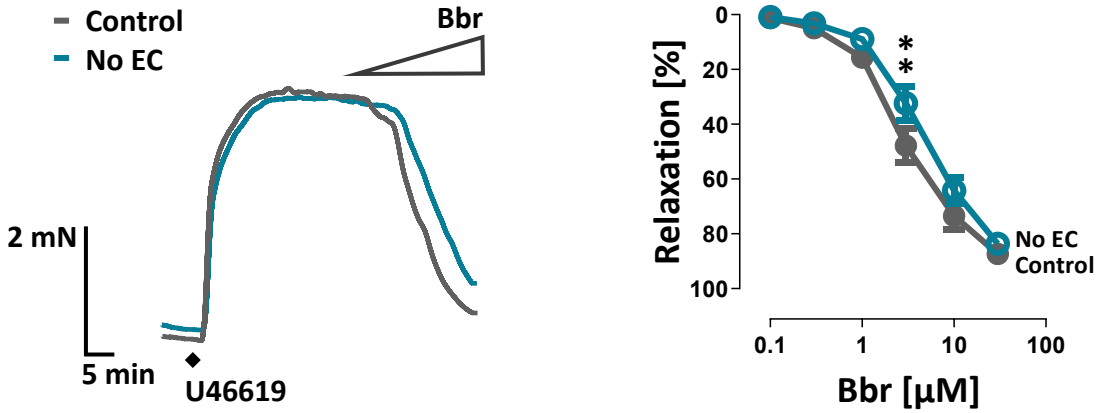

(**a**)

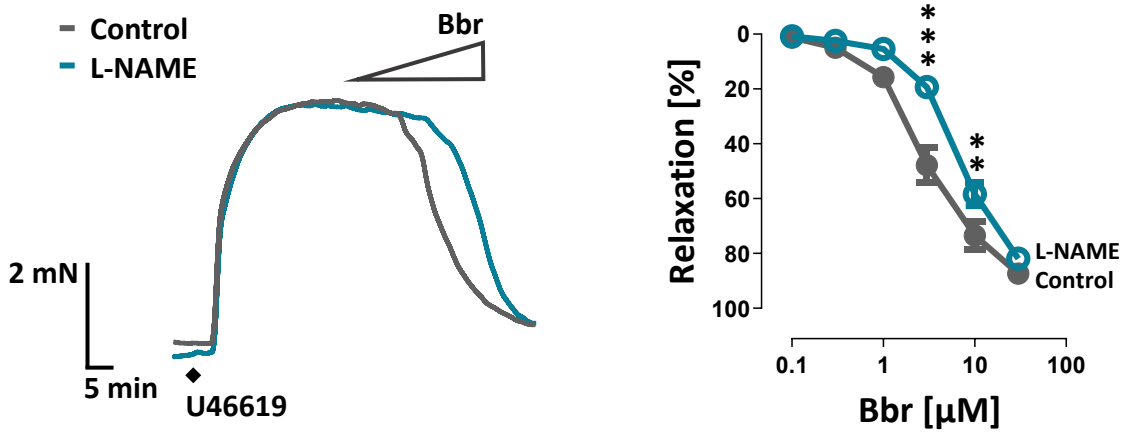

(**b**)

Figure 5. The role of endothelium in Bbr-mediated vasorelaxation. (a-b) Representative isometric tension measurements of Bbr-mediated vasorelaxation of U46619 pre-constricted mouse pulmonary arteries (left) showing endothelial contribution of Bbr effectiveness (right) with either endothelium removed (no EC; a) or incubation with L-NAME (b) (n = 4-7). ** $p < 0.01$, *** $p < 0.001$, **** $p < 0.0001$, two-way ANOVA with Bonferroni post-hoc test. (Obtained with the help from Neha Sharma, Medical University of Graz; reproduced from (1) in accordance with the MDPI and the CC BY 4.0 license).

4.2. IPAH PAECs are hallmarked by increased TMEM16A activity

Cl^- channels are prominent mediators of EC homeostasis. Their activity influences not only the electrophysiological properties of EC but Cl^- anions function as an important second messengers as well. TMEM16A represents the most recognized Ca^{2+}-activated Cl^- channel. I have demonstrated that its pharmacological inhibition affects the endothelial homeostasis and it has been shown before that its expression in idiopathic pulmonary arterial hypertension (IPAH) PAECs is increased. Therefore in the continuation of the project I studied the link between established IPAH endothelial dysfunction and the role of TMEM16A in this cascade. First, the localization of TMEM16A expression was investigated (**Figure 6a-c and Figure 7a-d**) in 3D precision-cut lung

slices (**Figure 6a**), lung sections (**Figure 6b**) and PAECs (**Figure 6c**) isolated from donor and IPAH patients. I could confirm the presence of TMEM16A in vWF^{+} cells, a marker of endothelium.

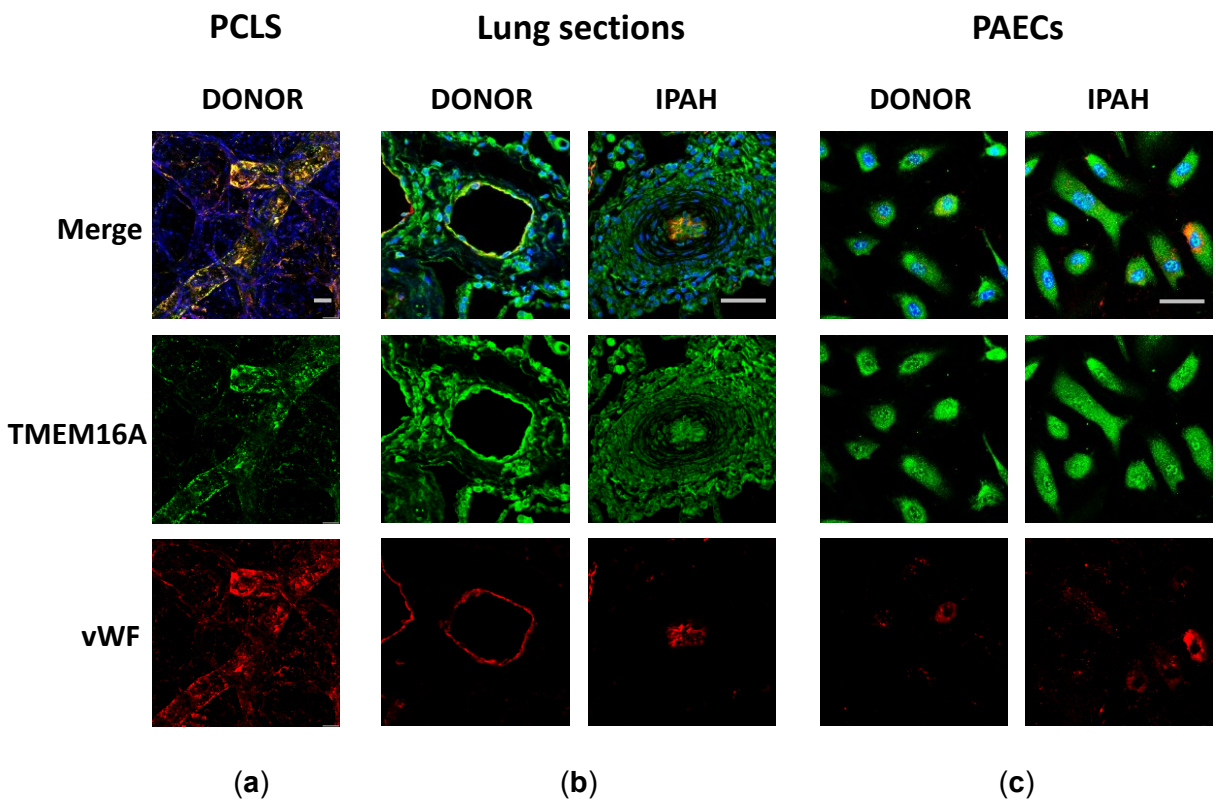

Figure 6. Localization of TMEM16A in the lung. Immunofluorescence staining of (a) 3D precision cut lung slices (PCLS), (b) lung sections and (c) PAECs obtained from healthy donor lungs and patients suffering from IPAH (BP=antibody blocking peptide, scale bar = 50 µm for PCLS, 50 µm for PAECs and 50 µm for lung sections). (PCLS results were obtained with the support from Diana Zabini, PhD, Medical University of Graz; reproduced from (1) in accordance with the MDPI and the CC BY 4.0 license).

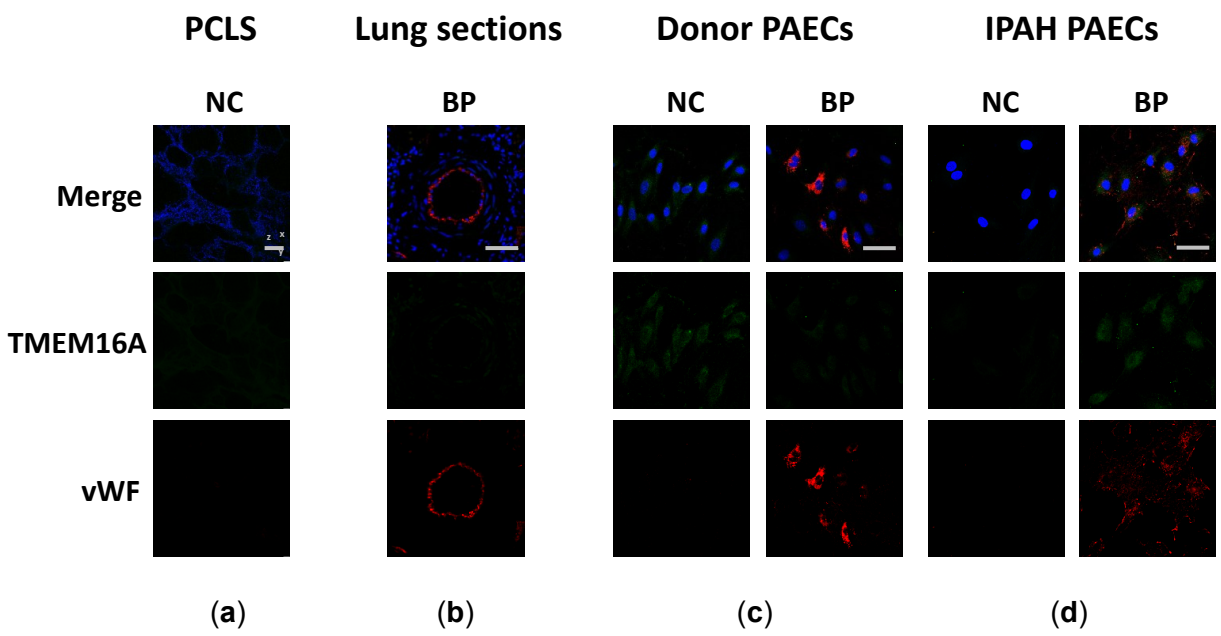

Figure 7. Control immunofluorescence staining of TMEM16A in PAECs. Control staining for detection of TMEM16A in PAECs. Immunofluorescence staining of 3D precision cut lung slices. (a) PCLS, (b) lung sections and (c) PAECs obtained from healthy donor lungs and (d) patients suffering from IPAH (BP=antibody blocking peptide, scale bar = 50 µm for PCLS, 50 µm for PAECs and 50 µm for lung sections). (PCLS staining and imaging was performed by dr. Diana Zabini, Medical University of Graz; reproduced from (1) in accordance with the MDPI and the CC BY 4.0 license).

Additionally I performed western blot analysis of donor and IPAH PAECs and showed that while in whole-cell protein, the level of TMEM16A at 114 kDa remains unchanged, there seems to be a staggering increase at approximately 80 kDa (**Figure 8**).

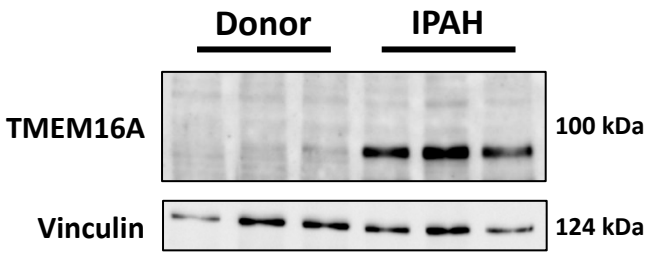

Figure 8. The expression of TMEM16A in PAECs isolated from IPAH patients. Western blot comparing TMEM16A expression in donor and IPAH PAECs. Figure was generated with N = 3 samples for both groups. (Reproduced from (1) in accordance with the MDPI and the CC BY 4.0 license).

It is possible that the product of 80 kDa belongs to an isoform of TMEM16A, since an isoform of this size was confirmed before in mouse and rat samples and was additionally predicted to be expressed in human as well. Thus the detected isoform could represent an IPAH-associated pathologically-relevant isoform. Finally, using whole-cell voltage clamp I was able to confirm increased I_{ClCa} corresponding to TMEM16A in IPAH PAECs (**Figure 9a**) supported by increased Bbr-mediated inhibition in these cells (**Figure 9b**).

Increased activity of TMEM16A could therefore represent the basis for endothelial dysfunction described in IPAH PAECs.

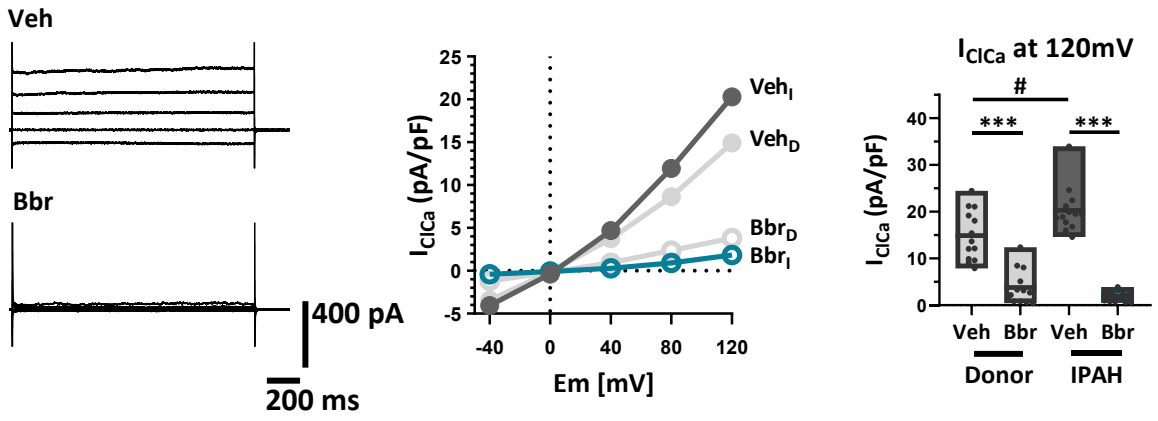

Figure 9. Increased I_{ClCa} in PAECs isolated from IPAH patients. (a) The effect of Bbr on representative whole-cell I_{ClCa} traces (left) and normalized current-voltage relationships (right) measured with voltage-clamp in donor and IPAH PAECs (Veh_I/Bbr_I = IPAH PAECs perfused with vehicle or Bbr; Veh_D/Bbr_D = donor PAECs perfused with vehicle or Bbr). (b) Comparison of the Ca^{2+}-activated Cl^- current density of donor and IPAH PAECs at 120 mV. Figures were generated with n = 12-13 cells from at least N = 4 patient samples. # $p < 0.01$, *** $p < 0.0001$, ANOVA with Bonferroni post-hoc test. (Reproduced from (1) in accordance with the MDPI and the CC BY 4.0 license).

4.3. TMEM16A overexpression-associated model of IPAH demonstrates endothelial dysfunction

To delineate the nature of endothelial dysfunction TMEM16A overactivity could cause, I acquired adenoviral vectors overexpressing full length TMEM16A (**Figure 10a**) and its control (**Figure 10b**). I infected human primary PAECs and followed the efficacy of infection by measuring mCherry fluorescence (**Figure 11a**). Using FACS analysis I tested different conditions of infection and could set the proper conditions of multiplicity of infection (MOI) to 50 and 72 h after adenoviral infection more than 90 % of the cells were $mCherry^+$ (**Figure 11b**).

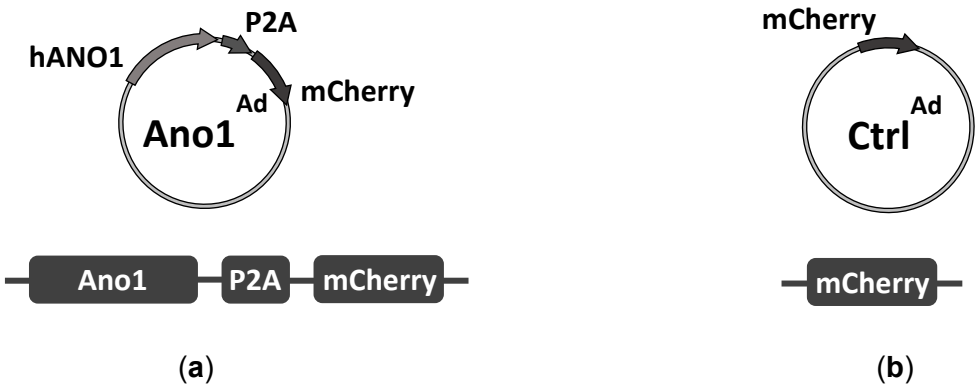

Figure 10. TMEM16A-overexpressing adenovirus and control. Two adenoviruses were acquired from Vectorbuilder Inc. (a) Ano1^{Ad} and (b) Ctrl^{Ad} expressing either mCherry connected to Ano1 via a self-cleaving peptide P2A or only mCherry respectively. (Reproduced from (1) in accordance with the MDPI and the CC BY 4.0 license).

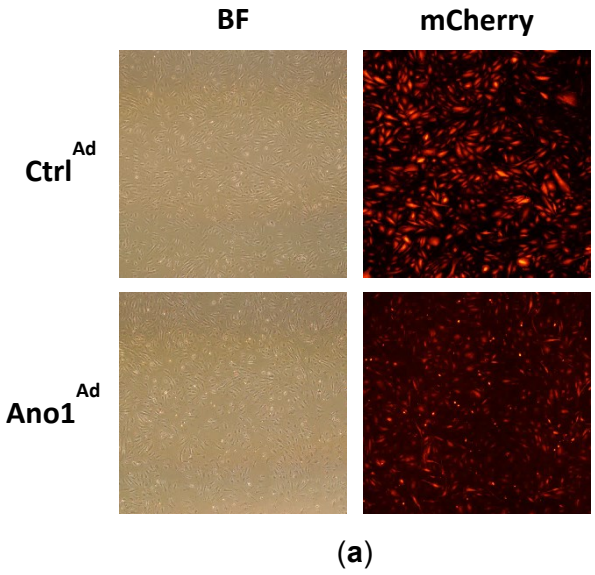

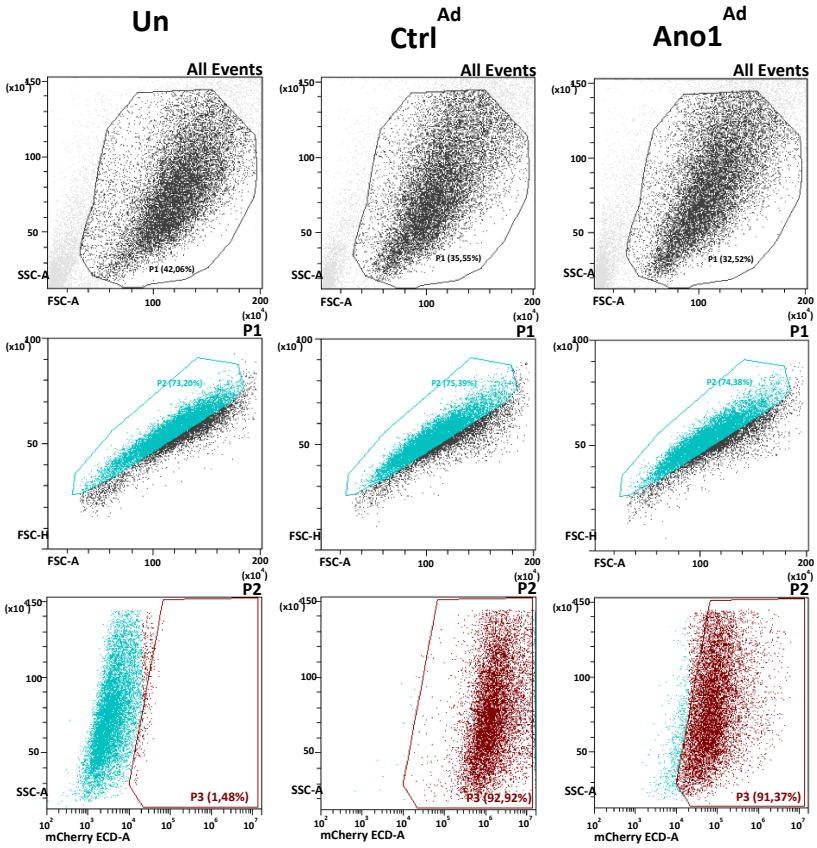

(**b**)

Figure 11. Adenoviral infection was followed by mCherry fluorescence. mCherry was chosen for the possibility of tracing the efficiency of the infection, seen here as (a) bright field (BF) and mCherry fluorescence pictures of primary PAECs 72 h after adenoviral infection (scale bar = 200 µm). (b) 72 h after adenoviral infection more than 90 % of the Ctrl^{Ad}- and Ano1^{Ad}-infected cells were mCherry^{+}. (Reproduced from (1) in accordance with the MDPI and the CC BY 4.0 license).

By performing western blot analysis and immunofluorescence staining of TMEM16A overexpressing PAECs, the increase in channel expression on protein level was confirmed (**Figure 12 and Figure** 13).

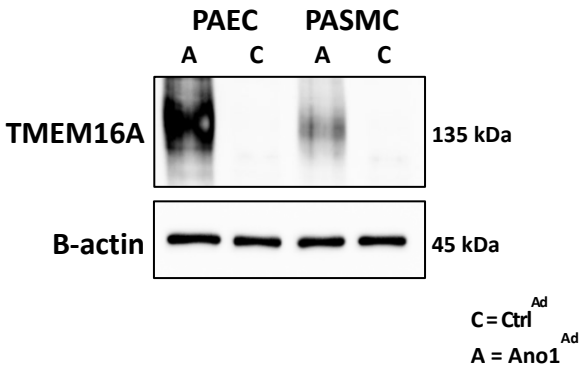

Figure 12. Overexpression of TMEM16A in primary vascular cells. Western blot displaying adenovirally-mediated TMEM16A expression in donor PAECs and PASMCs. (Reproduced from (1) in accordance with the MDPI and the CC BY 4.0 license).

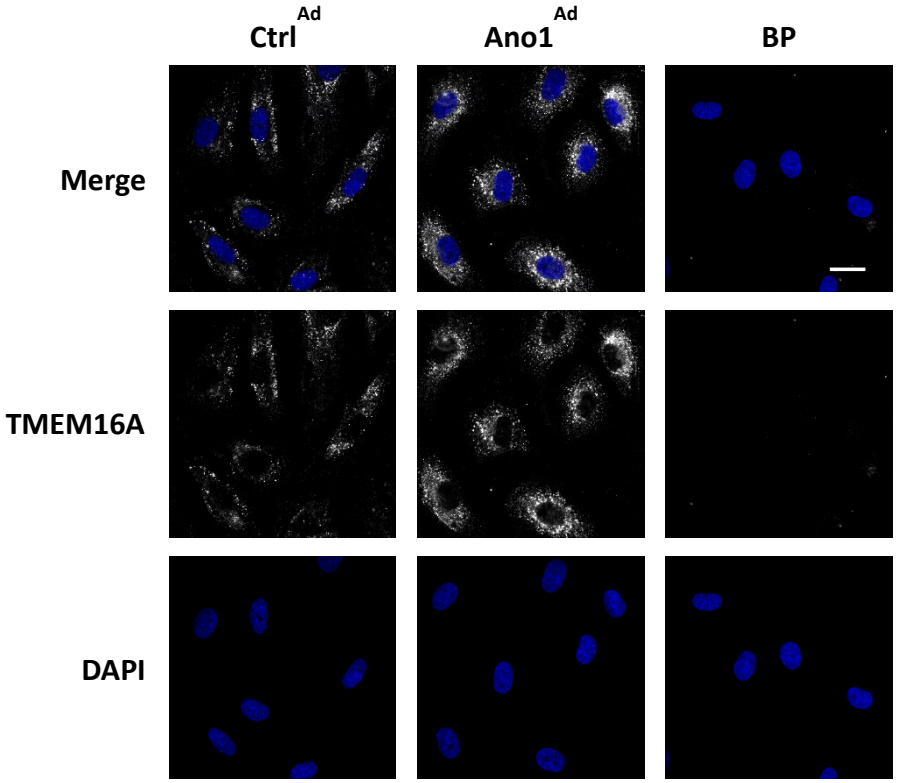

Figure 13. Immunofluorescence staining of TMEM16A-overexpressing PAECs. Primary PAECs were infected either with $Ctrl^{Ad}$ or $Ano1^{Ad}$ and stained for TMEM16A expression (scale bar = 20 µm). (Reproduced from (1) in accordance with the MDPI and the CC BY 4.0 license).

In order to determine that the increase in channel expression correlates with an increase in I_{ClCa}, I used whole-cell voltage clamp in the subsequent measurements. TMEM16A-overexpressing PAECs demonstrated approximately 5-fold increase in I_{ClCa} compared to control virus-infected PAECs (**Figure 14a-b**) and further supported by more than 5-fold increase in Bbr-sensitive current (**Figure 14c**). These results indicate that the adenoviral overexpression led to a production of a functional ion channel located in the outer cell membrane.

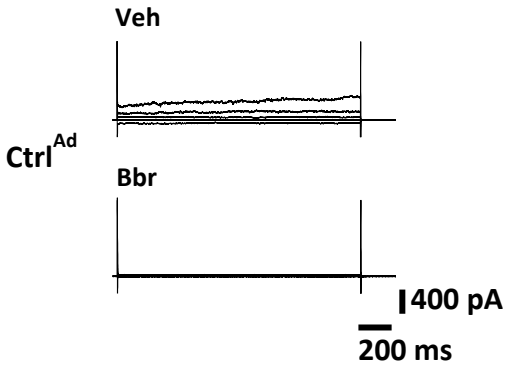

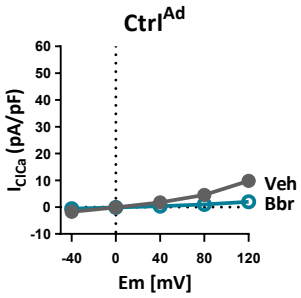

(**a**)

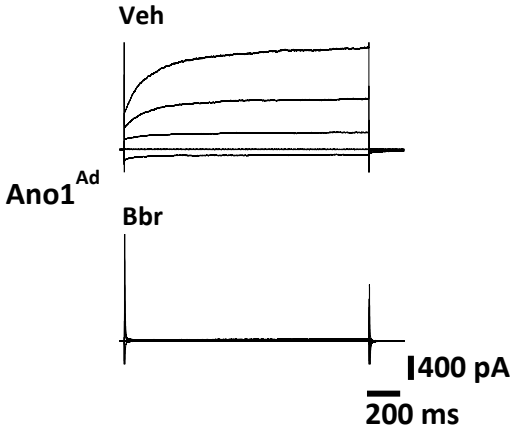

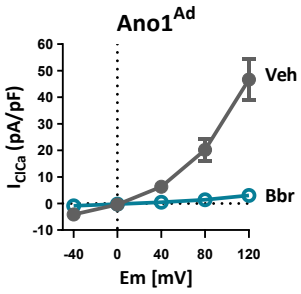

(**b**)

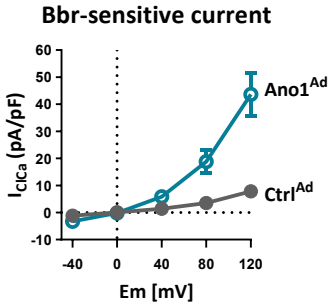

(**c**)

Figure 14. Adenoviral infection of primary PAECs results in increased I_{ClCa}. (a-b) Representative whole-cell I_{ClCa} traces (left) and normalized current-voltage relationships (right) measured with voltage-clamp showing the effect of Bbr in donor PAECs transfected with either $Ctrl^{Ad}$ (a) or TMEM16A-overexpressing $Ano1^{Ad}$ (b). (c) Calculated Bbr-sensitive current comparing primary PAECs infected with $Ctrl^{Ad}$ or $Ano1^{Ad}$. Figures were generated with 8-13 cells from N = 2 healthy donors. (Reproduced from (1) in accordance with the MDPI and the CC BY 4.0 license).

As Cl^- channels represent an important mechanism of cell membrane potential (E_m) regulation, I looked into possible electrophysiological consequences of increased TMEM16A activity. Adenoviral overexpression of TMEM16A caused significant increase in mean fluorescence intensity indicating E_m depolarization in primary PAECs (**Figure 15**).

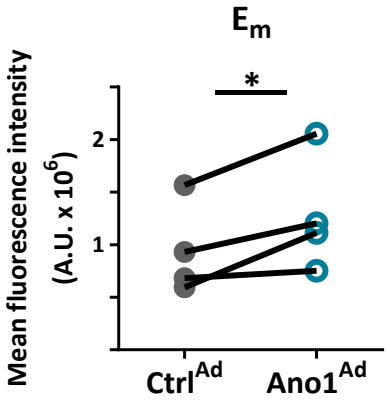

Figure 15. TMEM16A-mediated changes in resting membrane potential of human PAECs. Fluorometric measurements indicating a shift in relative resting membrane potential (E_m) of donor PAECs infected with $Ctrl^{Ad}$ or $Ano1^{Ad}$ using $DiBAC_4(3)$ dye. Figure was generated from 4 separate experiments. * $p < 0.05$, paired t-test. (Reproduced from (1) in accordance with the MDPI and the CC BY 4.0 license).

Since E_m fluctuation in turn is tightly interconnected with cell Ca^{2+} dynamics, a protocol enabling us to distinguish between divergent Ca^{2+} dynamics of cell Ca^{2+} stores and extracellular Ca^{2+} influx was implemented (**Figure 16a**). Increase in TMEM16A activity elevated the cytosolic Ca^{2+} concentration of PAECs (**Figure 16b**). Upon closer look, the extracellular Ca^{2+} influx was

decreased (**Figure 16c**) and could not be responsible for the observed rise in cytosolic Ca^{2+} concentration, however the store depletion step highlighted increased store Ca^{2+} content in TMEM16A-overexpressing PAECs (**Figure 16d**).

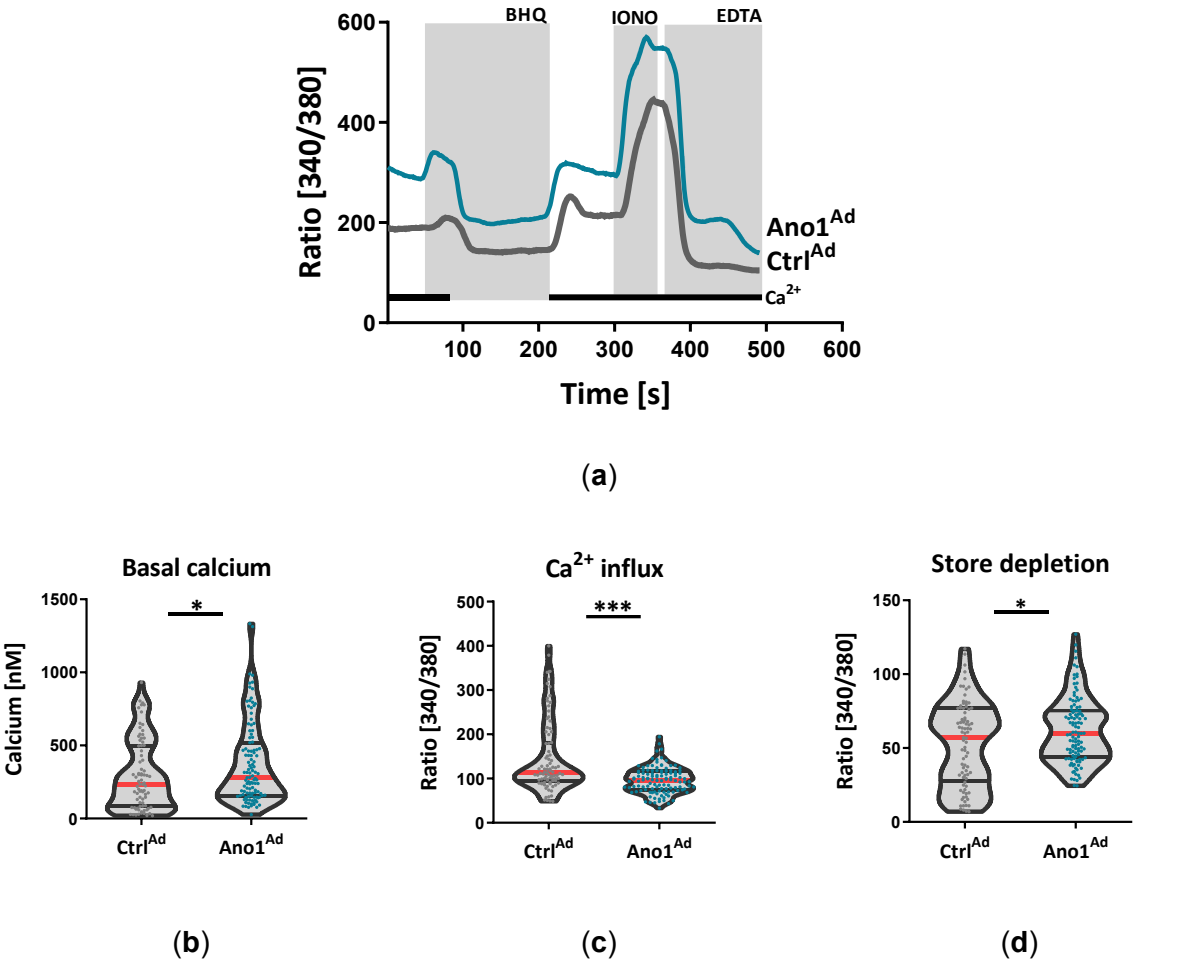

Figure 16. TMEM16A disrupts Ca^{2+} dynamics of human PAECs. (a) Representative traces depicting changes in intracellular Ca^{2+} of PAECs transfected either with $Ctrl^{Ad}$ or $Ano1^{Ad}$. (b-d) The effect of TMEM16A overexpression on cytosolic baseline Ca^{2+} concentration (b), store depletion (c) and Ca^{2+} influx (d) of donor PAECs. (BHQ = butylhydroquinone). Figures were generated with 80-116 cells from N = 3 healthy donors. * $p < 0.05$, unpaired t-tests. (The results were obtained with the support from Diana Zabini, PhD, Medical University of Graz; reproduced from (1) in accordance with the MDPI and the CC BY 4.0 license).

Since Ca^{2+} signalling changes are an essential part of IPAH PASMC pathological changes, I additionally investigated the effect of TMEM16A on the electrophysiological and Ca^{2+} dynamics of primary PASMCs (**Figure 17**). PASMCs had a tendency to be depolarized upon TMEM16A overexpression (**Figure 17a**), however changes on the Ca^{2+} landscape revealed different strategies of intracellular Ca^{2+} regulation between the cell types (**Figure 17b**). Similar to PAECs, cytosolic Ca^{2+} concentration was increased upon TMEM16A modulation (**Figure 17c)** with the exception of extracellular Ca^{2+} influx highly increased and Ca^{2+} store content decreased (**Figure 17d-e**).

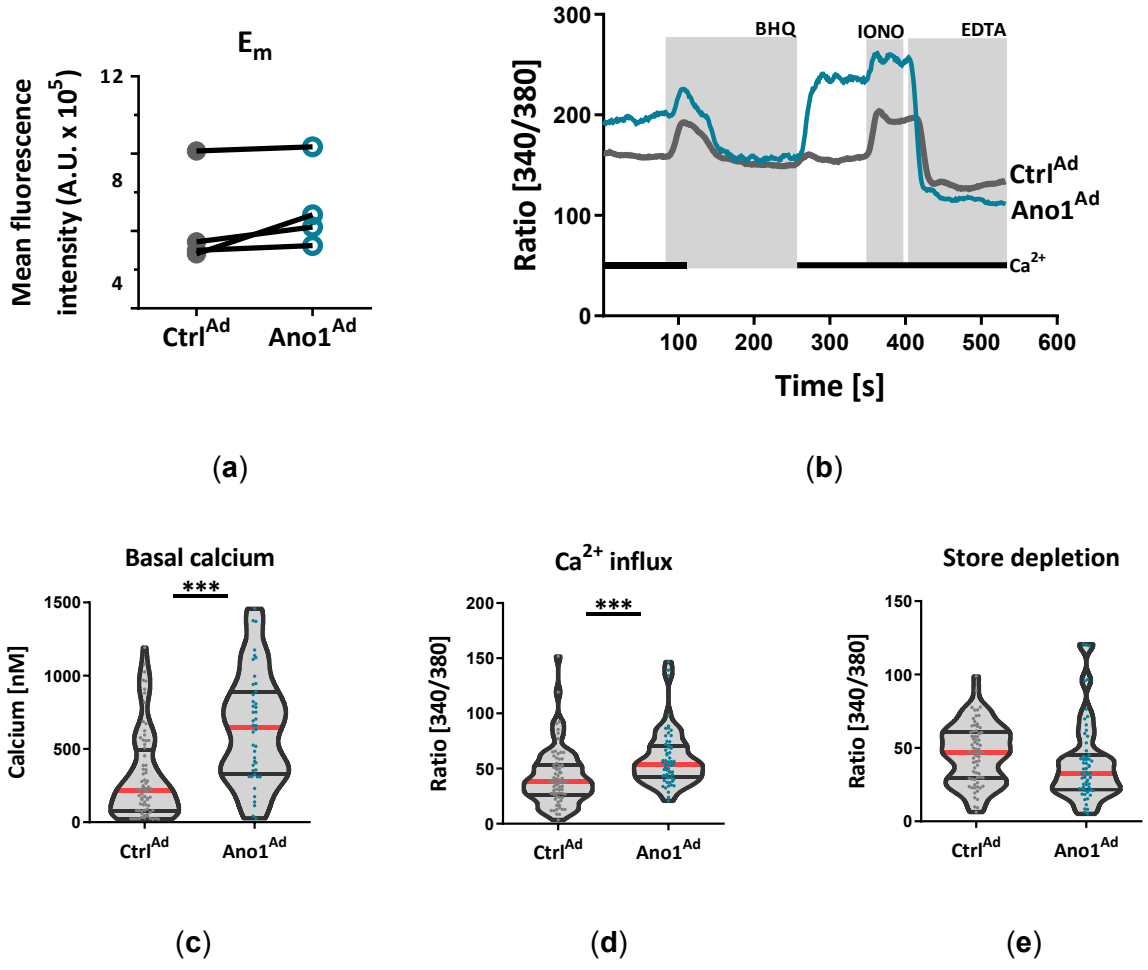

Figure 17. TMEM16A-mediated membrane depolarization disrupts Ca^{2+} dynamics of human PASMCs. TMEM16A-mediated membrane depolarization disrupts Ca^{2+} dynamics of human PASMCs. (a) Fluorometric measurements indicating relative resting membrane potential

(E_m) shift of donor PASMCs infected with $Ctrl^{Ad}$ or $Ano1^{Ad}$ using $DiBAC_4(3)$ dye. (b) Representative traces depict changes in intracellular Ca^{2+} measured in PASMCs transfected with $Ctrl^{Ad}$ or $Ano1^{Ad}$. (c-e) The effect of TMEM16A overexpression on cytosolic baseline Ca^{2+} concentration ($[Ca^{2+}]_i$), store depletion and Ca^{2+} influx using Fura-2 in donor PASMCs infected with $Ctrl^{Ad}$ or $Ano1^{Ad}$. (BHQ = butylhydroquinone). Figures were generated with 44-72 cells from N = 3 healthy donors. * $p < 0.05$, *** $p < 0.001$, unpaired t-tests. (Reproduced from (1) in accordance with the MDPI and the CC BY 4.0 license).

Taken together, TMEM16A causes significant changes to cell E_m and Ca^{2+} landscape, both important components of overall cell homeostasis.

4.4. TMEM16A-primed PAECs selectively suppress ERK1/2 pathway

TMEM16A activity was reported previously to affect the signalling of mitogen-activated protein kinases (MAPK), yet in sometime opposing ways. In the case of TMEM16A-primed primary PAECs, the activity of Akt and most MAPK remained unaffected (**Figure 18**), yet I could show a significant decrease in the ERK1/2 signalling pathway (**Figure 19**).

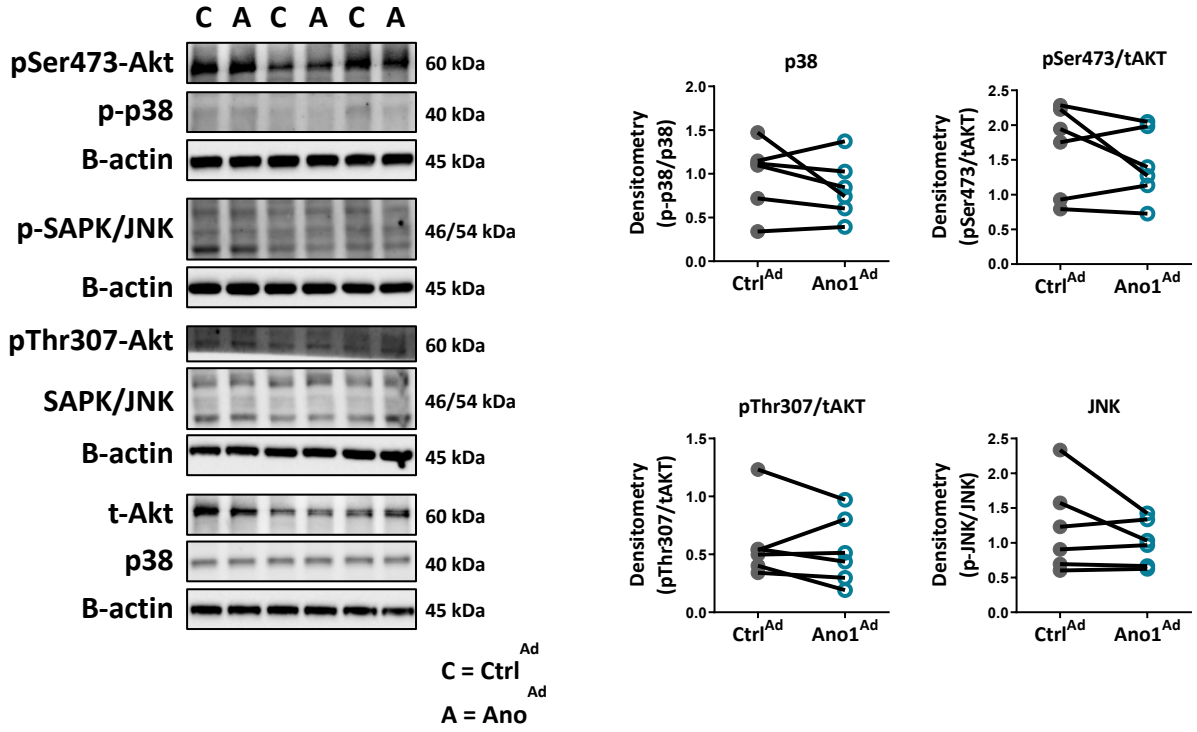

Figure 18. Elevated TMEM16A activity retains Akt, p38 and JNK signalling. Western blots showing protein levels of p38, Akt and SAPK/JNK obtained from PAECs infected with either Ano1^{Ad} or control Ctrl^{Ad}. Figures were generated from 6 separate experiments. (Reproduced from (1) in accordance with the MDPI and the CC BY 4.0 license).

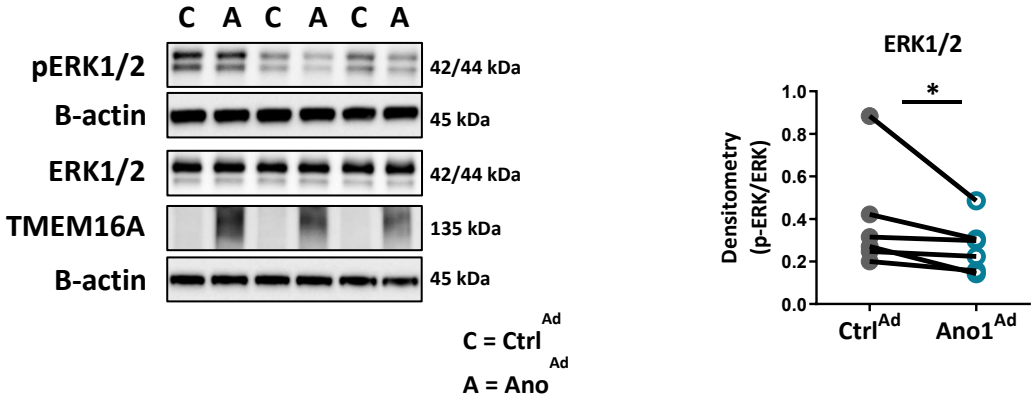

Figure 19. Elevated TMEM16A activity alters ERK1/2 signalling. Western blots showing ERK1/2 pathway activation in PAECs infected with either Ano1^{Ad} or Ctrl^{Ad} with quantification. Figures were generated with 6 samples. ** $p < 0.01$, ratio-paired t-test. (Reproduced from (1) in accordance with the MDPI and the CC BY 4.0 license).

ERK1/2 is a prominent endothelial cell regulator of angiogenesis, proliferation and wound-healing, which prompted me to look further into how tuning down of ERK1/2 signalling affects these functions. TMEM16A overexpression reduced the capability of PAECs to form tubular structures (**Figure 20**).

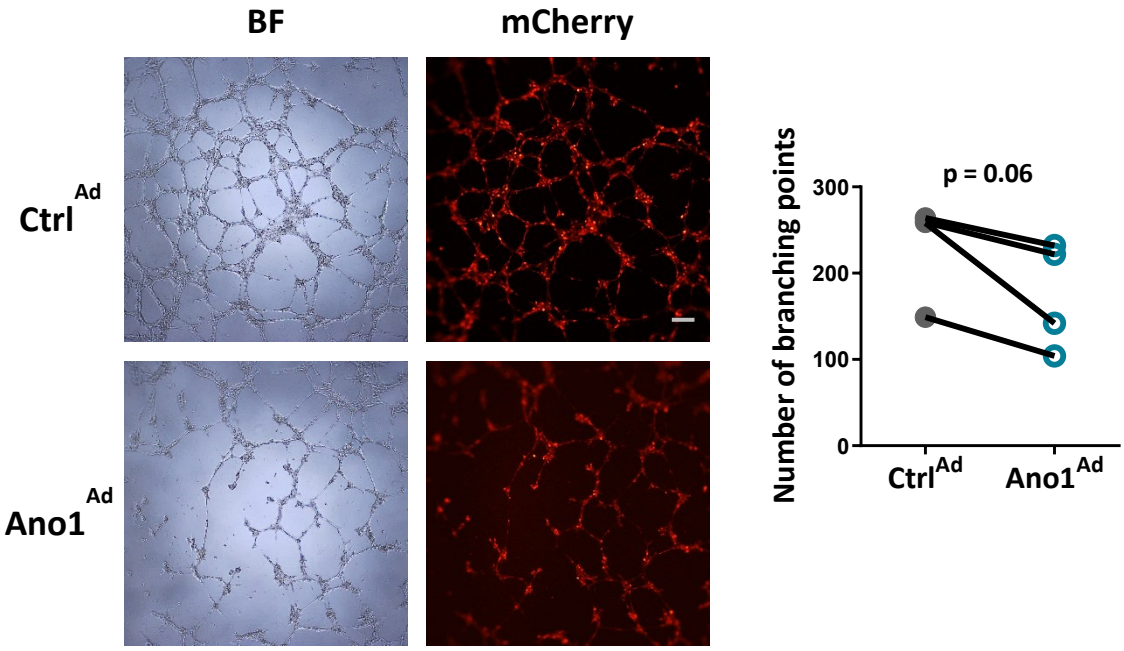

Figure 20. Increased TMEM16A activity causes angiogenic dysfunction. Matrigel tube-formation assay with representative bright-field (BF) and mCherry fluorescence pictures of Ano1^{Ad} or Ctrl^{Ad}-infected PAECs (scale bar = 200µm). Quantification showing the number of branching points in comparison to Ctrl^{Ad}. Figures were generated with 4 separate sets of experiments with triplicates in each group. * $p < 0.05$, paired t-test. (Reproduced from (1) in accordance with the MDPI and the CC BY 4.0 license).

I further supported hindered angiogenic ability with disrupted wound-healing potential (**Figure 21**) and a prominent decrease in their proliferative potential by measuring ^{3}H-thymidine incorporation (**Figure 22**).

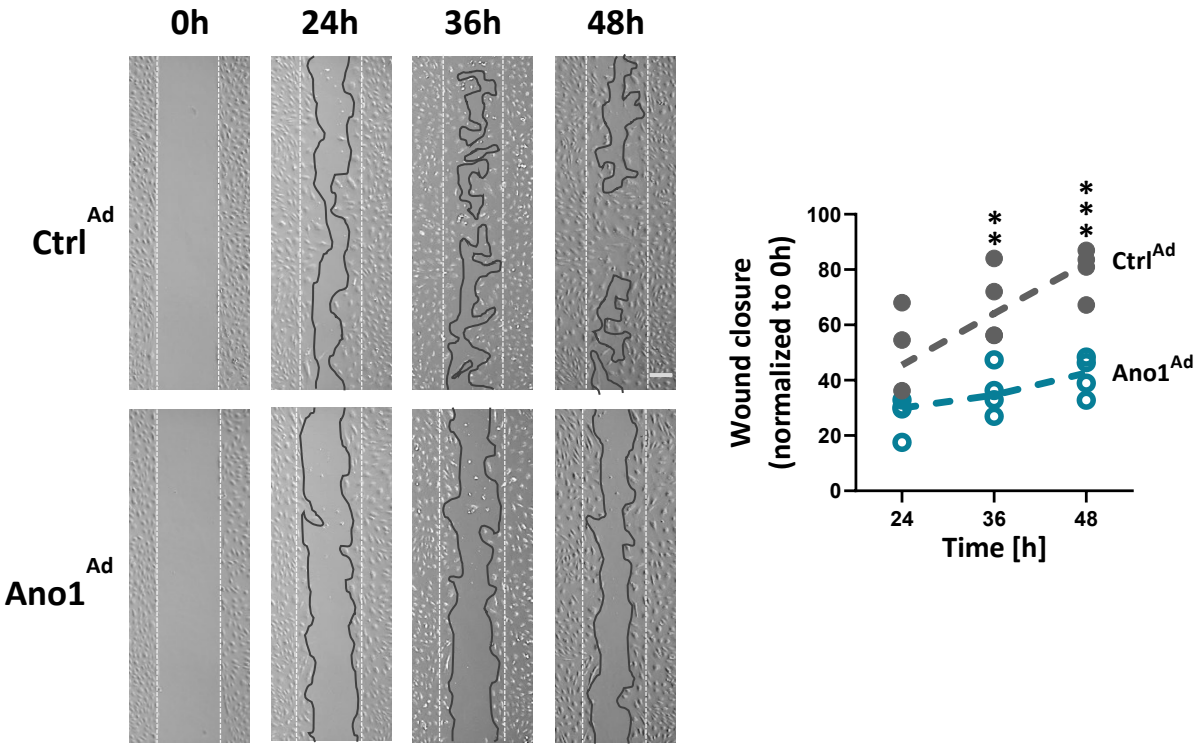

Figure 21. **Increased TMEM16A activity disrupts wound-healing.** Representative pictures of PAECs wound healing assay, expressing either Ano1^{Ad} or control Ctrl^{Ad}, taken after 24, 36 and 48 h and quantification (scale bar = 200 µm). Figure was generated with 4 separate sets of experiments. ** $p < 0.01$, *** $p < 0.001$, ANOVA with Bonferroni post-hoc test. (Reproduced from (1) in accordance with the MDPI and the CC BY 4.0 license).

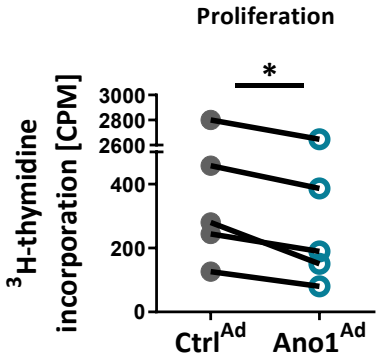

Figure 22. TMEM16A causes a reduction in PAEC proliferative potential. Proliferation of human PAECs overexpressing TMEM16A measured with ^{3}H-thymidine incorporation (n = 5). Changes are expressed as percentage compared to the PAECs treated with Ctrl^{Ad}. * $p < 0.05$, paired t-test. (Reproduced from (1) in accordance with the MDPI and the CC BY 4.0 license).

On the other hand, Cas3/Cas7 activity and cell cycle analysis revealed no changes thus confirming that apoptotic and cell cycle disruptions were not responsible for the observed change in cell numbers (**Figure 23 and Figure** 24).

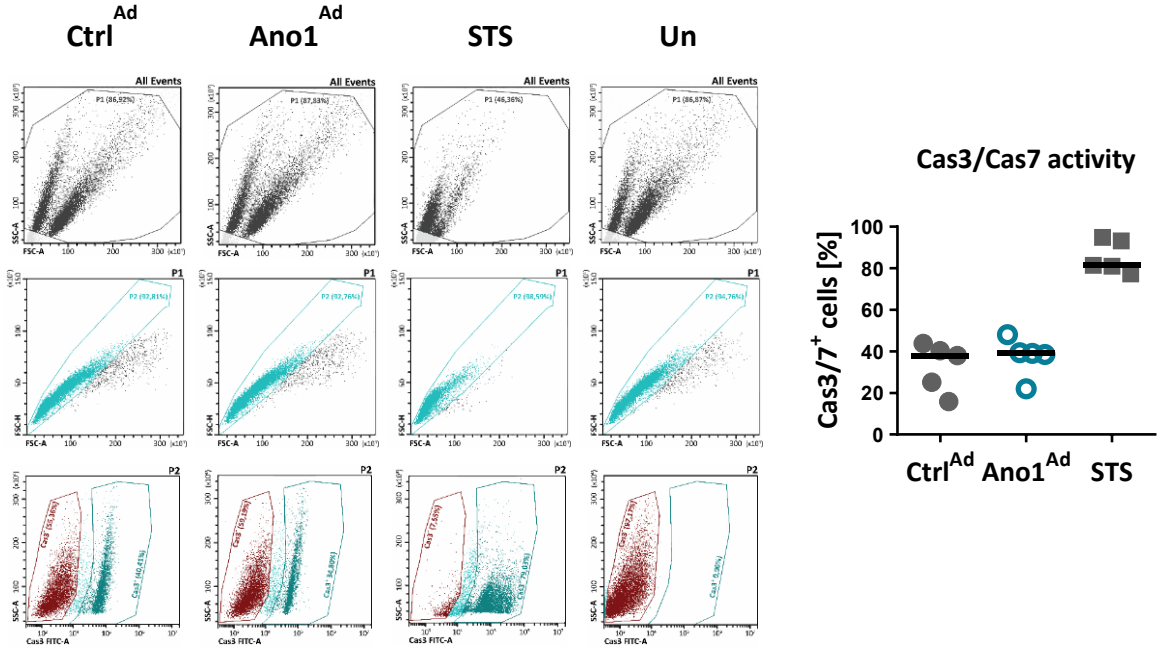

Figure 23. Cas3/Cas7 activity upon TMEM16A modulation. Cas3/Cas7 apoptosis assay of human PAECs overexpressing TMEM16A. Results are presented as percentage of parent cells. (Reproduced from (1) in accordance with the MDPI and the CC BY 4.0 license).

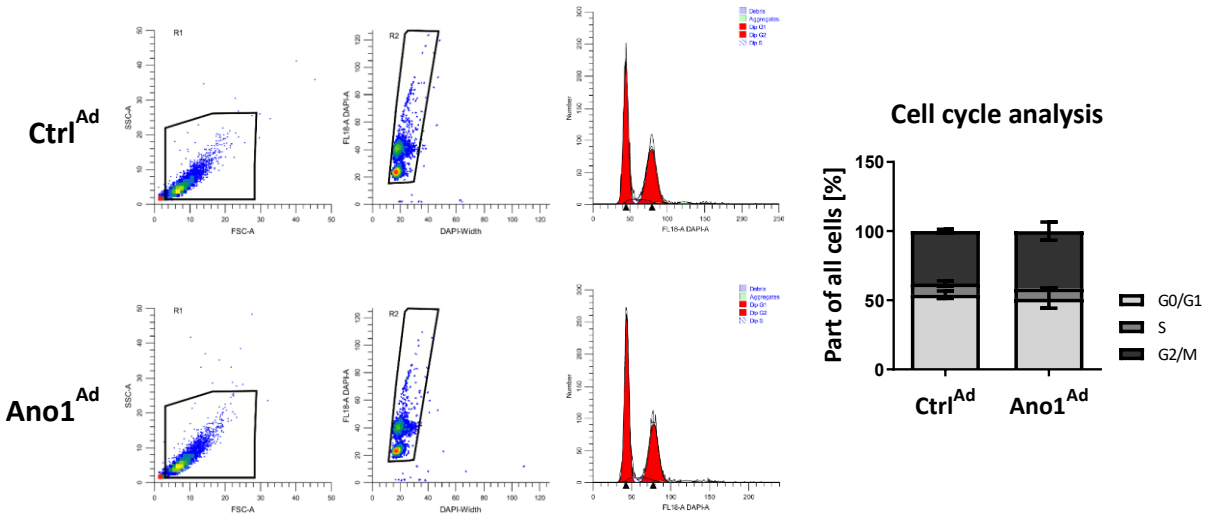

Figure 24. Cell-cycle analysis of TMEM16A-overexpressing PAECs. Cell-cycle analysis of human PAECs overexpressing TMEM16A. Results are presented as percentage of cells. (Reproduced from (1) in accordance with the MDPI and the CC BY 4.0 license).

These findings were further supported by western blot analysis showing unchanged PCNA and cyclin D1 levels, however cleavage of PARP seemed to be slightly reduced (**Figure 25**).

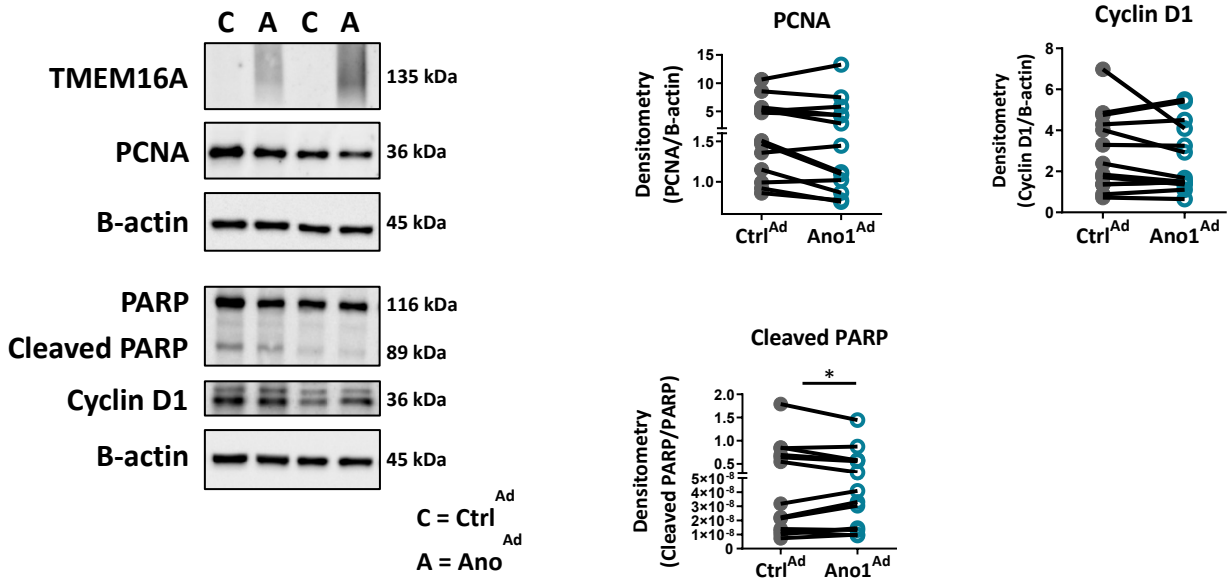

Figure 25. Processing of proliferation, apoptosis and cell-cycle markers upon TMEM16A modulation in PAECs. Western blots of PAECs infected with TMEM16A-overexpressing Ano1^{Ad} or control with quantifications of PCNA, cleaved PARP/PARP and Cyclin D1. Figures were generated with 13 separate sets of experiments. * $p < 0.05$, paired t-test. (Reproduced from (1) in accordance with the MDPI and the CC BY 4.0 license).

Moreover, there were no changes in the processing of autophagy-associated microtubule-associated protein 1A/1B-light chain 3 (LC3) (**Figure 26)**. These data suggest that tuning down ERK1/2 severely disrupts the vessel formation capability of primary PAECs. Seeing prominent changes in endothelial cell ability to proliferate and form tubules, I looked further into their metabolic footprint (**Figure 27 and Figure 28**).

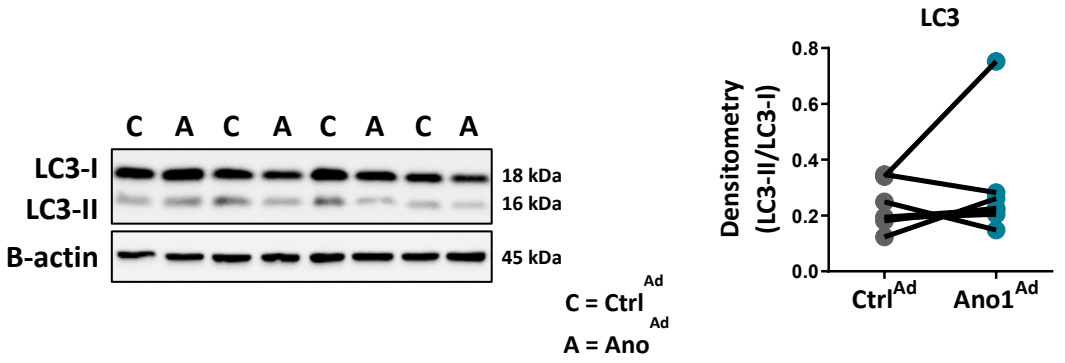

Figure 26. **TMEM16A-overexpressing PAECs retain autophagy intact.** Western blot of PAECs infected with TMEM16A-overexpressing Ano1^{Ad} and control Ctrl^{Ad} showing the processing of autophagy-associated microtubule-associated protein 1A/1B-light chain 3 (LC3). Figures were generated with n = 7 samples from 3 different donors. (Reproduced from (1) in accordance with the MDPI and the CC BY 4.0 license).

Aerobic glycolysis is the predominant bioenergetic pathway in endothelial cells. I implemented SeaHorse Cell Mito Stress Test and Glycolysis Stress Test to assess the bioenergetic pathways in TMEM16A-overexpressing cells. While glycolysis remained unaffected in primary PAECs, the cells demonstrated a shift to oxidative phosphorylation upon TMEM16A modulation, as shown by ratio of oxygen consumption rate to extracellular acidification rate (OCR/ECAR) (**Figure 27a-b and Figure 28**).

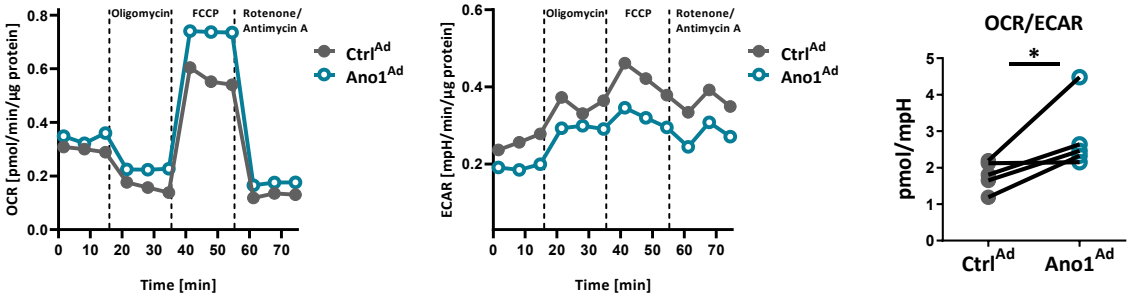

(**a**)

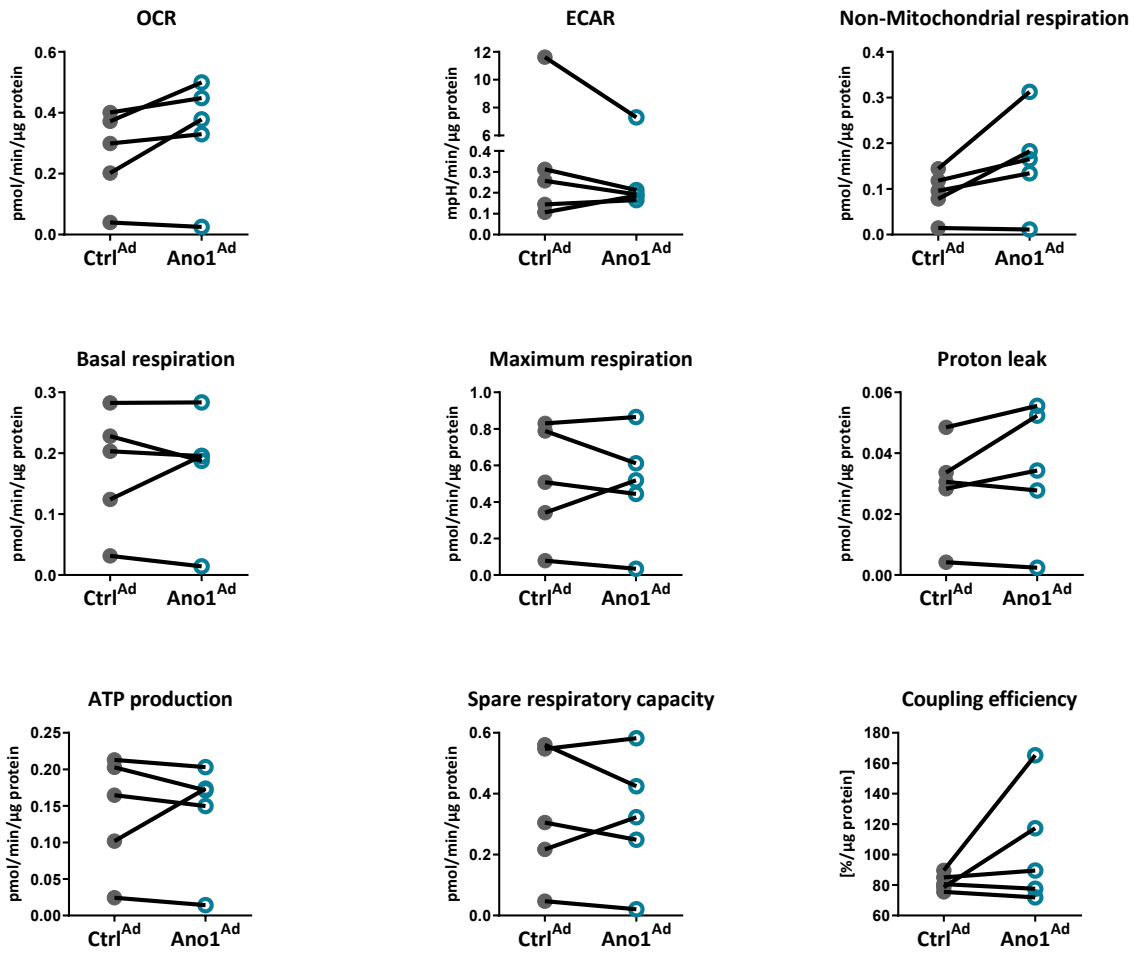

(**b**)

Figure 27. Mitochondrial metabolic footprint of TMEM16A-overexpressing PAECs. (a) SeaHorse Cell Mito Stress experiment showing the effect of TMEM16A overexpression on ratio of oxygen consumption rate to extracellular acidification rate (OCR/ECAR) in donor PAECs. (b) The effect of TMEM16A overexpression on OCR, ECAR, non-mitochondiral respiration, basal respiration, maximum respiration, proton leak, ATP production, spare respiratory capacity and coupling efficiency in donor PAECs. The figures were generated from 5 separate experiments performed in triplicate and normalized to protein content. * $p < 0.05$, paired t-test. (Reproduced from (1) in accordance with the MDPI and the CC BY 4.0 license).

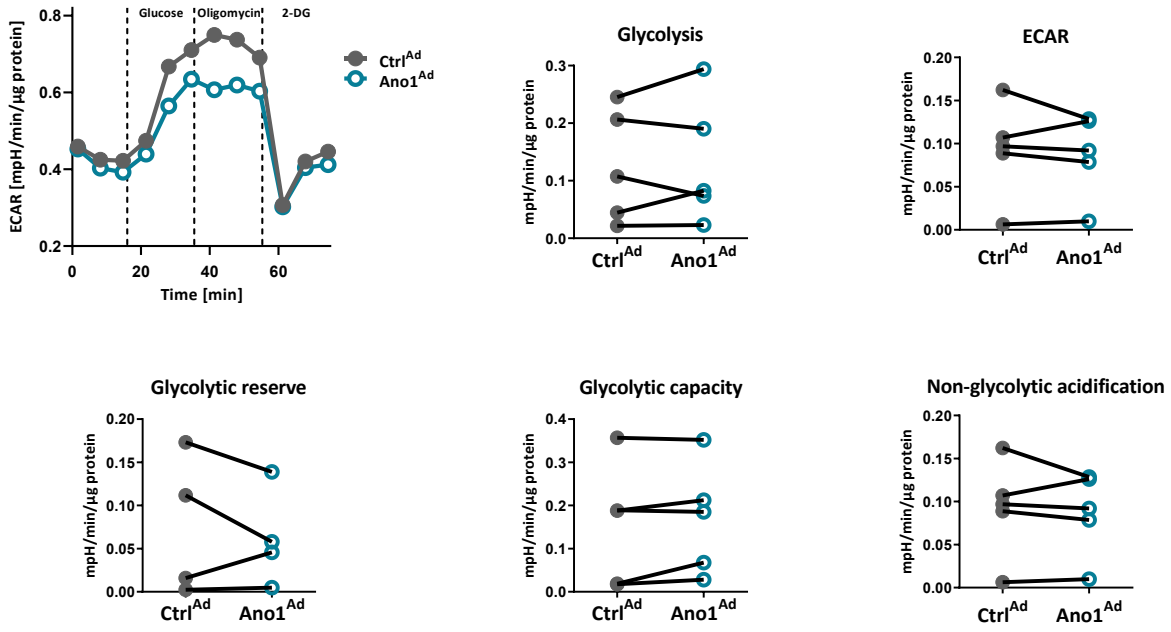

Figure 28. Glycolytic metabolic footprint of TMEM16A-overexpressing PAECs. SeaHorse Glycolysis Stress experiment showing the effect of TMEM16A overexpression in donor PAECs on glycolysis, glycolytic reserve, glycolytic capacity, ECAR and non-glycolytic acidification. The figures were generated from 5 separate experiments performed in triplicate and normalized to protein content.

On the other hand it has been shown before that adenoviral increase in TMEM16A expression stimulates proliferation of primary PASMCs, possibly through increased intracellular Ca^{2+} concentration (57). I have additionally supported this finding with unchanged Cas3/Cas7 activity (**Figure 29**) and cell-cycle modulation (**Figure 30**).

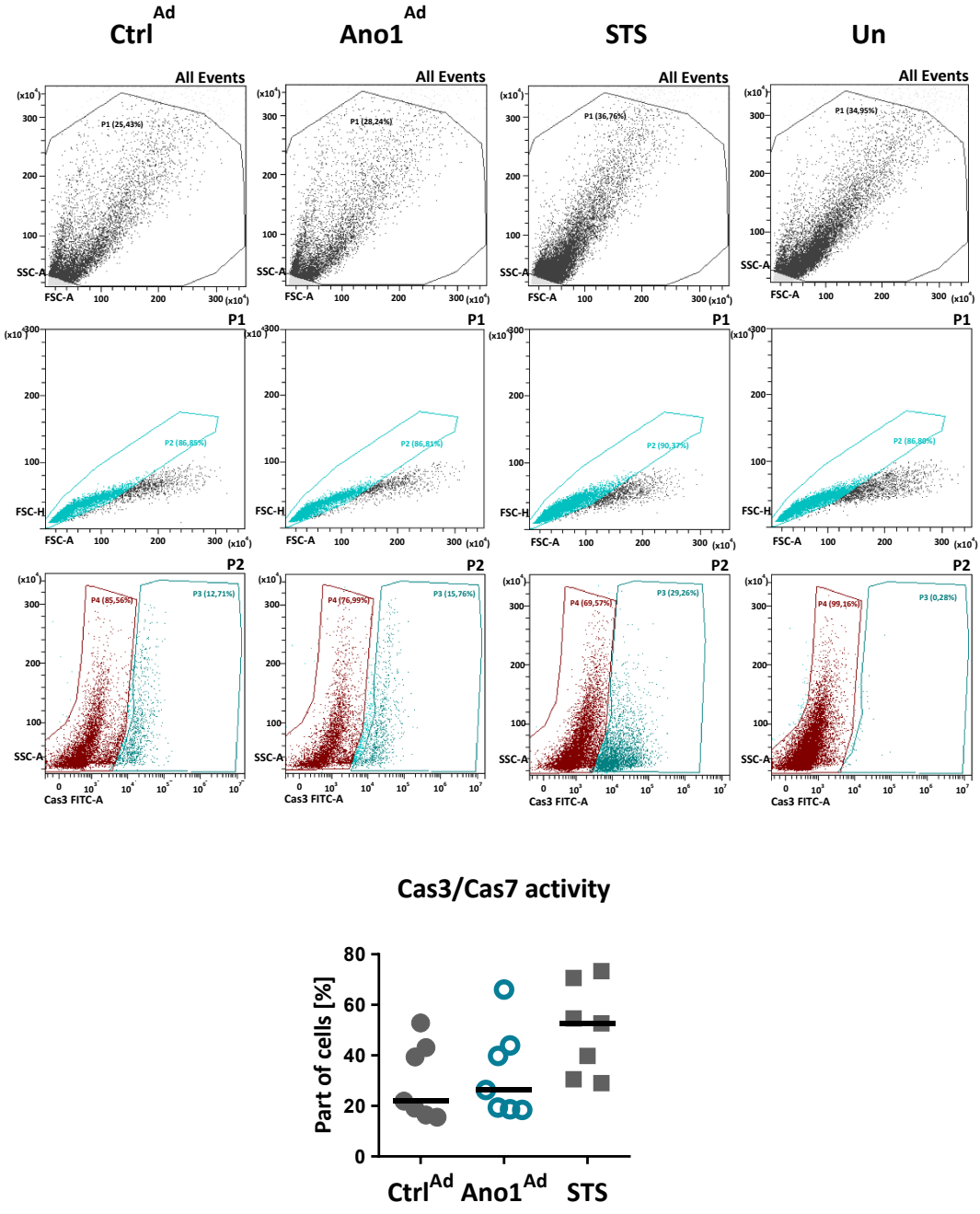

Figure 29. Cas3/Cas7 activity in PASMCs upon TMEM16A modulation. Cas3/Cas7 apoptosis assay of human PASMCs overexpressing TMEM16A. Results are presented as percentage of parent cells (STS = staurosporin; un = unstained control).

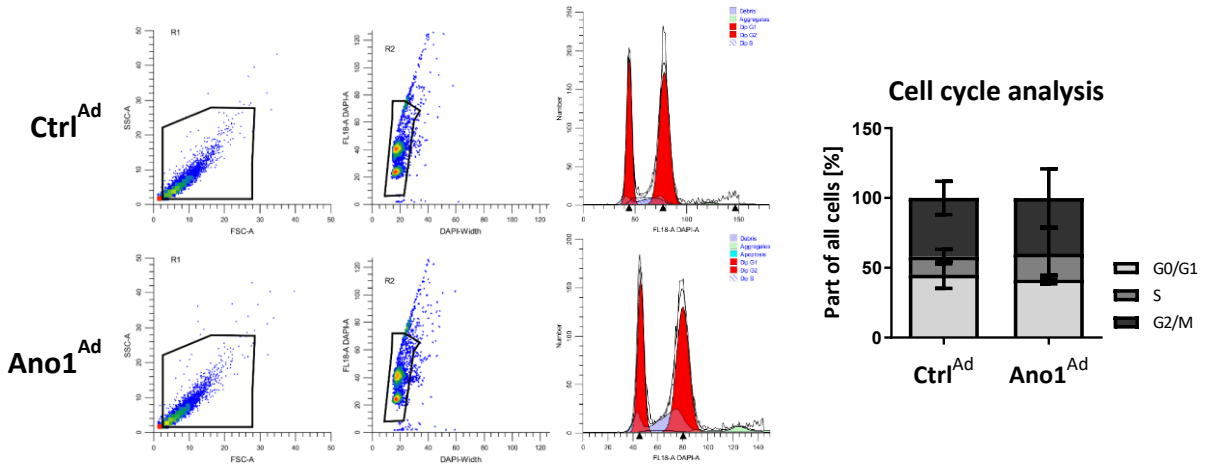

Figure 30. Cell-cycle analysis of TMEM16A-overexpressing PASMCs. Cell-cycle analysis of human PASMCs overexpressing TMEM16A. Results are presented as percentage of cells.

By performing western blot analysis I could support the observed phenotype by increased PCNA levels and unchanged cleavage of PARP, however Cyclin D1 levels were increased (**Figure 31**).

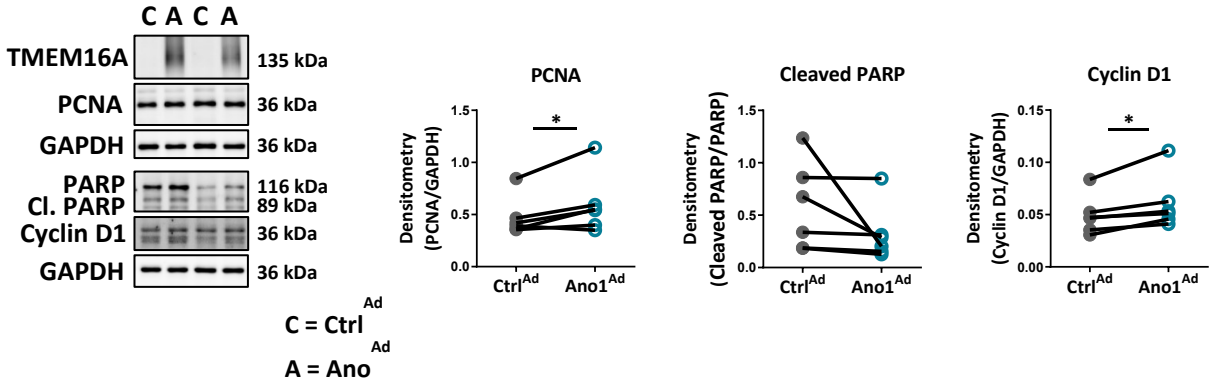

Figure 31. Processing of proliferation, apoptosis and cell-cycle markers upon TMEM16A modulation in PASMCs. Western blots of PASMCs infected with TMEM16A-overexpressing Ano1^{Ad} or control with quantifications of PCNA, cleaved PARP/PARP and Cyclin D1. Figures were generated with 6 separate sets of experiments. * $p < 0.05$, paired t-test.

Moreover, TMEM16A-associated rise in intracellular Ca^{2+} concentration did not affect the wound-healing capability (**Figure 32**) nor oxidative phosphorylation or glycolysis pathways of primary PASMCs, with the exception of glycolytic capacity (**Figure 33 and Figure 34**).

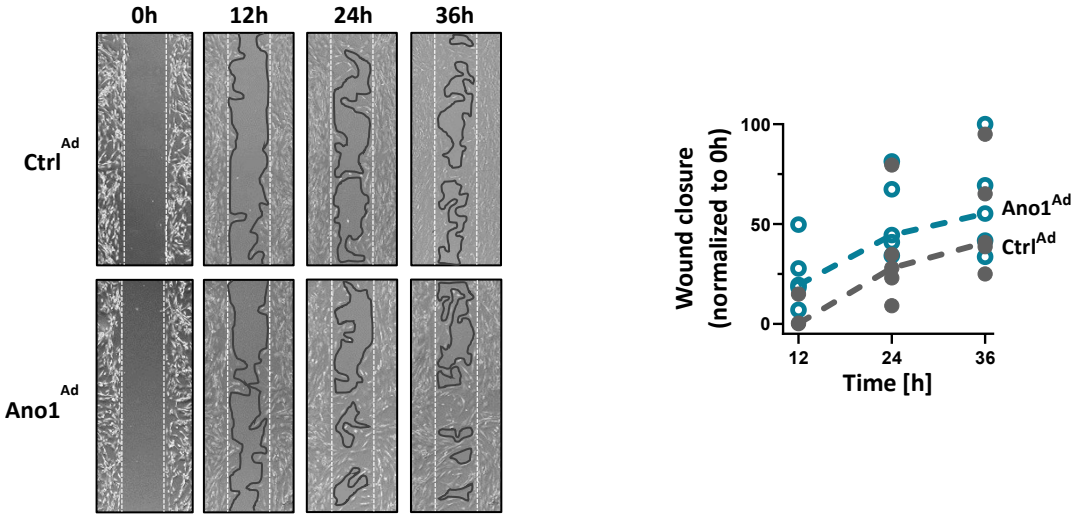

Figure 32. Wound healing of TMEM16A-overexpressing PASMCs. Representative pictures of PASMCs wound healing assay infected with either control or TMEM16A-overexpressing adenovirus. Figure was generated with 5 separate sets of experiments.

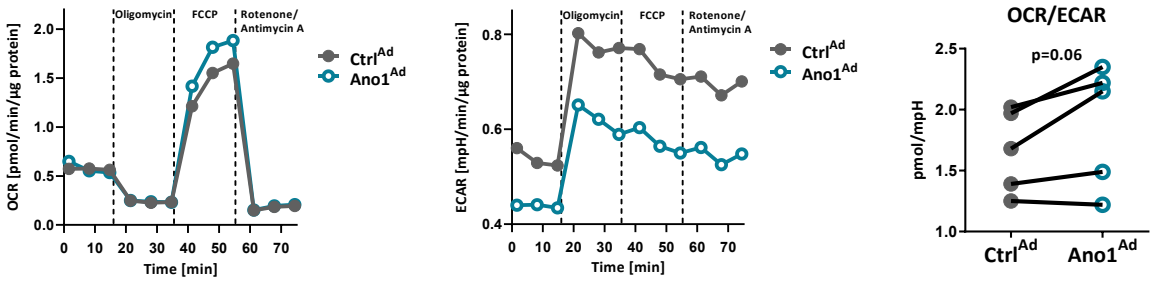

(**a**)

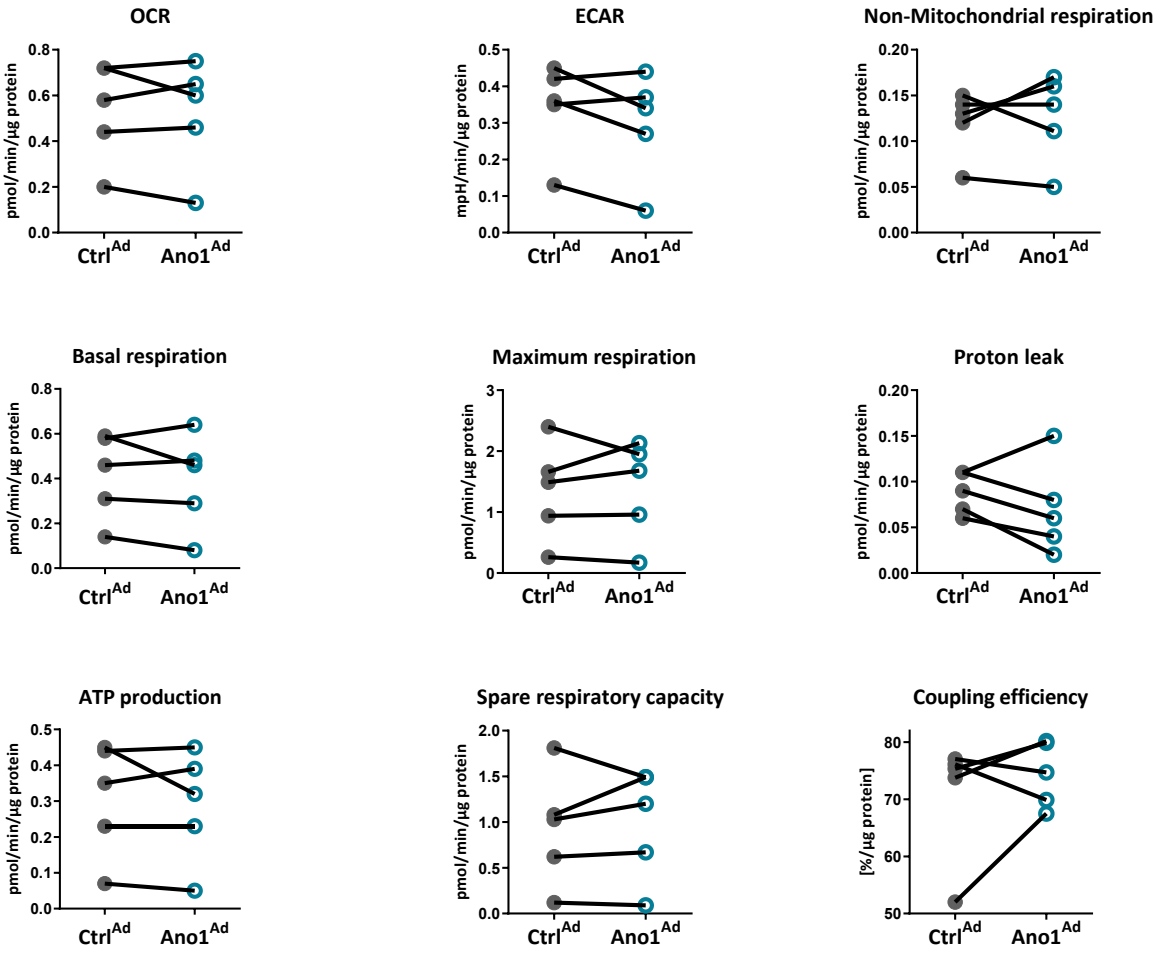

(**b**)

Figure 33. Mitochondrial metabolic footprint of TMEM16A-overexpressing PASMCs. (a) SeaHorse Cell Mito Stress experiment showing the effect of TMEM16A overexpression on ratio of oxygen consumption rate to extracellular acidification rate (OCR/ECAR) in donor PASMCs. (b) The effect of TMEM16A overexpression on OCR, ECAR, non-mitochondiral respiration, basal respiration, maximum respiration, proton leak, ATP production, spare respiratory capacity and coupling efficiency in donor PASMCs. The figures were generated from 5 separate experiments performed in triplicate and normalized to protein content. Paired t-test.

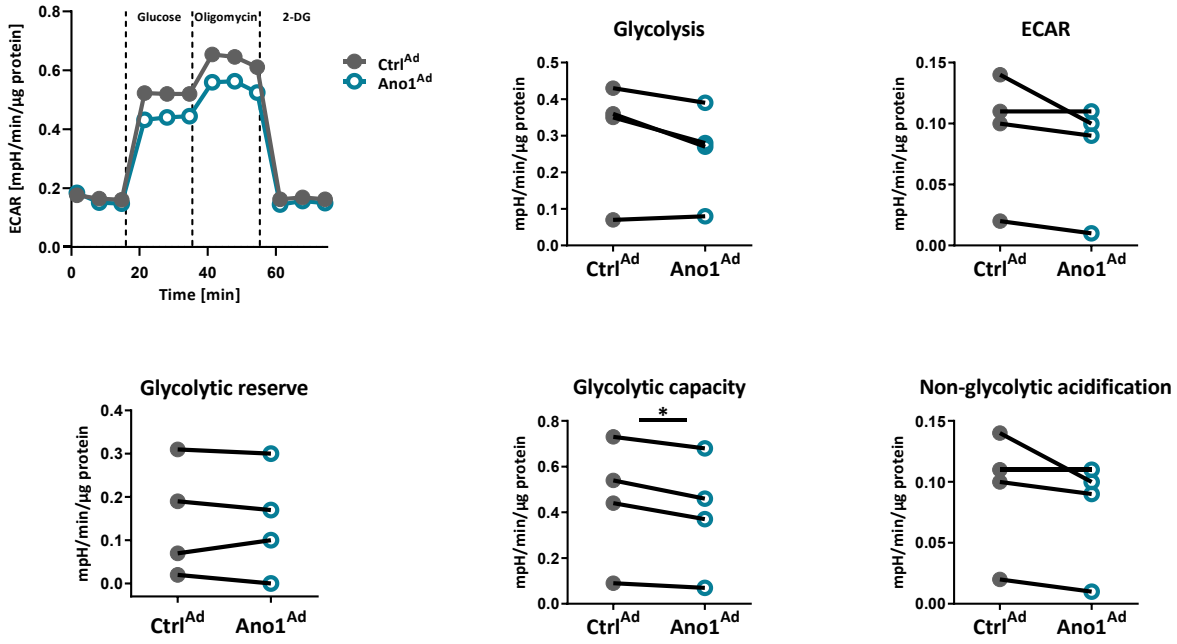

Figure 34. Glycolytic metabolic footprint of TMEM16A-overexpressing PASMCs. SeaHorse Glycolysis Stress experiment showing the effect of TMEM16A overexpression in donor PASMCs on glycolysis, glycolytic reserve, glycolytic capacity, ECAR and non-glycolytic acidification. The figures were generated from 4 separate experiments performed in triplicate and normalized to protein content. * $p < 0.05$, paired t-test.

TMEM16A modulation therefore affects the metabolic footprint of PAECs making them more dependent on oxidative phosphorylation. This further confirms TMEM16A as a modulator of endothelial homeostasis affecting the basic processes defining endothelial cell identity.

4.5. Disrupted eNOS activity underlining endothelial dysfunction

The reduction in ERK1/2 activity on the one hand affected the proliferation, wound-healing and angiogenesis of PAECs, yet ERK1/2 signalling is commonly associated with eNOS activity as well (176). NO production represents one of the most fundamental functions of endothelial cells and defines the healthy endothelium. Using a fluorescence NO-monitoring dye, I measured NO production in healthy, control adenovirus-infected PAECs on the one hand and TMEM16A-overexpressing PAECs on the other. Measurement of basal non-induced NO production did not

distinguish between the groups (**Figure 35a**), yet upon acetylcholine (ACh) stimulation, the control PAECs greatly increased NO production, while the levels in TMEM16A-overexpressing group remained low (**Figure 35b**).

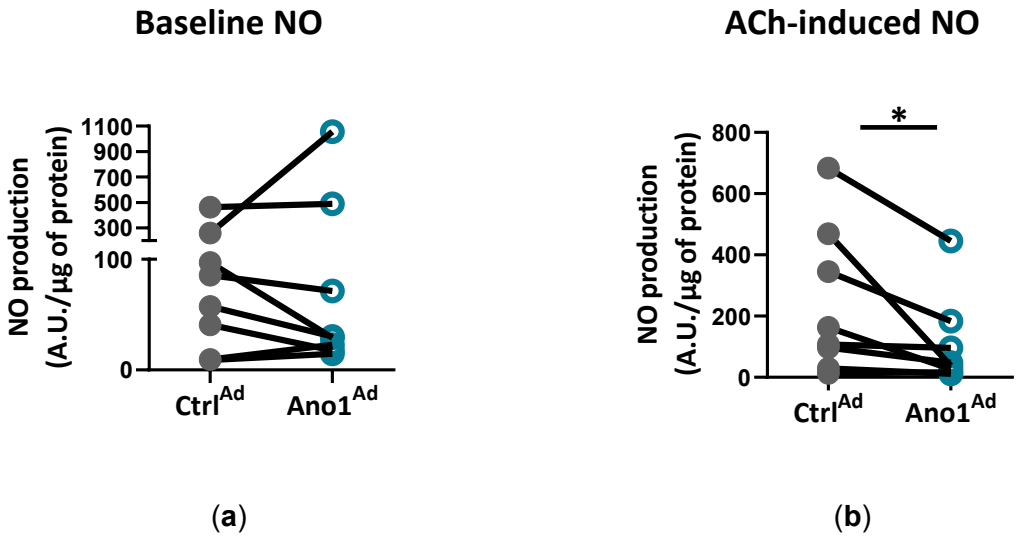

Figure 35. Elevated TMEM16A disturbs acetylcholine-induced nitric oxide production. (a) Non-induced nitric oxide levels and (b) acetylcholine-induced nitric oxide production of control and TMEM16A-overexpressing ($Ano1^{Ad}$) human PAECs. Figures were generated with 8 sets of experiments with quadruplicate in each group and normalized to protein content. * $p < 0.05$, ratio-paired t-test. (Reproduced from (1) in accordance with the MDPI and the CC BY 4.0 license).

The predominant source of NO production in endothelium is endothelial nitric oxide synthase (eNOS). eNOS is activated by Ca^{2+} on the one hand and by posttranslational modifications on the other. Two of the phosphorylation sites are especially important in its activity, the activatory Ser1177 and inhibitory Thr495. In order to explain changes in NO production, I defined activated state of eNOS by increased Ser1177 and decreased Thr495 phosphorylation. I stimulated control and TMEM16A-overexpressing PAECs with ACh in a time-dependent manner in order to follow the activation dynamics of eNOS (**Figure 36**).

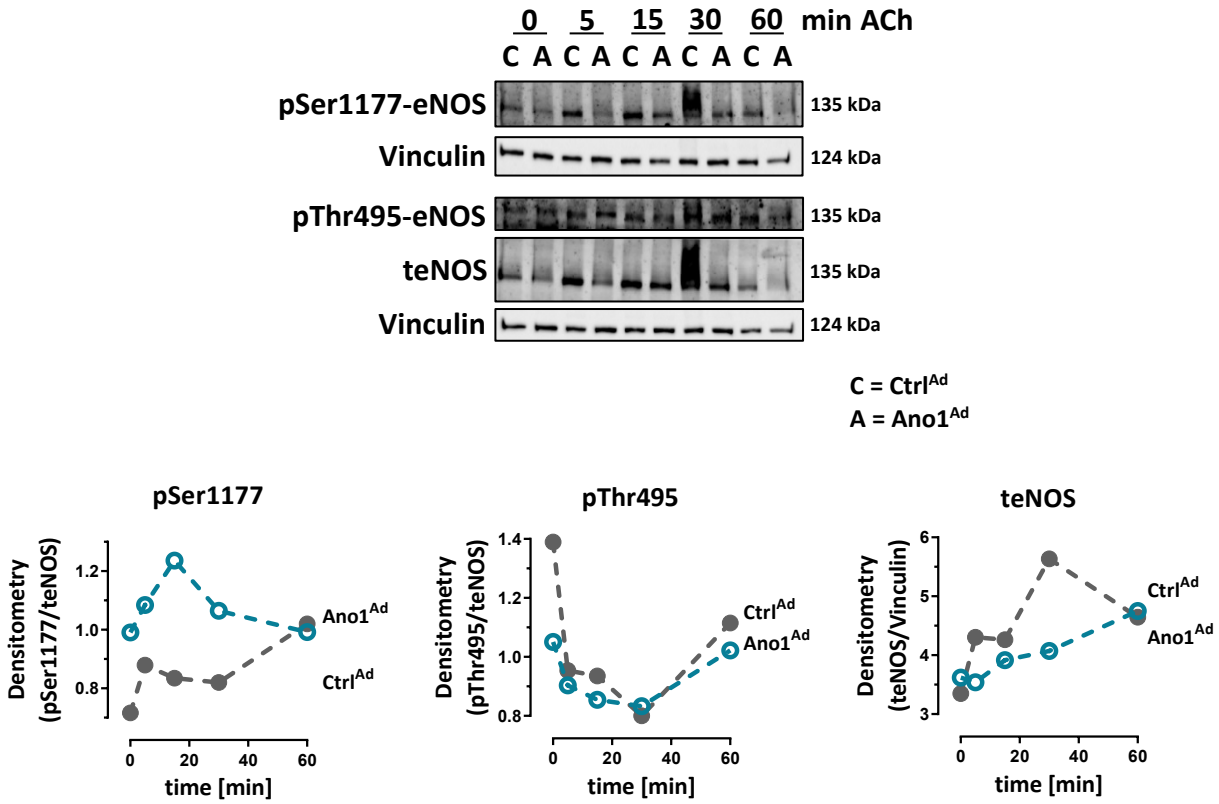

Figure 36. Increased TMEM16A activity disturbs eNOS activation. Western blots showing ACh-induced changes of Ctrl^{Ad} and Ano1^{Ad}-infected donor PAECs with quantification following the dynamic of total eNOS as well as its phosphorylation pattern at activatory Ser1177 and inhibitory Thr495 sites. (Reproduced from (1) in accordance with the MDPI and the CC BY 4.0 license).

I could show that at non-stimulated baseline, TMEM16A-overexpressing PAECs demonstrate emphasized activated state of eNOS with increased Ser1177 and decreased Thr495 phosphorylation (**Figure 37a**). After 15 min of ACh stimulation, the activatory Ser1177 phosphorylation persisted in TMEM16A-overexpressing cells and in control cells the phosphorylation of Thr495 decreased with time almost leveling with TMEM16A-overexpressing cells (**Figure 37b**).

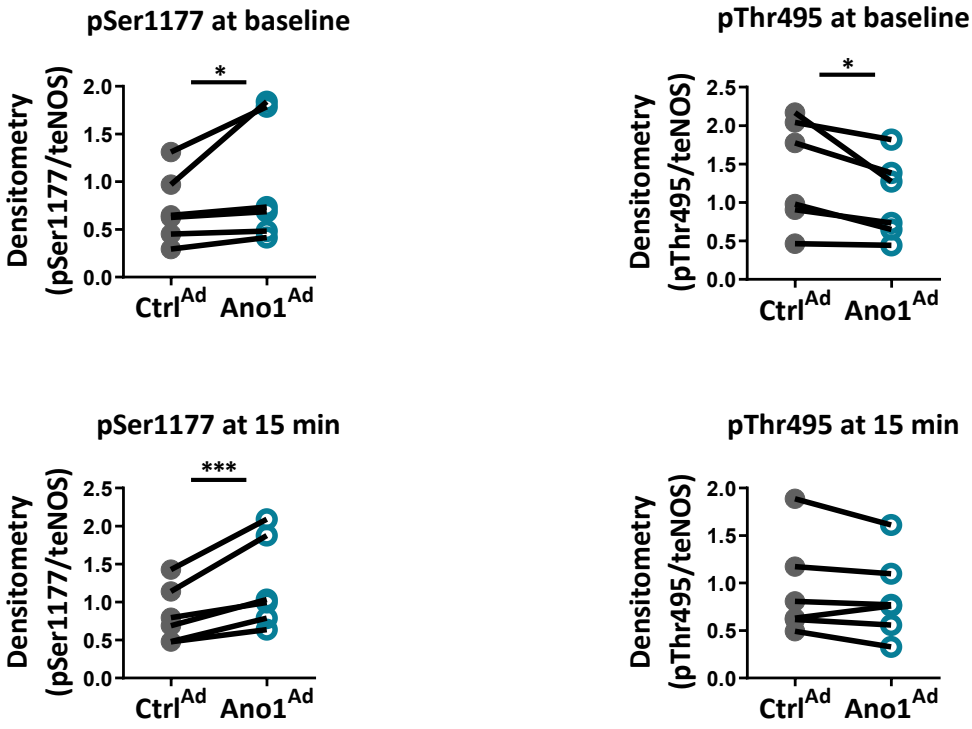

Figure 37. **TMEM16A-associated changes in eNOS activity.** Quantification of western blots from Figure 25 showing basal, non-induced level of eNOS phosphorylation at Ser1177 and Thr495 (a) and after 15 min of ACh stimulation (b). Figures were generated with 6 samples. * $p < 0.05$, ** $p < 0.01$, ratio-paired t-test. (Reproduced from (1) in accordance with the MDPI and the CC BY 4.0 license).

In a separate set of experiments, I incubated primary PAECs in a Ringer´s solution containing physiological concentration of Cl^- (N) or in a Cl^--reduced solution (M) for 24 h in order to simulate chronic intracellular Cl^- concentration decrease as caused by increased TMEM16A activity (**Figure 38, Figure** 39 **and Figure** 40). Following 24 h of incubation, primary PAECs retained morphological features (**Figure 38**).

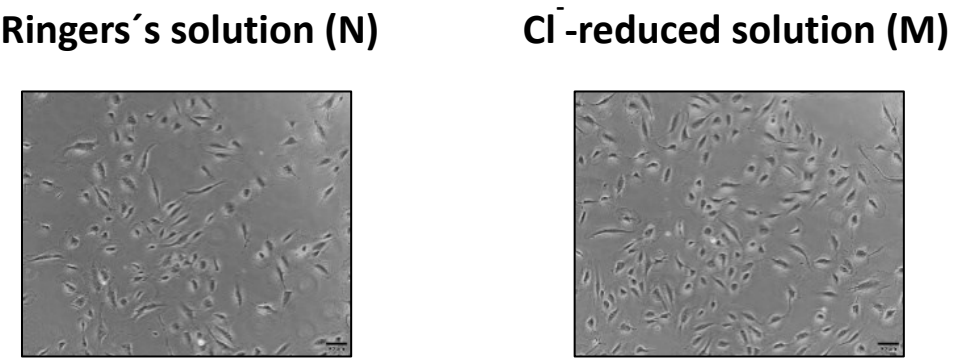

Figure 38. Donor PAECs retain morphology after isosmotic Cl^- reduction. Bright-field pictures of donor PAECs incubated in either Ringer´s (N) or Cl^--reduced (M) solution for 24 h before collecting the protein for further analysis (scale bar = 50µm). (Reproduced from (1) in accordance with the MDPI and the CC BY 4.0 license).

I stimulated both groups of cells with ACh in a time-dependent manner in order to follow the activation dynamics of eNOS (**Figure 39**).

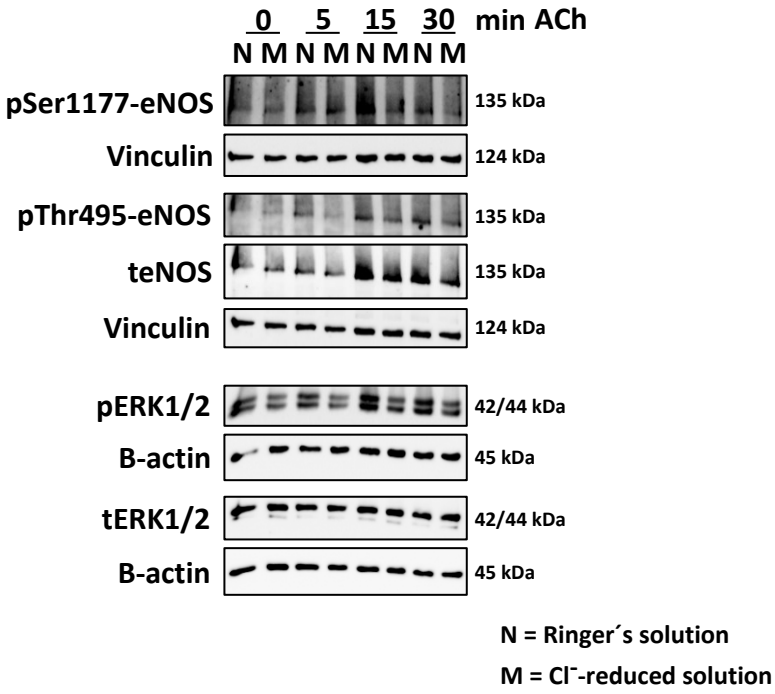

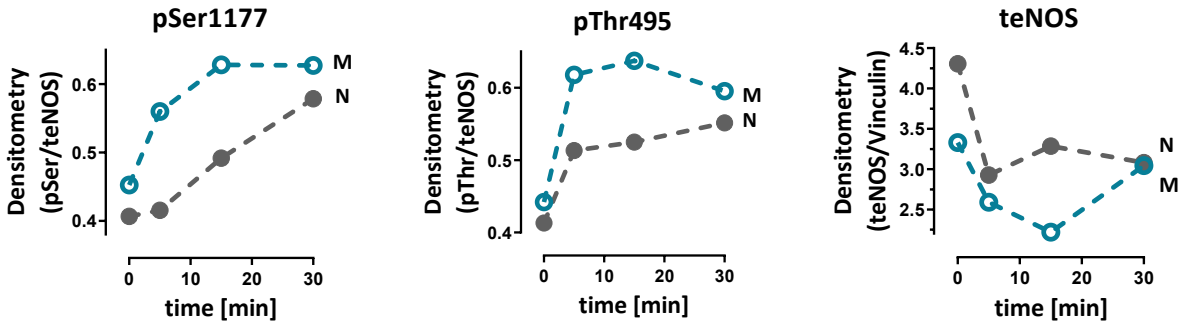

Figure 39. Chronic Cl^- reduction disturbs eNOS activation. Western blots showing ACh-induced changes following N and M-incubated donor PAECs with quantification following the dynamic of total eNOS as well as its phosphorylation pattern at activatory Ser1177 and inhibitory Thr495 sites. (Reproduced from (1) in accordance with the MDPI and the CC BY 4.0 license).

I could show that at non-stimulated baseline and after 15 min of ACh stimulation, M-incubated PAECs show tendency of higher Ser1177 phosphorylation, while Thr495 phosphorylation remains unchanged between the groups (**Figure 40a-b**). Incubation of primary PAECs in solution M caused tendency of PAECs to decrease ERK1/2 signalling (**Figure 40c**).

Taken together, increased TMEM16A represents a severe disturbance of endothelial cell homeostasis and is responsible for the development of endothelial dysfunction.

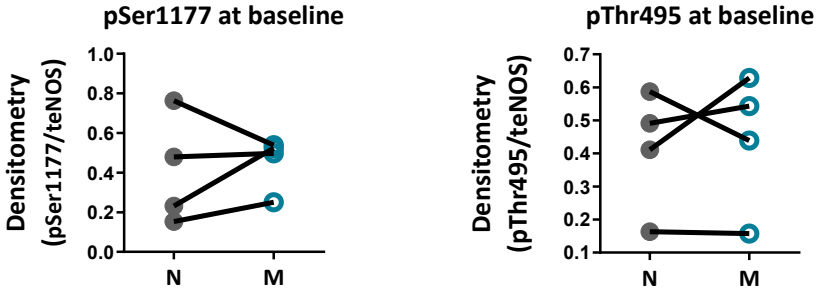

(**a**)

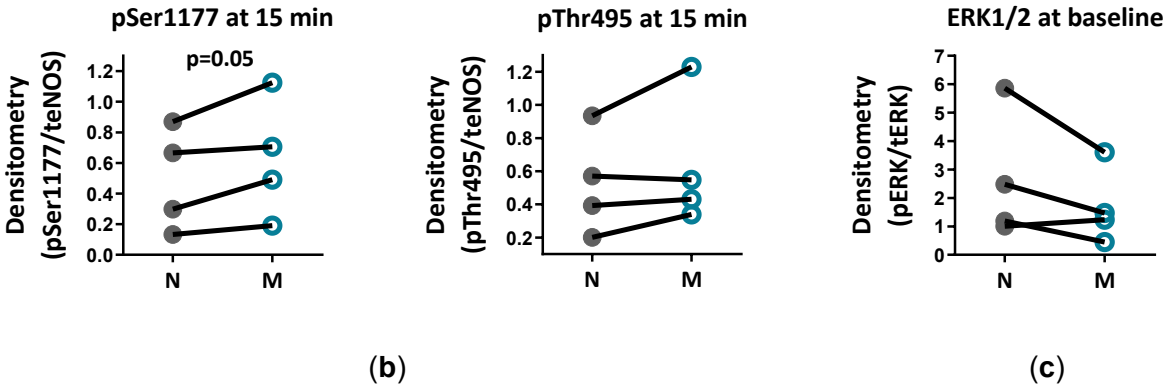

(**b**) (**c**)

Figure 40. Chronic Cl^- reduction-associated changes in eNOS activity. Quantification of western blots from Figure 28 showing basal, non-induced level of eNOS phosphorylation at Ser1177 and Thr495 (a) and after 15 min of ACh stimulation (b). (c) Quantification of western blots from Figure 28 showing changes in ERK1/2 signalling pathway upon incubation of PAECs in N or M. Figures were generated with 4 samples. Ratio-paired t-test. (Reproduced from (1) in accordance with the MDPI and the CC BY 4.0 license).

4.6. TMEM16A-associated endothelial dysfunction leads to a malfunctioned pulmonary arterial vasodilation

Increased TMEM16A proved to be disruptive for eNOS productivity, significantly lowering the production of NO, the main endothelium-derived vasodilatory factor. Therefore, I looked further into the possible functional consequences on a larger, more complex system. Freshly-isolated human PAs were incubated with control or TMEM16A-overexpressing adenovirus and left in culture for 48 h to achieve sufficient increase in TMEM16A level. I confirmed this with a western blot analysis showing a rise in TMEM16A expression after 48 h (**Figure 41)**.

Alternatively, using the same protocol lead to the overexpression in donor PCLS. By immunofluorescence staining I could show that TMEM16A is localized to vWF^+ compartment (**Figure 42**).

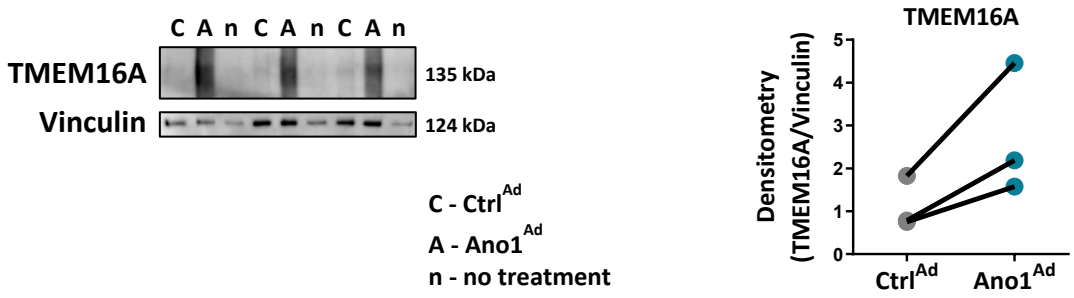

Figure 41. Overexpression of TMEM16A in donor pulmonary arteries. Western blot of healthy donor pulmonary artery infected with either $Ctrl^{Ad}$ or $Ano1^{Ad}$ with quantification of TMEM16A overexpression (right). (Reproduced from (1) in accordance with the MDPI and the CC BY 4.0 license).

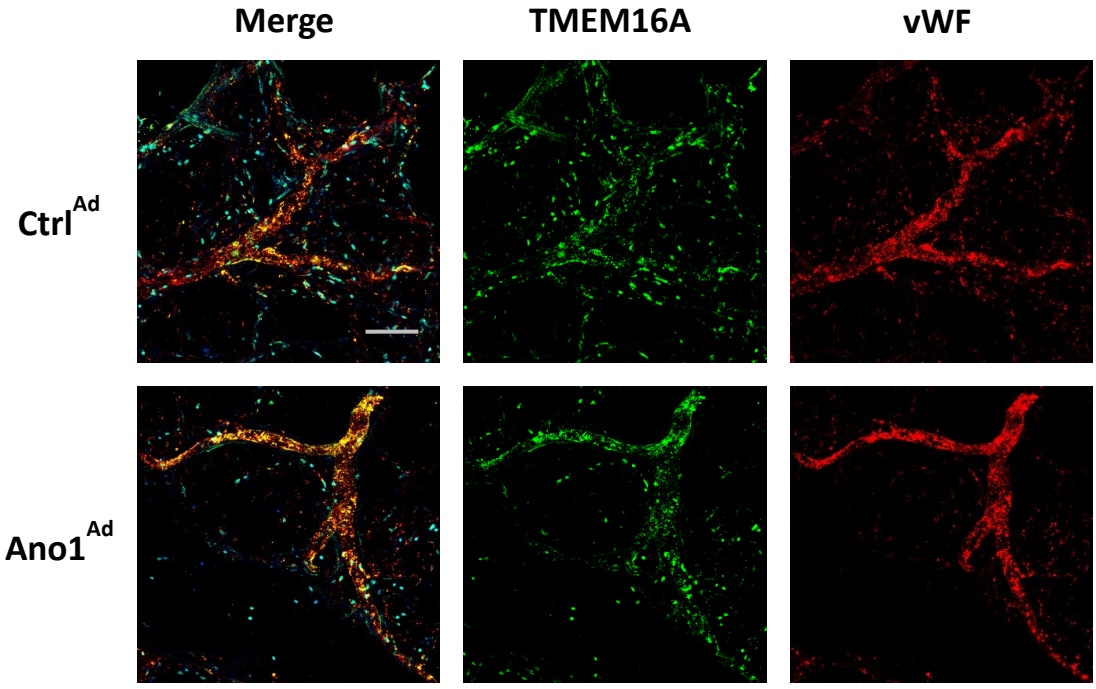

Figure 42. Immunofluorescence staining of adenovirus-infected precision-cut lung slices. Immunofluorescence staining of donor 3D precision-cut lung slices (PCLSs) infected

either with Ctrl^{Ad} or Ano1^{Ad} (scale bar = 100 µm). (PCLS processing was performed by dr. Diana Zabini, Medical University of Graz).

Having established TMEM16A overexpression in isolated donor PAs, I implemented isometric tension measurements to address if differences in NO production result in changes in vascular dilation *ex vivo* (**Figure 43a**). By using increasing concentrations of ACh I observed relaxation in both groups of vessels, yet the TMEM16A-overexpressing group demonstrated tendency for blunted ACh-mediated vasorelaxation (**Figure 43b**).

Taken together, this data suggests that TMEM16A overexpression causes disruption in ACh-mediated vasorelaxation with possibly other factors ultimately affecting the overall effect on the vessel tone.

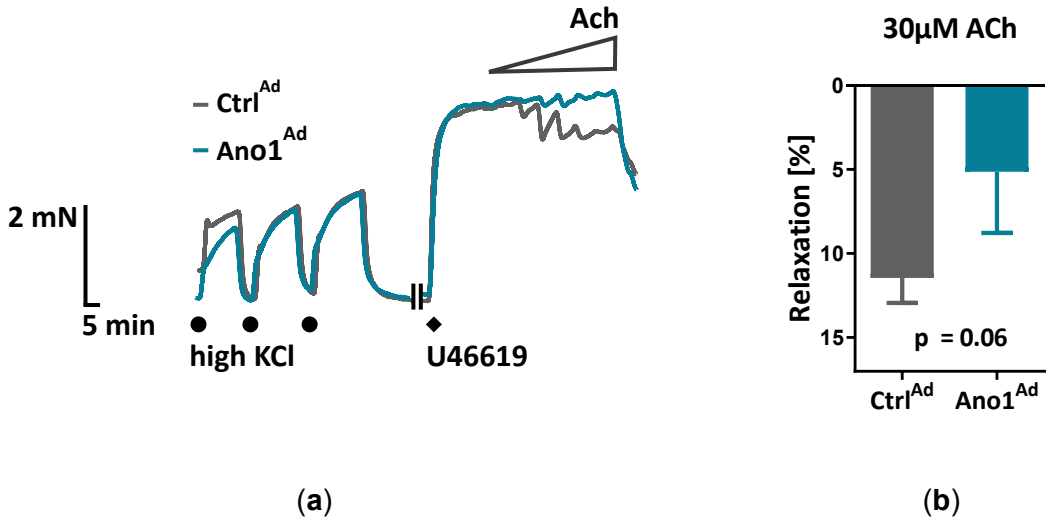

Figure 43. Acetylcholine-induced vasodilation of TMEM16A-overexpressing donor pulmonary arteries. (a) Representative isometric tension measurements of ACh-mediated vasorelaxation in pulmonary arteries (PAs) infected with either Ctrl^{Ad} or Ano1^{Ad}. (b) The effect of TMEM16A overexpression on 30 µM ACh-induced vasorelaxation of U46619 pre-constricted healthy donor pulmonary arteries. Figure was generated with 7 pairs of vessels taken from N = 3 donors. Unpaired t-test. (Obtained with the support from Neha Sharma, Medical University of Graz; reproduced from (1) in accordance with the MDPI and the CC BY 4.0 license).

5. Discussion

TMEM16A determines (patho)physiological characteristics of PAECs

Pulmonary arterial endothelial cells (PAECs) are an important source of factors maintaining homeostasis within the pulmonary vascular compartment. However, when dysfunctional they are also perfectly-positioned driver of pathological development. Ion-channelome represents an essential part in this balancing act, regulating all the aspects of maintaining endothelial cell identity and their progression towards endothelial dysfunction (3,53).

Cl^- channels have only recently gained importance, with their significance extending beyond the electrophysiological effects to reports of Cl^- anions acting as secondary signalling molecules (184). Even so, their contribution to the resting membrane potential (E_m) should not be underestimated. Although Cl^- channels have small open probability at negative potentials, they are partially active at E_m in endothelial cells. Thus, small changes in the activity of these channels in non-stimulated endothelial cells could significantly affect their homeostasis (51,56,59–62). An important part of Cl^- conductivity is the Ca^{2+}-activated Cl^- current (CaCC), which is mainly mediated by TMEM16A, first described in 2008 (215,216,237). Since then, its activity has been connected to the maintenance of different physiological processes in healthy organ systems. Likewise, its pathological footprint has been highlighted in several pathologies, including of systemic and pulmonary vasculature (57,65,243,245,353).

Within the vasculature, TMEM16A has been mostly studied in its effect on smooth muscle cells. We have previously shown, that TMEM16A regulates CaCC of PASMCs (57). Owing to the essential communication of vascular cells on the one hand and the strategical position of PAECs as regulators in the vessel lumen on the other, we hypothesized that TMEM16A plays an important regulatory role in the homeostasis of PAECs and thus homeostasis of the vasculature. In the current study, we have investigated TMEM16A expression in different compartments of the lung (PASMCs, PAECs and lung homogenate) and detected high protein level of the channel in PAECs. Using whole-cell voltage clamp studies and TMEM16A-specific inhibitor benzbromarone (Bbr) we not only demonstrated higher CaCC in PAECs but also attributed the observed CaCC to the activity of TMEM16A. In relation, we are the first to show the presence of a functional TMEM16A in the plasma membrane of primary human PAECs.

We have chosen Bbr for TMEM16A inhibition because it proved to be the most effective. There are multiple inhibitors of TMEM16A on the market showing different levels of potency but their specificity has been questioned, since these inhibitors sometimes demonstrate an additional effect on a highly similar TMEM16B on the one hand, CFTR on the other or interact with intracellular Ca^{2+} signalling (354–356). A new potent inhibitor Ani9 has been reported to be highly specific, not affecting TMEM16B or intracellular Ca^{2+} signalling (357). We confirmed its potency with patch-clamp studies and its potential as a therapeutic agent with isometric tension measurements of preconstricted mouse PAs on the one hand and in isolated and perfused rat lung studies on the other. Even though Ani9 elicited up to 50 % vasorelaxation effect, Bbr proved to be a better vasorelaxation-eliciting pharmacological agent (57). In isometric tension measurements of preconstricted mouse PAs Bbr caused up to 90 % vasorelaxation and though this effect was mostly mediated by its action on PASMCs, we could nevertheless show that the effect is partly mediated by TMEM16A localized in pulmonary endothelium. Furthermore, using eNOS inhibitor L-NAME, we could provide valuable insight into the mechanism of Bbr connecting TMEM16A and eNOS further emphasizing the importance of a healthy, balanced endothelium.

IPAH is pathologically determined by TMEM16A dysbalance

Idiopathic pulmonary arterial hypertension (IPAH) is a progressive disease hallmarked by dysbalanced ion-channelome and endothelial dysfunction. Traditionally potassium channels were featured in understanding the detrimental role of dysbalanced ion conductance (64). More recently, Cl^- channels have proven to be another pathologically-relevant factor and an intriguing target (57). Targeting TMEM16A alleviated established pathophysiological and pathomorphological developments in hypoxic mouse and monocrotaline rat models of pulmonary hypertension (57). On the other hand, TMEM16A has been shown elevated in PAECs isolated from IPAH (65), yet its role in driving the endothelial dysfunction has remained underrepresented. Our western blot analysis of whole cell lysate could not demonstrate an increase of TMEM16A expression in PAECs isolated from IPAH patients at the expected 114 kDa size. However, we could detect a prominent increase at the size of approximately 70-80 kDa. It is known that TMEM16A gene *Ano1* goes through several different alternative splicing events producing several isoforms that can (i) demonstrate different activity characteristics, (ii) localize to specific tissues or (iii) are themselves hallmarking pathological states (230). This highlights the heterogeneity of Cl^-

current and its importance in the homeostasis of healthy tissue on the one hand and in the pathogenesis of diseased tissue on the other. While further investigation would be needed to delineate the specifics of the detected isoform in IPAH PAECs, isoforms of this size have been reported before (230). In murine portal vein, guinea pig brain and colon cells a band of similar size was detected (358,359). In the former, they speculated the band cannot be an isoform omitting a, b, c and d parts of the protein since the size difference is too big. They hypothesize that the differences in TMEM16A size are either due to a new, previously not shown alternative splicing and/or posttranslational modification processes (358). On the other hand, a Δ3'exon 21 tandem splice site, reported conserved in human, would shift the protein out of frame at the amino acid M702 (mouse TMEM16A; NP_848757) resulting in a truncated TMEM16A with an altered C-terminus and a size of approximately 84 kDa (230). Since the previous report of increased TMEM16A in IPAH PAECs does not report its size (65), it is plausible we have confirmed their finding at the level of whole-cell protein or found an additional mechanism of dysfunctional Cl^- conductance in IPAH PAECs. It would be interesting to determine, whether the isolation and western blot analysis of outer cell membrane protein fraction would change the relative levels of any specific TMEM16A isoforms. Moreover, further investigations would be needed if an isoform of approximately 70-80 kDa represents TMEM16A and to determine its electrophysiological characteristics. If confirmed, it could potentially represent an IPAH-specific TMEM16A in PAECs; otherwise not expressed but increased levels can be detected in the pathological environment of PAECs isolated from IPAH patients. Even so, we could show for the first time increased TMEM16A-associated I_{ClCa} in PAECs isolated from IPAH patients, emphasized by I_{ClCa} correlating with Bbr-mediated inhibition.

IPAH-mimicking TMEM16A increase leads to endothelial dysfunction

To mimic increased TMEM16A activity as determined in IPAH PAECs, we developed a model using healthy donor PAECs in combination with adenoviral overexpression of TMEM16A. With the use of this model, we determined increased TMEM16A protein level going in hand with increased activity in the outer cell membrane. TMEM16A-overexpressing PAECs and PASMCs were chronically depolarized and demonstrated aberrancies in Ca^{2+} dynamics; we defined these as changes in (i) basal Ca^{2+} concentration, (ii) extracellular Ca^{2+} influx and (iii) endoplasmic reticulum-(ER) allocated Ca^{2+} level.

While TMEM16A overexpression caused an increase in cytosolic Ca^{2+} concentration of PAECs and PASMCs, it had opposite effects on extracellular Ca^{2+} influx and store Ca^{2+} levels further emphasizing key differences between the cell types. We suggest that observed TMEM16A-mediated intracellular Ca^{2+} increase might be a consequence of VGCC activity in PASMCs, whereas in PAECs the mechanisms of store-operated Ca^{2+} entry (SOCE) are more likely. By emptying the ER with the help of 2,5-Di-*t*-butyl-1,4-benzohydroquinone (BHQ), we could define that the Ca^{2+} store of TMEM16A-overexpressing PAECs, as opposed to PASMCs, holds higher amount of Ca^{2+}. On the other hand, after the removal and reintroduction of extracellular Ca^{2+}, the influx in PAECs is lower as opposed to PASMCs, suggesting that the extracellular influx is probably not responsible for the cytosolic nor store-related Ca^{2+} rise via increased sequestration of cytosolic Ca^{2+}. This opposite effect could represent key cell-type-specific differences in ion channelome signature, e.g. voltage-gated Ca^{2+} channels (VGCC) and transient receptor potential (TRP) channels. In contrast to PAECs (106–108), PASMCs express L-type Ca^{2+} channels, which represent the main voltage-sensitive Ca^{2+} entry pathway. Their absence in PAECs might explain the decreased Ca^{2+} influx, since resident T-type VGCC have lower conductivity and deactivate faster thus seem unlikely to link chronic membrane depolarization to the observed Ca^{2+} disruptions (109). Moreover, TRP channels, specifically TRPC, are important for the ion homeostasis of both cell types, having been implicated in the pathogenesis of different diseases (112–114). In TMEM16A-overexpressing PASMCs, TRP channels could be responsible for the voltage-independent increase in Ca^{2+} influx, thus account for the rise in cytosolic concentration (114). Finally, R-type Ca^{2+} channels could be responsible for a sustained Ca^{2+} influx during long-lasting depolarization (111).

We propose that TMEM16A-overexpressing PAECs develop an ER leak and hypothesize that this could represent either (i) a dysfunctional store-operated Ca^{2+} entrance (SOCE) whereas higher activation of SOCE would cause continuous ER leak or (ii) dysfunctional ER leak continuously emptying the store thus repeatedly activating SOCE. In connection, ER Ca^{2+} sensors STIM1 and STIM2 (83,84) have been implicated in SOCE-associated Ca^{2+} disruptions across different conditions, including IPAH albeit in PASMCs (85–87). With ER stress being an important part of PAH endothelial dysfunction (77,88) and Ca^{2+} leak being an essential part of ER stress (89), STIM1 and 2 could be of interest in further delineating mechanisms of endothelial dysfunction in IPAH (90). In relation, the discrepancies in the activation of apoptotic pathways reported here and shown by Allawzi *et al*. (65) could likewise be attributed to Ca^{2+} dynamics. ER leak-associated

increase in cytosolic and mitochondrial Ca^{2+} concentrations promotes oxidative phosphorylation in the early stages (360), yet chronically it activates apoptotic pathways (78). An imbalanced rate of basal Ca^{2+} flux out of the ER would therefore be a plausible option, since there is a precedence in Alzheimers disease, where these changes have been associated with observed changes in Ca^{2+} homeostasis (361,362). Furthermore, changes in basal Ca^{2+} homeostasis have been connected to endothelial dysfunction in general and various diseases, ranging from neurodegenerative to cardiac and kidney disease (87). Moreover, there seems to be a communication between numerous ER leak channels and SERCA pumps keeping the balance in the ER and cytosol Ca^{2+} levels. Besides leak channels, these cells could alternatively have either a SERCA dysregulation or a prevalence of a different isomer.

TMEM16A-ERK1/2 axis could be connected to vascular and eNOS homeostasis

Ca^{2+} dynamics represents one of the most important cellular signalling pathways. An increase in Ca^{2+} levels of PAECs should be an important signal for proliferation, wound-healing, angiogenesis and NO production (127). Even though TMEM16A-primed PAECs develop increased cytosolic Ca^{2+} concentration, we identified many of these processes lacking the Ca^{2+}-associated response. The connection between TMEM16A and the activation of Akt or MAPK has been explored before in the field of cancer (194,196,363–366), and it was similarly established that Akt and MAPK ERK1/2, JNK and p38 respond to intracellular Cl^- concentration (367–371). Furthermore, it has been shown before that TMEM16A is able to modulate intracellular Cl^- concentration leading to E_m depolarization and Ca^{2+} increase (66), yet its activity affects downstream pathways in sometimes opposing ways (194,195,243,244,372,373), implying that there are other factors determining its influence on cell physiology. We hypothesized that TMEM16A-mediated chronic Cl^- decrease would, apart from E_m and Ca^{2+} dynamics, affect other pathways necessary to maintain endothelial cell identity. We could show that increased TMEM16A activity in primary human PAECs leaves Akt and MAPK signalling intact, except for ERK1/2. ERK1/2 is a positive regulator of endothelial cell proliferation and angiogenesis and interestingly its deletion does not affect apoptosis (161–166). Furthermore, ERK1/2 silencing could be a part of the observed metabolic change shifting PAECs from angiogenesis- and migration-favoured glycolytic to oxidative metabolism (141). To this end, we are the first to demonstrate the tendency of ERK1/2 pathway deactivation by chronic intracellular Cl^- reduction of primary human PAECs, which in

healthy vascular endothelial cells positively responds to brief increases in intracellular Ca^{2+} concentration (156–158). We propose that TMEM16A-ERK1/2 axis represents a novel mechanism of angiogenic dysfunction in pulmonary endothelium.

Our results suggest that TMEM16A affects NO production. ERK1/2 has been connected to eNOS activation and NO production before, yet its eNOS target sites have been somewhat controversial (156,171–178). During our experimental setup, we have looked into the phosphorylation of two main target sites, activatory Ser1177 and inhibitory Thr495. Other ERK1/2 target sites have been reported but were not the focus of this study (176). In the absence of other reported eNOS-manipulating pathways, we assumed that complex ERK1/2 signalling could prove to mediate eNOS dysfunction. Since TMEM16A-primed PAECs demonstrated downregulated ERK1/2 pathway and counterintuitively increased Ser1177 eNOS phosphorylation, the role of ERK1/2 would be difficult to define without further investigations. In this manner, the effect of implementing ERK1/2 inhibitor or activator would be interesting. On another hand ERK1/2 has been reported responsible for continuous phosphorylation of the inhibitory site Thr495, meaning a decrease in ERK1/2 activity could explain an increase in the background activity of eNOS upon TMEM16A overexpression (178,374). Since background eNOS activity and stable production of NO is an essential part of maintaining low vascular tone in normoxic conditions (4), this could make TMEM16A-primed PAECs mediator of a dysfunctional background eNOS activity thus affecting the vascular tone in normoxic conditions.

On a similar note, we demonstrated increased TMEM16A-associated activation of eNOS. The pathway remained intact, supported by responding to ACh stimulation with even further intensification of the activated state. However, the measured NO level was significantly lower. Several mechanism could contribute to the reduction of detected NO; on the one hand eNOS activation may not be complete, mediated by the uncoupling of the enzyme, dimer disruption or cofactor BH4 depletion (176,349,375,376). On the other hand, the reduced NO might correlate with its reduced bioavailability, i.e. produced NO could be scavenged by reactive oxygen species producing reactive nitrogen species likewise detrimental to the vascular homeostasis in PAH (349).

Alterations in angiogenic (21,32,377), eNOS (38–45) and ERK1/2 (378) pathways observed in our and previous IPAH studies emphasizes their role in the development of the disease. We could show that our TMEM16A-primed PAEC model of IPAH causes a decrease in ERK1/2

phosphorylation. In contrast, IPAH studies could observe an activation of the ERK1/2 pathway (378). This may indicate that the high presence of growth factors in IPAH patients (379–383) strongly activate ERK1/2 (141,384,385), while increased TMEM16A is meant to counteract this effect, seemingly unsuccessful at a late stage of the disease. On the other hand, our study reveals several important roles of TMEM16A in PAECs. On the one hand TMEM16A-mediated CaCC maintains E_m and thus defines the Ca^{2+} landscape of healthy cells, on the other it maintains the diseased PAEC phenotype, thus becoming a part of the IPAH-PAEC signature. In IPAH patients (38–45) as well as in animal models of pulmonary hypertension (PH) (386–389), disrupted eNOS pathway has been shown. Hypoxic mice and monocrotaline rat models of PH have impaired ACh-mediated vasorelaxation (46) and persistent eNOS activation induces PH in mice and humans with the vasodilation defect (35). In our study we could show the influence of increased TMEM16A on the weakening of ACh-mediated vasorelaxation, further emphasizing the role of TMEM16A.

Our study has some limitations. (i) Concerning the NO pathway, we have shown lower NO levels going together with higher eNOS activation. We have not looked at the level of any eNOS cofactors, eNOS localization nor if there is less NO production or is the existing being siphoned into peroxynitrite. Many of existing questions could be addressed with either live-cell NO or peroxynitrite imaging following NO dynamics within TMEM16A-overexpressing PAECs. Furthermore, even though ERK1/2 modulates eNOS activation, we have not been able to connect it via the observed phosphorylating sites. On the other hand it is possible that lack of ERK1/2 prevents the complete eNOS activation, resulting in lower NO output. We could start addressing the question by systematically looking at all of the ERK1/2 target eNOS sites.

(ii) Concerning the TMEM16A / reduced [Cl^-] - ERK1/2 axis: we have no direct evidence of ERK1/2 involvement in the pathogenesis of endothelial dysfunction. Further studies involving pharmacological modulation of ERK1/2 would be useful in addressing if manipulation of the pathway could either reproduce or save the observed phenotype.

(iii) Concerning the IPAH PAECs: we cannot exclude changes in the biophysical properties of the TMEM16A channel in IPAH PAECs including its activation or Ca^{2+}-binding properties. Furthermore, we have shown an increase in TMEM16A level in IPAH PAECs but at a size that could belong to a different isoform. Even though we show higher whole-cell Ca^{2+}-activated Cl^- current as well as the Bbr-responsive current, we cannot be sure whether the observed is a

TMEM16A isoform nor of its activation properties. These could be investigated by systematically isolating and biophysically characterizing the observed protein. Moreover, we did not investigate other readouts in IPAH PAECs besides patch-clamp. Therefore, we cannot provide direct evidence that silencing of TMEM16A would normalize the IPAH phenotype. Especially useful would be the contribution of an endothelial cell-specific TMEM16A overexpression or knock-out mouse model.

(iv) While TMEM16A-mediated changes in PAEC phenotype described here are consistent with ERK1/2 deactivation, the effects could possibly be traced back to the efficacy of growth factor signalling, e.g. VEGFR2 (390), otherwise essentially interconnected with ERK1/2 and eNOS (90). In this manner the ultimate effect of TMEM16A-mediated chronic intracellular Cl^- decrease could interference with growth factor pathways indirectly disturbing ERK1/2 signalling.

6. Conclusion

Within the scope of this work we were able to extend the pathological footprint of TMEM16A beyond its effect on smooth muscle cell physiology and show its role in the fundamental disruption of downstream signalling pathways otherwise essential to the identity of an endothelial cell. Increased Ca^{2+} levels of PAECs should promote proliferation, angiogenesis and nitric oxide production, however increased TMEM16A activity weakens the Ca^{2+} responsiveness of these processes. We traced these detrimental effects to ERK1/2 inactivation, a pathway essentially interconnected with all the crucial endothelial-defining processes. As a result, we have established that disease-associated TMEM16A activity pathologically primes healthy pulmonary arteries and ultimately causes severe deficiencies resembling of that found in PAH.

7. Bibliography

1. Skofic Maurer D, Zabini D, Nagaraj C, Sharma N, Lengyel M, Nagy BM, et al. Endothelial Dysfunction Following Enhanced TMEM16A Activity in Human Pulmonary Arteries. Cells. 2020;9(9):1984.
2. Kovacs G, Berghold A, Scheidl S, Olschewski H. Pulmonary arterial pressure during rest and exercise in healthy subjects: A systematic review. Eur Respir J. 2009;34(4):888–94.
3. Huertas A, Guignabert C, Barberà JA, Bärtsch P, Bhattacharya J, Bhattacharya S, et al. Pulmonary vascular endothelium: The orchestra conductor in respiratory diseases. Eur Respir J. 2018;51(4):1700745.
4. Dinh-Xuan AT. Endothelial modulation of pulmonary vascular tone. Eur Respir J. 1992;5(6):757–62.
5. Simonneau G, Montani D, Celermajer DS, Denton CP, Gatzoulis MA, Krowka M, et al. Haemodynamic definitions and updated clinical classification of pulmonary hypertension. Eur Respir J. 2019;53(1).
6. Rabinovitch M. Molecular pathogenesis of pulmonary arterial hypertension. J Clin Invest. 2012 Dec 3;122(12):4306–13.
7. Stacher E, Graham BB, Hunt JM, Gandjeva A, Groshong SD, McLaughlin V V., et al. Modern age pathology of pulmonary arterial hypertension. Am J Respir Crit Care Med. 2012;186(3):261–72.
8. Tuder RM, Stacher E, Robinson J, Kumar R, Graham BB. Pathology of pulmonary hypertension. Vol. 34, Clinics in Chest Medicine. 2013. p. 639–50.
9. Sheikh AQ, Lighthouse JK, Greif DM. Recapitulation of developing artery muscularization in pulmonary hypertension. Cell Rep. 2014;6(5):809–17.
10. Fourie PR, Coetzee AR, Bolliger CT. Pulmonary artery compliance: Its role in right ventricular-arterial coupling. Cardiovasc Res. 1992;26(9):839–44.
11. Vonk-Noordegraaf A, Haddad F, Chin KM, Forfia PR, Kawut SM, Lumens J, et al. Right heart adaptation to pulmonary arterial hypertension: Physiology and pathobiology. J Am

Coll Cardiol. 2013;62(25 SUPPL.):D22–33.

12. Bogaard HJ, Abe K, Noordegmaf AV, Voelkel NF. The right ventricle under pressure. Chest. 2009;135(3):794–804.

13. Humbert M, Sitbon O, Chaouat A, Bertocchi M, Habib G, Gressin V, et al. Survival in patients with idiopathic, familial, and anorexigen-associated pulmonary arterial hypertension in the modern management era. Circulation. 2010;122(2):156–63.

14. Stenmark KR, McMurtry IF. Vascular remodeling versus vasoconstriction in chronic hypoxic pulmonary hypertension: A time for reappraisal? Circ Res. 2005;97(2):95–8.

15. Abe K, Shinoda M, Tanaka M, Kuwabara Y, Yoshida K, Hirooka Y, et al. Haemodynamic unloading reverses occlusive vascular lesions in severe pulmonary hypertension. Cardiovasc Res. 2016;111(1):16–25.

16. Huertas A, Perros F, Tu L, Cohen-Kaminsky S, Montani D, Dorfmüller P, et al. Immune dysregulation and endothelial dysfunction in pulmonary arterial hypertension: A complex interplay. Circulation. 2014;129(12):1332–40.

17. Guignabert C, Tu L, Girerd B, Ricard N, Huertas A, Montani D, et al. New molecular targets of pulmonary vascular remodeling in pulmonary arterial hypertension: Importance of endothelial communication. Chest. 2015;147(2):529–37.

18. Schermuly RT, Ghofrani HA, Wilkins MR, Grimminger F. Mechanisms of disease: Pulmonary arterial hypertension. Nat Rev Cardiol. 2011;8(8):443–55.

19. Humbert M, Guignabert C, Bonnet S, Dorfmüller P, Klinger JR, Nicolls MR, et al. Pathology and pathobiology of pulmonary hypertension: state of the art and research perspectives. Eur Respir J. 2019;53(1):1801887.

20. Morrell NW, Adnot S, Archer SL, Dupuis J, Lloyd Jones P, MacLean MR, et al. Cellular and Molecular Basis of Pulmonary Arterial Hypertension. J Am Coll Cardiol. 2009;54(1 SUPPL. 1):S20–31.

21. Masri FA, Xu W, Comhair SAA, Asosingh K, Koo M, Vasanji A, et al. Hyperproliferative apoptosis-resistant endothelial cells in idiopathic pulmonary arterial hypertension. Am J Physiol - Lung Cell Mol Physiol. 2007;293(3):L548–54.

22. TARASEVICIENE-STEWART L, KASAHARA Y, ALGER L, HIRTH P, MAHON GM, WALTENBERGER J, et al. Inhibition of the VEGF receptor 2 combined with chronic hypoxia causes cell death-dependent pulmonary endothelial cell proliferation and severe pulmonary hypertension. FASEB J. 2001;15(2):427–38.

23. Abe K, Toba M, Alzoubi A, Ito M, Fagan KA, Cool CD, et al. Formation of plexiform lesions in experimental severe pulmonary arterial hypertension. Circulation. 2010;121(25):2747–54.

24. Lee S Do, Shroyer KR, Markham NE, Cool CD, Voelkel NF, Tuder RM. Monoclonal endothelial cell proliferation is present in primary but not secondary pulmonary hypertension. J Clin Invest. 1998;101(5):927–34.

25. Deng Z, Morse JH, Slager SL, Cuervo N, Moore KJ, Venetos G, et al. Familial primary pulmonary hypertension (Gene PPH1) is caused by mutations in the bone morphogenetic protein receptor-II gene. Am J Hum Genet. 2000;67(3):737–44.

26. Lane KB, Machado RD, Pauciulo MW, Thomson JR, Phillips JA, Loyd JE, et al. Heterozygous germline mutations in BMPR2, encoding a TGF-β receptor, cause familial primary pulmonary hypertension. Nat Genet. 2000;26(1):81–4.

27. Morisaki H, Nakanishi N, Kyotani S, Takashima A, Tomoike H, Morisaki T. BMPR2 mutations found in Japanese patients with familial and sporadic primary pulmonary hypertension. Hum Mutat. 2004;23(6):632.

28. Koehler R, Grünig E, Pauciulo MW, Hoeper MM, Olschewski H, Wilkens H, et al. Low frequency of BMPR2 mutations in a German cohort of patients with sporadic idiopathic pulmonary arterial hypertension. J Med Genet. 2004;41(12):e127.

29. Ulrich S, Szamalek-Hoegel J, Hersberger M, Fischler M, Garcia JS, Huber LC, et al. Sequence variants in BMPR2 and genes involved in the serotonin and nitric oxide pathways in idiopathic pulmonary arterial hypertension and chronic thromboembolic pulmonary hypertension: Relation to clinical parameters and comparison with left heart diseas. Respiration. 2010;79(4):279–87.

30. Austin ED, Ma L, LeDuc C, Rosenzweig EB, Borczuk A, Phillips JA, et al. Whole exome sequencing to identify a novel gene (Caveolin-1) associated with human pulmonary arterial

hypertension. Circ Cardiovasc Genet. 2012;5(3):336–43.

31. Upton PD, Morrell NW. The transforming growth factor-β-bone morphogenetic protein type signalling pathway in pulmonary vascular homeostasis and disease. Exp Physiol. 2013;98(8):1262–6.

32. Geraci MW, Moore M, Gesell T, Yeager ME, Alger L, Golpon H, et al. Gene expression patterns in the lungs of patients with primary pulmonary hypertension: A gene microarray analysis. Circ Res. 2001;88(6):555–62.

33. Schermuly RT, Stasch JP, Pullamsetti SS, Middendorff R, Müller D, Schlüter KD, et al. Expression and function of soluble guanylate cyclase in pulmonary arterial hypertension. Eur Respir J. 2008;32(4):881–91.

34. Wharton J, Strange JW, Møller GMO, Growcott EJ, Ren X, Franklyn AP, et al. Antiproliferative effects of phosphodiesterase type 5 inhibition in human pulmonary artery cells. Am J Respir Crit Care Med. 2005;172(1):105–13.

35. Zhao YY, Zhao YD, Mirza MK, Huang JH, Potula HHSK, Vogel SM, et al. Persistent eNOS activation secondary to caveolin-1 deficiency induces pulmonary hypertension in mice and humans through PKG nitration. J Clin Invest. 2009;119(7):2009–18.

36. Bowers R, Cool C, Murphy RC, Tuder RM, Hopken MW, Flores SC, et al. Oxidative Stress in Severe Pulmonary Hypertension. Am J Respir Crit Care Med. 2004;169(6):764–9.

37. Cracowski JL, Cracowski C, Bessard G, Pepin JL, Bessard J, Schwebel C, et al. Increased lipid peroxidation in patients with pulmonary hypertension. Am J Respir Crit Care Med. 2001;164(6):1038–42.

38. Giaid A, Saleh D. Reduced expression of endothelial nitric oxide synthase in the lungs of patients with pulmonary hypertension. N Engl J Med. 1995;333(4):214–21.

39. Özkan M, Dweik RA, Laskowski D, Arroliga AC, Erzurum SC. High levels of nitric oxide in individuals with pulmonary hypertension receiving epoprostenol therapy. Lung. 2001;179(4):233–43.

40. Kaneko FT, Arroliga AC, Dweik RA, Comhair SA, Laskowski D, Oppedisano R, et al. Biochemical reaction products of nitric oxide as quantitative markers of primary pulmonary

hypertension. Am J Respir Crit Care Med. 1998;158(3):917–23.

41. Tuder RM, Cool CD, Geraci MW, Wang J, Abman SH, Wright L, et al. Prostacyclin synthase expression is decreased in lungs from patients with severe pulmonary hypertension. Am J Respir Crit Care Med. 1999;159(6):1925–32.

42. Xue C, Johns RA, Giaid A, Saleh D. Endothelial nitric oxide synthase in the lungs of patients with pulmonary hypertension. N Engl J Med. 1995;333(24):1642–4.

43. Mason NA, Springall DR, Burke M, Pollock J, Mikhail G, Yacoub MH, et al. High expression of endothelial nitric oxide synthase in plexiform lesions of pulmonary hypertension. J Pathol. 1998;185(3):313–8.

44. Fagan KA, Morrissey B, Fouty BW, Sato K, Harral JW, Morris KG, et al. Upregulation of nitric oxide synthase in mice with severe hypoxia-induced pulmonary hypertension. Respir Res. 2001;2(5):306–13.

45. Xu W, Kaneko FT, Zheng S, Comhair SAA, Janocha AJ, Goggans T, et al. Increased arginase II and decreased NO synthesis in endothelial cells of patients with pulmonary arterial hypertension. FASEB J. 2004;18(14):1746–8.

46. Mam V, Tanbe AF, Vitali SH, Arons E, Christou HA, Khalil RA. Impaired vasoconstriction and nitric oxide-mediated relaxation in pulmonary arteries of hypoxia- and monocrotaline-induced pulmonary hypertensive rats. J Pharmacol Exp Ther. 2010;332(2):455–562.

47. Achcar ROD, Demura Y, Rai PR, Taraseviciene-Stewart L, Kasper M, Voelkel NF, et al. Loss of caveolin and heme oxygenase expression in severe pulmonary hypertension. Chest. 2006;129(3):696–705.

48. Gratton JP, Fontana J, O'Connor DS, García-Cardeña G, McCabe TJ, Sessa WC. Reconstitution of an endothelial nitric-oxide synthase (eNOS), hsp90, and caveolin-1 complex in vitro: Evidence that hsp90 facilitates calmodulin stimulated displacement of eNOS from caveolin-1. J Biol Chem. 2000;275(29):22268–72.

49. Wertz JW, Bauer PM. Caveolin-1 regulates BMPRII localization and signaling in vascular smooth muscle cells. Biochem Biophys Res Commun. 2008;375(4):557–61.

50. Bonor J, Adams EL, Bragdon B, Moseychuk O, Czymmek KJ, Nohe A. Initiation of BMP2

signaling in domains on the plasma membrane. J Cell Physiol. 2012;227(7):2880–8.

51. Nilius B, Droogmans G. Ion channels and their functional role in vascular endothelium. Physiol Rev. 2001;81(4):1415–59.

52. Aird WC. Endothelium as an organ system. Crit Care Med. 2004;32(5 Suppl):S271-279.

53. Makino A, Firth AL, Yuan JXJ. Endothelial and smooth muscle cell ion channels in pulmonary vasoconstriction and vascular remodeling. Compr Physiol. 2011;1(3):1555–602.

54. Kamouchi M, Droogmans G, Nilius B. Membrane potential as a modulator of the free intracellular Ca2+ concentration in agonist-activated endothelial cells. Gen Physiol Biophys. 1999;18(2):199–208.

55. Lückhoff A, Busse R. Calcium influx into endothelial cells and formation of endothelium-derived relaxing factor is controlled by the membrane potential. Pflügers Arch Eur J Physiol. 1990;416(3):305–11.

56. Voets T, Droogmans G, Nilius B. Membrane currents and the resting membrane potential in cultured bovine pulmonary artery endothelial cells. J Physiol [Internet]. 1996;497(1):95–107. Available from: papers://d8e9569c-3053-4f4e-bfb0-c8b1b3194e73/Paper/p4650%5Cnhttp://doi.wiley.com/10.1113/jphysiol.1996.sp021752

57. Papp R, Nagaraj C, Zabini D, Nagy BM, Lengyel M, Maurer DS, et al. Targeting TMEM16A to reverse vasoconstriction and remodelling in idiopathic pulmonary arterial hypertension. Eur Respir J. 2019;53(6):1800965.

58. Mehrke G, Pohl U, Daut J. Effects of vasoactive agonists on the membrane potential of cultured bovine aortic and guinea-pig coronary endothelium. J Physiol. 1991;439(1):277–99.

59. Olschewski A, Olschewski H, Bräu ME, Hempelmann G, Vogel W, Safronov B V. Basic electrical properties of in situ endothelial cells of small pulmonary arteries during postnatal development. Am J Respir Cell Mol Biol. 2001;25(3):285–90.

60. Hogg DS, Albarwani S, Davies ARL, Kozlowski RZ. Endothelial cells freshly isolated from resistance-sized pulmonary arteries possess a unique K+ current profile. Biochem Biophys Res Commun. 1999;263(2):405–9.

61. Antigny F, Hautefort A, Meloche J, Belacel-Ouari M, Manoury B, Rucker-Martin C, et al. Potassium channel subfamily K member 3 (KCNK3) contributes to the development of pulmonary arterial hypertension. Circulation. 2016;133(14):1371–85.

62. Johns A, Lategan TW, Lodge NJ, Ryan US, Van Breemen C, Adams DJ. Calcium entry through receptor-operated channels in bovine pulmonary artery endothelial cells. Tissue Cell. 1987;19(6):733–45.

63. Wu G, Hamill OP. NPPB block of Ca++-activated Cl- currents in Xenopus oocytes. Pflügers Arch Eur J Physiol. 1992;420(2):227–9.

64. Lambert M, Capuano V, Olschewski A, Sabourin J, Nagaraj C, Girerd B, et al. Ion channels in pulmonary hypertension: A therapeutic interest? Int J Mol Sci. 2018;19(10):3162.

65. Allawzi AM, Vang A, Clements RT, Jhun BS, Kue NR, Mancini TJ, et al. Activation of anoctamin-1 limits pulmonary endothelial cell proliferation via p38–Mitogen-activated protein Kinase–dependent apoptosis. Am J Respir Cell Mol Biol. 2018;58(5):658–67.

66. He M, Ye W, Wang WJ, Sison ES, Jan YN, Jan LY. Cytoplasmic Cl- couples membrane remodeling to epithelial morphogenesis. Proc Natl Acad Sci U S A. 2017;114(52):E11161–9.

67. Parekh AB, Penner R. Store depletion and calcium influx. Physiol Rev. 1997;77(4):901–30.

68. Wood PG, Gillespie JI. Evidence for mitochondrial Ca2+-induced Ca2+ release in permeabilised endothelial cells. Biochem Biophys Res Commun. 1998;246(2):543–8.

69. Macer DRJ, Koch GLE. Identification of a set of calcium-binding proteins in reticuloplasm, the luminal content of the endoplasmic reticulum. J Cell Sci. 1988;91(1):61–70.

70. Ichas F, Jouaville LS, Mazat JP. Mitochondria are excitable organelles capable of generating and conveying electrical and calcium signals. Cell. 1997;89(7):1145–53.

71. Falcke M, Hudson JL, Camacho P, Lechleiter JD. Impact of mitochondrial Ca2+ cycling on pattern formation and stability. Biophys J. 1999;77(1):37–44.

72. Scheitlin CG, Julian JA, Shanmughapriya S, Madesh M, Tsoukias NM, Alevriadou BR. Endothelial mitochondria regulate the intracellular Ca2+ response to fluid shear stress. Am J Physiol - Cell Physiol. 2016;310(6):C479–90.

73. Csordás G, Thomas AP, Hajnóczky G. Quasi-synaptic calcium signal transmission between endoplasmic reticulum and mitochondria. EMBO J. 1999;18(1):96–108.

74. Hajnóczky G, Hager R, Thomas AP. Mitochondria suppress local feedback activation of inositol 1,4,5- trisphosphate receptors by Ca2+. J Biol Chem. 1999;274(20):14157–62.

75. Malli R, Frieden M, Trenker M, Graier WF. The role of mitochondria for Ca2+ refilling of the endoplasmic reticulum. J Biol Chem. 2005;280(13):12114–22.

76. Paulin R, Michelakis ED. The metabolic theory of pulmonary arterial hypertension. Circ Res. 2014;115(1):148–64.

77. Hu Y, Yang W, Xie L, Liu T, Liu H, Liu B. Endoplasmic reticulum stress and pulmonary hypertension. Pulm Circ. 2020;10(1):2045894019900121.

78. Bravo R, Vicencio JM, Parra V, Troncoso R, Munoz JP, Bui M, et al. Increased ER-mitochondrial coupling promotes mitochondrial respiration and bioenergetics during early phases of ER stress. J Cell Sci. 2011;124(13):2143–52.

79. Jacob R, Merritt JE, Hallam TJ, Rink TJ. Repetitive spikes in cytoplasmic calcium evoked by histamine in human endothelial cells. Nature. 1988;335(6185):40–5.

80. Brailoiu GC, Gurzu B, Gao X, Parkesh R, Aley PK, Trifa DI, et al. Acidic NAADP-sensitive calcium stores in the endothelium: Agonist-specific recruitment and role in regulating blood pressure. J Biol Chem. 2010;285(48):37133–7.

81. Faviaa A, Desiderib M, Gambaraa G, D'Alessioa A, Ruas M, Esposito B, et al. VEGF-induced neoangiogenesis is mediated by NAADP and two-pore channel-2 -dependent ca2+signaling. Proc Natl Acad Sci U S A. 2014;111(44):4706–15.

82. Berridge MJ, Lipp P, Bootman MD. The versatility and universality of calcium signalling. Nat Rev Mol Cell Biol. 2000;1(1):11–21.

83. Brandman O, Liou J, Park WS, Meyer T. STIM2 Is a Feedback Regulator that Stabilizes Basal Cytosolic and Endoplasmic Reticulum Ca2+ Levels. Cell. 2007;131(7):1327–39.

84. Cheng KT, Liu X, Ong HL, Swaim W, Ambudkar IS. Local Ca2+ entry via Orai1 regulates plasma membrane recruitment of TRPC1 and controls cytosolic Ca2+ signals required for specific cell functions. PLoS Biol. 2011;9(3):e1001025.

85. Song MY, Makino A, Yuan JXJ. STIM2 contributes to enhanced store-operated Ca2+ entry in pulmonary artery smooth muscle cells from patients with idiopathic pulmonary arterial hypertension. Pulm Circ. 2011;1(1):84–94.

86. Song S, Carr SG, McDermott KM, Rodriguez M, Babicheva A, Balistrieri A, et al. STIM2 (Stromal Interaction Molecule 2)–mediated increase in resting cytosolic free Ca2+ concentration stimulates PASMC proliferation in pulmonary arterial hypertension. Hypertension. 2018;71(3):518–29.

87. Camello C, Lomax R, Petersen OH, Tepikin A V. Calcium leak from intracellular store - The enigma of calcium signalling. Cell Calcium. 2002;32(5–6):355–61.

88. Smith P, Heath D. Electron microscopy of the plexiform lesion. Thorax. 1979;34(2):177–86.

89. Maamoun H, Benameur T, Pintus G, Munusamy S, Agouni A. Crosstalk between oxidative stress and endoplasmic reticulum (ER) stress in endothelial dysfunction and aberrant angiogenesis associated with diabetes: A focus on the protective roles of heme oxygenase (HO)-1. Front Physiol. 2019;10(FEB):70.

90. Moccia F, Negri S, Shekha M, Faris P, Guerra G. Endothelial Ca2+ signaling, angiogenesis and vasculogenesis: Just what it takes to make a blood vessel. Int J Mol Sci. 2019;20(16):3962.

91. Flavahan NA, Shimokawa H, Vanhoutte PM. Pertussis toxin inhibits endothelium-dependent relaxations to certain agonists in porcine coronary arteries. J Physiol. 1989;408(1):549–60.

92. Boulanger CM, Vanhoutte PM. G proteins and endothelium-dependent relaxations. J Vasc Res. 1997;34(3):175–85.

93. Shimokawa H, Flavahan NA, Vanhoutte PM. Loss of endothelial pertussis toxin-sensitive G protein function in atherosclerotic porcine coronary arteries. Circulation. 1991;83(2):652–60.

94. Berridge MJ. Inositol trisphosphate and calcium signalling. Nature. 1993;361(6410):315–25.

95. He H, Venema VJ, Gu X, Venema RC, Marrero MB, Caldwell RB. Vascular endothelial

growth factor signals endothelial cell production of nitric oxide and prostacyclin through Flk-1/KDR activation of c-Src. J Biol Chem. 1999;274(35):25130–5.

96. Meyer RD, Latz C, Rahimi N. Recruitment and activation of phospholipase Cγ1 by vascular endothelial growth factor receptor-2 are required for tubulogenesis and differentiation of endothelial cells. J Biol Chem. 2003;278(18):16347–55.

97. Prasad ARS, Logan SA, Nerem RM, Schwartz CJ, Sprague EA. Flow-related responses of intracellular inositol phosphate levels in cultured aortic endothelial cells. Circ Res. 1993;72(4):827–36.

98. Streb H, Irvine RF, Berridge MJ, Schulz I. Release of Ca2+ from a nonmitochondrial intracellular store in pancreatic acinar cells by inositol-1,4,5-trisphosphate. Nature. 1983;306(5938):67–9.

99. Zhang AY, Li PL. Vascular physiology of a Ca2+ mobilizing second messenger - Cyclic ADP-ribose. J Cell Mol Med. 2006;10(2):407–22.

100. Galione A, Lee HC, Busa WB. Ca2+-induced Ca2+ release in sea urchin egg homogenates: Modulation by cyclic ADP-Ribose. Science (80-). 1991;253(5024):1143–6.

101. Kwong TC, Liu X, Hwei LO, Ambudkar IS. Functional requirement for Orai1 in store-operated TRPC1-STIM1 channels. J Biol Chem. 2008;283(19):12935–40.

102. Abdullaev IF, Bisaillon JM, Potier M, Gonzalez JC, Motiani RK, Trebak M. Stim1 and orai1 mediate crac currents and store-operated calcium entry important for endothelial cell proliferation. Circ Res. 2008;103(11):1289–99.

103. Oike M, Gericke M, Droogmans G, Nilius B. Calcium entry activated by store depletion in human umbilical vein endothelial cells. Cell Calcium. 1994;16(5):367–76.

104. Catterall WA. Voltage-gated calcium channels. Cold Spring Harb Perspect Biol. 2011;3(8):1–23.

105. Franco-Obregón A, López-Barneo J. Differential oxygen sensitivity of calcium channels in rabbit smooth muscle cells of conduit and resistance pulmonary arteries. J Physiol. 1996;491(2):511–8.

106. Zhou C, Wu S. T-type calcium channels in pulmonary vascular endothelium.

Microcirculation. 2006;13(8):645–56.

107. Zhang B, Naik JS, Jernigan NL, Walker BR, Resta TC. Reduced membrane cholesterol limits pulmonary endothelial Ca2+ entry after chronic hypoxia. Am J Physiol - Hear Circ Physiol. 2017;312(6):H1176–84.

108. Braunstein TH, Inoue R, Cribbs L, Oike M, Ito Y, Holstein-Rathlou NH, et al. The role of L- and T-type calcium channels in local and remote calcium responses in rat mesenteric terminal arterioles. J Vasc Res. 2009;46(2):138–51.

109. Monteil A, Chemin J, Bourinet E, Mennessier G, Lory P, Nargeot J. Molecular and functional properties of the human α(1G) subunit that forms T-type calcium channels. J Biol Chem. 2000;275(9):6090–100.

110. Wu S, Haynes J, Taylor JT, Obiako BO, Stubbs JR, Li M, et al. CaV3.1 (α1G) T-type Ca2+ channels mediate vaso-occlusion of sickled erythrocytes in lung microcirculation. Circ Res. 2003;93(4):346–53.

111. Bkaily G, D'Orléans-Juste P, Naik R, Pérodin J, Stankova J, Abdulnour E, et al. PAF activation of a voltage-gated R-type Ca2+ channel in human and canine aortic endothelial cells. Br J Pharmacol. 1993;110(2):519–20.

112. Moccia F. Update on vascular endothelial Ca2+ signalling: A tale of ion channels, pumps and transporters. World J Biol Chem. 2012;3(7):127–58.

113. Gonzalez-Cobos JC, Trebak M. TRPC channels in smooth muscle cells. Front Biosci. 2010;15(3):1023–39.

114. Yu Y, Fantozzi I, Remillard C V., Landsberg JW, Kunichika N, Platoshyn O, et al. Enhanced expression of transient receptor potential channels in idiopathic pulmonary arterial hypertension. Proc Natl Acad Sci U S A [Internet]. 2004;101(38):13861–6. Available from: http://www.pubmedcentral.nih.gov/articlerender.fcgi?artid=518765&tool=pmcentrez&rendertype=abstract

115. Firth AL, Remillard C V., Yuan JXJ. TRP channels in hypertension. Vol. 1772, Biochimica et Biophysica Acta - Molecular Basis of Disease. 2007. p. 895–906.

116. Pedersen SF, Owsianik G, Nilius B. TRP channels: An overview. Cell Calcium. 2005;38(3-

4 SPEC. ISS.):233–52.

117. Tiruppathi C, Freichel M, Vogel SM, Paria BC, Mehta D, Flockerzi V, et al. Impairment of store-operated Ca2+ entry in TRPC4-/- mice interferes with increase in lung microvascular permeability. Circ Res. 2002;91(1):70–6.

118. Freichel M, Suh SH, Pfeifer A, Schweig U, Trost C, Weißgerber P, et al. Lack of an endothelial store-operated Ca2+ current impairs agonist-dependent vasorelaxation in TRP4-/- mice. Nat Cell Biol. 2001;3(2):121–7.

119. Lin MJ, Leung GPH, Zhang WM, Yang XR, Yip KP, Tse CM, et al. Chronic hypoxia-induced upregulation of store-operated and receptor-operated Ca2+ channels in pulmonary arterial smooth muscle cells: A novel mechanism of hypoxic pulmonary hypertension. Circ Res. 2004;95(5):496–505.

120. Wang XY, Mo D, Tian W, Liu XX, Zhou YG, Sun Y, et al. Inhibition of RhoA/ROCK signaling pathway ameliorates hypoxic pulmonary hypertension via HIF-1α-dependent functional TRPC channels. Toxicol Appl Pharmacol. 2019;369:60–72.

121. Hofmann T, Schaefer M, Schultz G, Gudermann T. Subunit composition of mammalian transient receptor potential channels in living cells. Proc Natl Acad Sci U S A. 2002;99(11):7461–6.

122. Wang J, Weigand L, Lu W, Sylvester JT, Semenza GL, Shimoda LA. Hypoxia inducible factor 1 mediates hypoxia-induced TRPC expression and elevated intracellular Ca 2+ in pulmonary arterial smooth muscle cells. Circ Res. 2006;98(12):1528–37.

123. Sweeney M, Yu Y, Platoshyn O, Zhang S, McDaniel SS, Yuan JXJ. Inhibition of endogenous TRP1 decreases capacitative Ca2+ entry and attenuates pulmonary artery smooth muscle cell proliferation. Am J Physiol - Lung Cell Mol Physiol [Internet]. 2002;283(1 27-1):L144-55. Available from: papers://d8e9569c-3053-4f4e-bfb0-c8b1b3194e73/Paper/p83

124. Fantozzi I, Zhang S, Platoshyn O, Remillard C V., Cowling RT, Yuan JXJ. Hypoxia increases AP-1 binding activity by enhancing capacitative Ca 2+ entry in human pulmonary artery endothelial cells. Am J Physiol - Lung Cell Mol Physiol. 2003;285(6 29-6):L1233–45.

125. Paria BC, Vogel SM, Ahmmed GU, Alamgir S, Shroff J, Malik AB, et al. Tumor necrosis

factor-α-induced TRPC1 expression amplifies store-operated Ca2+ influx and endothelial permeability. Am J Physiol - Lung Cell Mol Physiol. 2004;287(6 31-6):L12303–L1313.

126. Vasauskas AA, Chen H, Wu S, Cioffi DL. The serine-threonine phosphatase calcineurin is a regulator of endothelial store-operated calcium entry. Pulm Circ. 2014;4(1):116–27.

127. Filippini A, D'Amore A, D'Alessio A. Calcium mobilization in endothelial cell functions. Int J Mol Sci. 2019;20(18):4525.

128. Knot HJ, Laher I, Sobie EA, Guatimosim S, Gomez-Viquez L, Hartmann H, et al. Twenty years of calcium imaging: Cell physiology to dye for. Mol Interv. 2005;5(2):112–27.

129. Patel V, Brown C, Goodwin A, Wilkie N, Boarder MR. Phosphorylation and activation of p42 and p44 mitogen-activated protein kinase are required for the P2 purinoceptor stimulation of endothelial prostacyclin production. Biochem J. 1996;320(1):221–6.

130. Graier WF, Sturek M, Kukovetz WR. Ca2+ Regulation and Endothelial Vascular Function. Endothelium. 1994;1(4):223–36.

131. Kajimura M, O'Donnell ME, Curry FE. Effect of cell shrinkage on permeability of cultured bovine aortic endothelia and frog mesenteric capillaries. J Physiol. 1997;503(2):413–25.

132. Kajimura M, Curry FE. Endothelial cell shrinkage increases permeability through a Ca2+-dependent pathway in single frog mesenteric microvessels. J Physiol. 1999;518(1):227–38.

133. Noll T, Hölschermann H, Koprek K, Gündüz D, Haberbosch W, Tillmanns H, et al. ATP reduces macromolecule permeability of endothelial monolayers despite increasing [Ca2+](i). Am J Physiol - Hear Circ Physiol. 1999;276(6):H1892–901.

134. Verin AD, Gilbert-McClain LI, Patterson CE, Garcia JGN. Biochemical regulation of the nonmuscle myosin light chain kinase isoform in bovine endothelium. Am J Respir Cell Mol Biol. 1998;19(5):767–76.

135. Wu H Mac, Yuan Y, Zawieja DC, Tinsley J, Granger HJ. Role of phospholipase C, protein kinase C, and calcium in VEGF-induced venular hyperpermeability. Am J Physiol - Hear Circ Physiol. 1999;276(2):H535–42.

136. Allen S, Khan S, Futwan-Al-Mohanna, Batten P, Yacoub M. Native low density lipoprotein-

induced calcium transients trigger VCAM- 1 and E-selectin expression in cultured human vascular endothelial cells. J Clin Invest. 1998;101(5):1064–75.

137. Mertens S, Noll T, Spahr R, Krutzfeldt A, Piper HM. Energetic response of coronary endothelial cells to hypoxia. Am J Physiol - Hear Circ Physiol. 1990;258(3):H689–94.

138. Dobrina A, Rossi F. Metabolic properties of freshly isolated bovine endothelial cells. BBA - Mol Cell Res. 1983;762(2):295–301.

139. De Bock K, Georgiadou M, Schoors S, Kuchnio A, Wong BW, Cantelmo AR, et al. Role of PFKFB3-driven glycolysis in vessel sprouting. Cell. 2013;154(3):651–63.

140. Culic O, Gruwel MLH, Schrader J. Energy turnover of vascular endothelial cells. Am J Physiol - Cell Physiol. 1997;273(1):C205–13.

141. Potente M, Carmeliet P. The Link between Angiogenesis and Endothelial Metabolism. Annu Rev Physiol. 2017;79:43–66.

142. Groschner LN, Waldeck-Weiermair M, Malli R, Graier WF. Endothelial mitochondria-less respiration, more integration. Pflugers Arch Eur J Physiol. 2012;464(1):63–76.

143. Kohn EC, Alessandro R, Spoonster J, Wersto RP, Liotta LA. Angiogenesis: Role of calcium-mediated signal transduction. Proc Natl Acad Sci U S A. 1995;92(5):1307–11.

144. Hamdollah Zadeh MA, Glass C, Magnussen A, Hancox J, Bates D. VEGF-Mediated elevated intracellular calcium and angiogenesis in human microvascular endothelial cells In vitro are inhibited by dominant negative TRPC6. Microcirculation. 2008;15(7):605–14.

145. Manolopoulos VG, Liekens S, Koolwijk P, Voets T, Peters E, Droogmans G, et al. Inhibition of angiogenesis by blockers of volume-regulated anion channels. Gen Pharmacol. 2000;34(2):107–16.

146. Apte RS, Chen DS, Ferrara N. VEGF in Signaling and Disease: Beyond Discovery and Development. Cell. 2019;176(6):1248–64.

147. Simons M, Gordon E, Claesson-Welsh L. Mechanisms and regulation of endothelial VEGF receptor signalling. Nat Rev Mol Cell Biol. 2016;17(10):611–25.

148. Mirzapoiazova T, Kolosova I, Usatyuk P V., Natarajan V, Verin AD. Diverse effects of vascular endothelial growth factor on human pulmonary endothelial barrier and migration.

Am J Physiol - Lung Cell Mol Physiol. 2006;291(4):L718–24.

149. Gupta K, Kshirsagar S, Li W, Gui L, Ramakrishnan S, Gupta P, et al. VEGF prevents apoptosis of human microvascular endothelial cells via opposing effects on MAPK/ERK and SAPK/JNK signaling. Exp Cell Res. 1999;247(2):495–504.

150. Meadows KN, Bryant P, Pumiglia K. Vascular Endothelial Growth Factor Induction of the Angiogenic Phenotype Requires Ras Activation. J Biol Chem. 2001;276(52):49289–98.

151. Faehling M, Kroll J, Föhr KJ, Fellbrich G, Mayr U, Trischler G, et al. Essential role of calcium in vascular endothelial growth factor A-induced signaling: mechanism of the antiangiogenic effect of carboxyamidotriazole. FASEB J. 2002;16(13):1805–7.

152. Dawson NS, Zawieja DC, Wu MH, Granger HJ, Dawson NS, Zawieja DC, et al. Signaling pathways mediating VEGF 165 -induced calcium transients and membrane depolarization in human endothelial cells . FASEB J. 2006;20(7):991–3.

153. Fearnley GW, Bruns AF, Wheatcroft SB, Ponnambalam S. VEGF-A isoform-specific regulation of calcium ion flux, transcriptional activation and endothelial cell migration. Biol Open. 2015;4(6):731–42.

154. Noren DP, Chou WH, Lee SH, Qutub AA, Warmflash A, Wagner DS, et al. Endothelial cells decode VEGF-mediated Ca2+ signaling patterns to produce distinct functional responses. Sci Signal. 2016;9(416):ra20.

155. Andrikopoulos P, Eccles SA, Yaqoob MM. Coupling between the TRPC3 ion channel and the NCX1 transporter contributed to VEGF-induced ERK1/2 activation and angiogenesis in human primary endothelial cells. Cell Signal. 2017;37:12–30.

156. Xiao Z, Wang T, Qin H, Huang C, Feng Y, Xia Y. Endoplasmic reticulum Ca2+ release modulates endothelial nitric-oxide synthase via Extracellular Signal-regulated Kinase (ERK) 1/2-mediated serine 635 phosphorylation. J Biol Chem. 2011;286(22):20100–8.

157. Fleming I, Fisslthaler B, Busse R. Calcium signaling in endothelial cells involves activation of tyrosine kinases and leads to activation of mitogen-activated protein kinases. Circ Res. 1995;76(4):522–9.

158. Katoch SS, Moreland RS. Agonist and membrane depolarization induced activation of MAP

kinase in the swine carotid artery. Am J Physiol - Hear Circ Physiol. 1995;269(1):H222–9.

159. Lee MY, Luciano AK, Ackah E, Rodriguez-Vitad J, Bancroft TA, Eichmann A, et al. Endothelial Akt1 mediates angiogenesis by phosphorylating multiple angiogenic substrates. Proc Natl Acad Sci U S A. 2014;111(35):12865–70.

160. Gélinas DS, Bernatchez PN, Rollin S, Bazan NG, Sirois MG. Immediate and delayed VEGF-mediated NO synthesis in endothelial cells: Role of PI3K, PKC and PLC pathways. Br J Pharmacol. 2002;137(7):1021–30.

161. Srinivasan R, Zabuawala T, Huang H, Zhang J, Gulati P, Fernandez S, et al. Erk1 and erk2 regulate endothelial cell proliferation and migration during mouse embryonic angiogenesis. PLoS One. 2009;4(12):e8283.

162. Nagasawa-Masuda A, Terai K. ERK activation in endothelial cells is a novel marker during neovasculogenesis. Genes to Cells. 2016;21(11):1164–75.

163. Narasimhan P, Liu J, Song YS, Massengale JL, Chan PH. VEGF stimulates the ERK 1/2 signaling pathway and apoptosis in cerebral endothelial cells after ischemic conditions. Stroke. 2009;40(4):1467–73.

164. Mebratu Y, Tesfaigzi Y. How ERK1/2 activation controls cell proliferation and cell death is subcellular localization the answer? Cell Cycle. 2009;8(8):1168–75.

165. Yamamoto T, Ebisuya M, Ashida F, Okamoto K, Yonehara S, Nishida E. Continuous ERK Activation Downregulates Antiproliferative Genes throughout G1 Phase to Allow Cell-Cycle Progression. Curr Biol. 2006;16(12):1171–82.

166. Berra E, Milanini J, Richard DE, Le Gall M, Viñals F, Gothié E, et al. Signaling angiogenesis via p42/p44 MAP kinase and hypoxia. Biochem Pharmacol. 2000;60(8):1171–8.

167. Savage AM, Kurusamy S, Chen Y, Jiang Z, Chhabria K, MacDonald RB, et al. tmem33 is essential for VEGF-mediated endothelial calcium oscillations and angiogenesis. Nat Commun. 2019;10(1):732.

168. Wilhelm K, Happel K, Eelen G, Schoors S, Oellerich MF, Lim R, et al. FOXO1 couples metabolic activity and growth state in the vascular endothelium. Nature. 2016;529(7585):216–20.

169. Menssen A, Hermeking H. Characterization of the c-MYC-regulated transcriptome by SAGE: Identification and analysis of c-MYC target genes. Proc Natl Acad Sci U S A. 2002;99(9):6274–9.

170. Vizán P, Sánchez-Tena S, Alcarraz-Vizán G, Soler M, Messeguer R, Pujol MD, et al. Characterization of the metabolic changes underlying growth factor angiogenic activation: Identification of new potential therapeutic targets. Carcinogenesis. 2009;30(6):946–52.

171. Liu S, Rockey DC. Cicletanine stimulates eNOS phosphorylation and NO production via Akt and MAP kinase/Erk signaling in sinusoidal endothelial cells. Am J Physiol - Gastrointest Liver Physiol. 2013;305(2):G163–71.

172. Mineo C, Yuhanna IS, Quon MJ, Shaul PW. High density lipoprotein-induced endothelial nitric-oxide synthase activation is mediated by Akt and MAP kinases. J Biol Chem. 2003;278(11):9142–9.

173. Corson MA, James NL, Latta SE, Nerem RM, Berk BC, Harrison DG. Phosphorylation of endothelial nitric oxide synthase in response to fluid shear stress. Circ Res. 1996;79(5):984–91.

174. Chen Z, Yuhanna IS, Galcheva-Gargova Z, Karas RH, Mendelsohn ME, Shaul PW. Estrogen receptor mediates the nongenomic activation of endothelial nitric oxide synthase by estrogen. J Clin Invest. 1999;103(3):401–6.

175. Li Y, Zheng J, Bird IM, Magness RR. Mechanisms of Shear Stress-Induced Endothelial Nitric-Oxide Synthase Phosphorylation and Expression in Ovine Fetoplacental Artery Endothelial Cells. Biol Reprod. 2004;70(3):785–96.

176. Vanhoutte PM, Zhao Y, Xu A, Leung SWS. Thirty Years of Saying NO: Sources, Fate, Actions, and Misfortunes of the Endothelium-Derived Vasodilator Mediator. Circ Res. 2016;119(2):375–96.

177. Salerno JC, Ghosh DK, Razdan R, Helms KA, Brown CC, McMurry JL, et al. Endothelial nitric oxide synthase is regulated by ERK phosphorylation at Ser602. Biosci Rep. 2014;34(5):e00137.

178. Kong X, Qu X, Li B, Wang Z, Chao Y, Jiang X, et al. Modulation of low shear stress-induced eNOS multi-site phosphorylation and nitric oxide production via protein kinase and ERK1/2

signaling. Mol Med Rep. 2017;15(2):908–14.

179. Papapetropoulos A, García-Cardeña G, Madri JA, Sessa WC. Nitric oxide production contributes to the angiogenic properties of vascular endothelial growth factor in human endothelial cells. J Clin Invest. 1997;100(12):3131–9.

180. Fukumura D, Gohongi T, Kadambi A, Izumi Y, Ang J, Yun CO, et al. Predominant role of endothelial nitric oxide synthase in vascular endothelial growth factor-induced angiogenesis and vascular permeability. Proc Natl Acad Sci U S A. 2001;98(5):2604–9.

181. Brouet A, Sonveaux P, Dessy C, Balligand JL, Feron O. Hsp90 Ensures the Transition from the Early Ca2+-dependent to the Late Phosphorylation-dependent Activation of the Endothelial Nitric-oxide Synthase in Vascular Endothelial Growth Factor-exposed Endothelial Cells. J Biol Chem. 2001;276(35):32663–9.

182. Liang W, Ray JB, He JZ, Backx PH, Ward ME. Regulation of proliferation and membrane potential by chloride currents in rat pulmonary artery smooth muscle cells. Hypertension. 2009;54(2):286–93.

183. Crutzen R, Virreira M, Markadieu N, Shlyonsky V, Sener A, Malaisse WJ, et al. Anoctamin 1 (Ano1) is required for glucose-induced membrane potential oscillations and insulin secretion by murine β-cells. Pflugers Arch Eur J Physiol. 2016;468(4):573–91.

184. Valdivieso ÁG, Santa-Coloma TA. The chloride anion as a signalling effector. Biol Rev. 2019;94(5):1839–56.

185. O'Rourke B. Mitochondrial ion channels. Annu Rev Physiol. 2007;69:19–49.

186. Tabares L, Mazzanti M, Clapham DE. Chloride channels in the nuclear membrane. J Membr Biol. 1991;123(1):49–54.

187. Bekar LK, Walz W. Evidence for chloride ions as intracellular messenger substances in astrocytes. J Neurophysiol. 1999;82(1):248–54.

188. Succol F, Fiumelli H, Benfenati F, Cancedda L, Barberis A. Intracellular chloride concentration influences the GABA A receptor subunit composition. Nat Commun. 2012;3:738.

189. Piala AT, Moon TM, Akella R, He H, Cobb MH, Goldsmith EJ. Chloride sensing by WNK1

involves inhibition of autophosphorylation. Sci Signal. 2014;7(324):ra41.

190. Rushworth CA, Guy JL, Turner AJ. Residues affecting the chloride regulation and substrate selectivity of the angiotensin-converting enzymes (ACE and ACE2) identified by site-directed mutagenesis. FEBS J. 2008;275(23):6033–42.

191. Miyazaki H, Shiozaki A, Niisato N, Ohsawa R, Itoi H, Ueda Y, et al. Chloride ions control the G1/S cell-cycle checkpoint by regulating the expression of p21 through a p53-independent pathway in human gastric cancer cells. Biochem Biophys Res Commun. 2008;366(2):506–12.

192. Klausen TK, Preisler S, Pedersen SF, Hoffmann EK. Monovalent ions control proliferation of Ehrlich Lettre ascites cells. Am J Physiol - Cell Physiol. 2010;299(3):C714–25.

193. Lai ZF, Chen YZ, Nishi K. Modulation of intracellular Cl- homeostasis by lectin-stimulation in Jurkat T lymphocytes. Eur J Pharmacol. 2003;482(1–3):1–8.

194. Wang H, Zou L, Ma K, Yu J, Wu H, Wei M, et al. Cell-specific mechanisms of TMEM16A Ca2+-activated chloride channel in cancer. Mol Cancer. 2017;16(1):152.

195. Wu H, Wang H, Guan S, Zhang J, Chen Q, Wang X, et al. Cell-specific regulation of proliferation by Ano 1/TMEM16A in breast cancer with different ER, PR, and HER2 status. Oncotarget. 2017;8(49):84996–5013.

196. Duvvuri U, Shiwarski DJ, Xiao D, Bertrand C, Huang X, Edinger RS, et al. TMEM16A induces MAPK and contributes directly to tumorigenesis and cancer progression. Cancer Res. 2012;72(13):3270–81.

197. Nilius B, Prenen J, Kamouchi M, Viana F, Voets T, Droogmans G. Inhibition by mibefradil, a novel calcium channel antagonist, of Ca2+- and volume-activated Cl- channels in macrovascular endothelial cells. Br J Pharmacol. 1997;121(3):547–55.

198. Pedersen SF, Okada Y, Nilius B. Biophysics and Physiology of the Volume-Regulated Anion Channel (VRAC)/Volume-Sensitive Outwardly Rectifying Anion Channel (VSOR). Pflugers Arch Eur J Physiol. 2016;468(3):371–83.

199. Sabirov RZ, Prenen J, Tomita T, Droogmans G, Nilius B. Reduction of ionic strength activates single volume-regulated anion channels (VRAC) in endothelial cells. Pflugers

Arch Eur J Physiol. 2000;439(3):315–20.

200. Voss FK, Ullrich F, Muñch J, Lazarow K, Lutte D, Mah N, et al. Identification of LRRC8 heteromers as an essential component of the volume-regulated anion channel VRAC. Science (80-). 2014;344(6184):634–8.

201. Tousson A, Van Tine BA, Naren AP, Shaw GM, Schwiebert LM. Characterization of CFTR expression and chloride channel activity in human endothelia. Am J Physiol - Cell Physiol. 1998;275(6 44-6):C1555–64.

202. Riordan JR, Rommens JM, Kerem BS, Alon NOA, Rozmahel R, Grzelczak Z, et al. Identification of the cystic fibrosis gene: Cloning and characterization of complementary DNA. Science (80-). 1989;245(4922):1066–73.

203. Totani L, Plebani R, Piccoli A, Di Silvestre S, Lanuti P, Recchiuti A, et al. Mechanisms of endothelial cell dysfunction in cystic fibrosis. Biochim Biophys Acta - Mol Basis Dis. 2017;1863(12):3243–53.

204. Rodriguez-Miguelez P, Thomas J, Seigler N, Crandall R, McKie KT, Forseen C, et al. Evidence of microvascular dysfunction in patients with cystic fibrosis. Am J Physiol - Hear Circ Physiol. 2016;310(11):H1479–85.

205. Benedetto R, Ousingsawat J, Cabrita I, Pinto M, Lérias JR, Wanitchakool P, et al. Plasma membrane–localized TMEM16 proteins are indispensable for expression of CFTR. J Mol Med. 2019;97:711–22.

206. Benedetto R, Ousingsawat J, Wanitchakool P, Zhang Y, Holtzman MJ, Amaral M, et al. Epithelial Chloride Transport by CFTR Requires TMEM16A. Sci Rep. 2017;7(1):12397.

207. Wei L, Vankeerberghen A, Cuppens H, Eggermont J, Cassiman JJ, Droogmans G, et al. Interaction between calcium-activated chloride channels and the cystic fibrosis transmembrane conductance regulator. Pflugers Arch Eur J Physiol. 1999;438(5):635–41.

208. Vennekens R, Trouet D, Vankeerberghen A, Voets T, Cuppens H, Eggermont J, et al. Inhibition of volume-regulated anion channels by expression of the cystic fibrosis transmembrane conductance regulator. J Physiol. 1999;515(1):75–85.

209. Ousingsawat J, Kongsuphol P, Schreiber R, Kunzelmann K. CFTR and TMEM16A are

separate but functionally related Cl - channels. Cell Physiol Biochem. 2011;28(4):715–24.

210. Legendre C, Mooij MJ, Adams C, O'Gara F. Impaired expression of hypoxia-inducible factor-1α in cystic fibrosis airway epithelial cells - A role for HIF-1 in the pathophysiology of CF? J Cyst Fibros. 2011;10(4):286–90.

211. Zheng W, Kuhlicke J, Jäckel K, Eltzschig HK, Singh A, Sjoblöm M, et al. Hypoxia inducible factor-1 (HIF-I)-mediated repression of cystic fibrosis transmembrane conductance regulator (CFTR) in the intestinal epithelium. FASEB J [Internet]. 2009;23(1):204–13. Available from: http://www.pubmedcentral.nih.gov/articlerender.fcgi?artid=2626614&tool=pmcentrez&rendertype=abstract

212. Sun H, Xia Y, Paudel O, Yang XR, Sham JSK. Chronic hypoxia-induced upregulation of Ca 2+-activated Cl - channel in pulmonary arterial myocytes: A mechanism contributing to enhanced vasoreactivity. J Physiol. 2012;590(15):3507–21.

213. Buchholz B, Schley G, Faria D, Kroening S, Willam C, Schreiber R, et al. Hypoxia-inducible factor-1α causes renal cyst expansion through calcium-activated chloride secretion. J Am Soc Nephrol [Internet]. 2014;25(3):465–74. Available from: http://www.jasn.org/cgi/doi/10.1681/ASN.2013030209

214. Barish ME. A transient calcium-dependent chloride current in the immature Xenopus oocyte. J Physiol. 1983;342(1):309–25.

215. Schroeder BC, Cheng T, Jan YN, Jan LY. Expression Cloning of TMEM16A as a Calcium-Activated Chloride Channel Subunit. Cell. 2008;134(6):1019–29.

216. Caputo A, Caci E, Ferrera L, Pedemonte N, Barsanti C, Sondo E, et al. TMEM16A, a membrane protein associated with calcium-dependent chloride channel activity. Science (80-) [Internet]. 2008;322(5901):590–4. Available from: http://www.sciencemag.org/cgi/doi/10.1126/science.1163518

217. Yang YD, Cho H, Koo JY, Tak MH, Cho Y, Shim WS, et al. TMEM16A confers receptor-activated calcium-dependent chloride conductance. Nature. 2008;455(7217):1210–5.

218. Kamouchi M, Trouet D, De Greef C, Droogmans G, Eggermont J, Nilius B. Functional effects of expression of hslo Ca2+ activated K+ channels in cultured macrovascular

endothelial cells. Cell Calcium. 1997;22(6):497–506.

219. Nilius B, Prenen J, Szücs G, Wei L, Tanzi F, Voets T, et al. Calcium-activated chloride channels in bovine pulmonary artery endothelial cells. J Physiol. 1997;498(2):381–96.

220. Xiao Q, Yu K, Perez-Cornejo P, Cui Y, Arreola J, Hartzell HC. Voltage- and calcium-dependent gating of TMEM16A/Ano1 chloride channels are physically coupled by the first intracellular loop. Proc Natl Acad Sci U S A [Internet]. 2011;108(21):8891–6. Available from: http://www.pnas.org/cgi/doi/10.1073/pnas.1102147108

221. Ma K, Wang H, Yu J, Wei M, Xiao Q. New Insights on the Regulation of Ca2+-Activated Chloride Channel TMEM16A. J Cell Physiol [Internet]. 2017;232(4):707–16. Available from: http://doi.wiley.com/10.1002/jcp.25621

222. Cabrita I, Benedetto R, Fonseca A, Wanitchakool P, Sirianant L, Skryabin B V., et al. Differential effects of anoctamins on intracellular calcium signals. FASEB J. 2017;31(5):2123–34.

223. Concepcion AR, Vaeth M, Wagner LE, Eckstein M, Hecht L, Jun Y, et al. Store-operated Ca2+ entry regulates Ca2+-activated chloride channels and eccrine sweat gland function. J Clin Invest. 2016;126(11):4303–18.

224. Wang Q, Dennis Leo M, Narayanan D, Kuruvilla KP, Jaggar JH. Local coupling of TRPC6 to ANO1/TMEM16A channels in smooth muscle cells amplifies vasoconstriction in cerebral arteries. Am J Physiol - Cell Physiol [Internet]. 2016;310(11):C1001–9. Available from: http://ajpcell.physiology.org/lookup/doi/10.1152/ajpcell.00092.2016

225. Paulino C, Kalienkova V, Lam AKM, Neldner Y, Dutzler R. Activation mechanism of the calcium-activated chloride channel TMEM16A revealed by cryo-EM. Nature. 2017;552(7685):421–5.

226. Dang S, Feng S, Tien J, Peters CJ, Bulkley D, Lolicato M, et al. Cryo-EM structures of the TMEM16A calciumactivated chloride channel. Nature. 2017;552(7685):426–9.

227. Xiao Q, Cui Y. Acidic amino acids in the first intracellular loop contribute to voltage- and calcium- dependent gating of Anoctamin1/TMEM16A. PLoS One. 2014;9(6):e99376.

228. Yu K, Duran C, Qu Z, Cui YY, Hartzell HC. Explaining calcium-dependent gating of

anoctamin-1 chloride channels requires a revised topology. Circ Res. 2012;110(7):990–9.

229. Ferrera L, Caputo A, Ubby I, Bussani E, Zegarra-Moran O, Ravazzolo R, et al. Regulation of TMEM16A chloride channel properties by alternative splicing. J Biol Chem. 2009;284(48):33360–8.

230. O'Driscoll KE, Pipe RA, Britton FC. Increased complexity of Tmem16a/Anoctamin 1 transcript alternative splicing. BMC Mol Biol. 2011;12:35.

231. Strege PR, Bernard CE, Mazzone A, Linden DR, Beyder A, Gibbons SJ, et al. A novel exon in the human Ca2+-activated Cl- channel Ano1 imparts greater sensitivity to intracellular Ca2+. Am J Physiol - Gastrointest Liver Physiol. 2015;309(9):G743–9.

232. Ertongur-Fauth T, Hochheimer A, Buescher JM, Rapprich S, Krohn M. A novel TMEM16A splice variant lacking the dimerization domain contributes to calcium-activated chloride secretion in human sweat gland epithelial cells. Exp Dermatol. 2014;23(11):825–31.

233. Mazzone A, Bernard CE, Strege PR, Beyder A, Galietta LJV, Pasricha PJ, et al. Altered expression of ano1 variants in human diabetic gastroparesis. J Biol Chem. 2011;286(15):13393–403.

234. Hwang SJ, Blair PJA, Britton FC, O'Driscoll KE, Hennig G, Bayguinov YR, et al. Expression of anoctamin 1/TMEM16A by interstitial cells of Cajal is fundamental for slow wave activity in gastrointestinal muscles. J Physiol. 2009;587(20):4887–904.

235. Huang F, Rock JR, Harfe BD, Cheng T, Huang X, Jan YN, et al. Studies on expression and function of the TMEM16A calcium-activated chloride channel. Proc Natl Acad Sci U S A [Internet]. 2009;106(50):21413–8. Available from: http://www.pnas.org/lookup/doi/10.1073/pnas.0911935106

236. Rock JR, O'Neal WK, Gabriel SE, Randell SH, Harfe BD, Boucher RC, et al. Transmembrane protein 16A (TMEM16A) is a Ca2+ -regulated Cl- secretory channel in mouse airways. J Biol Chem. 2009;284(22):14875–80.

237. Rock JR, Futtner CR, Harfe BD. The transmembrane protein TMEM16A is required for normal development of the murine trachea. Dev Biol. 2008;321(1):141–9.

238. Schenk LK, Buchholz B, Henke SF, Michgehl U, Daniel C, Amann K, et al. Nephron-specific

knockout of TMEM16A leads to reduced number of glomeruli and albuminuria. Am J Physiol - Ren Physiol. 2018;315(6):F1777–86.

239. Hong GS, Lee SH, Lee B, Choi JH, Oh SJ, Jang Y, et al. ANO1/TMEM16A regulates process maturation in radial glial cells in the developing brain. Proc Natl Acad Sci U S A. 2019;116(25):12494–9.

240. Pedemonte N, Galietta LJV. Structure and function of tmem16 proteins (anoctamins). Physiol Rev [Internet]. 2014;94(2):419–59. Available from: http://physrev.physiology.org/cgi/doi/10.1152/physrev.00039.2011

241. Sondo E, Caci E, Galietta LJV. The TMEM16A chloride channel as an alternative therapeutic target in cystic fibrosis. Vol. 52, International Journal of Biochemistry and Cell Biology. 2014. p. 73–6.

242. Wang B, Li C, Huai R, Qu Z. Overexpression of ANO1/TMEM16A, an arterial Ca2+-activated Cl- channel, contributes to spontaneous hypertension. J Mol Cell Cardiol. 2015;82:22–32.

243. Ma MM, Gao M, Guo KM, Wang M, Li XY, Zeng XL, et al. TMEM16A Contributes to Endothelial Dysfunction by Facilitating Nox2 NADPH Oxidase-Derived Reactive Oxygen Species Generation in Hypertension. Hypertension. 2017;69(5):892–901.

244. Wang M, Yang H, Zheng LY, Zhang Z, Tang YB, Wang GL, et al. Downregulation of TMEM16A calcium-activated chloride channel contributes to cerebrovascular remodeling during hypertension by promoting basilar smooth muscle cell proliferation. Circulation. 2012;125(5):697–707.

245. Heinze C, Seniuk A, Sokolov M V., Huebner AK, Klementowicz AE, Szijártó IA, et al. Disruption of vascular Ca2+-activated chloride currents lowers blood pressure. J Clin Invest. 2014;124(2):675–86.

246. Furchgott RF, Zawadzki J V. The obligatory role of endothelial cells in the relaxation of arterial smooth muscle by acetylcholine. Nature. 1980;288(5789):373–6.

247. Palmer RMJ, Ferrige AG, Moncada S. Nitric oxide release accounts for the biological activity of endothelium-derived relaxing factor. Nature. 1987;327(6122):524–6.

248. Domeier TL, Segal SS. Electromechanical and pharmacomechanical signalling pathways for conducted vasodilatation along endothelium of hamster feed arteries. J Physiol. 2007;579(1):175–86.

249. Ignarro LJ, Byrns RE, Buga GM, Wood KS. Endothelium-derived relaxing factor from pulmonary artery and vein possesses pharmacologic and chemical properties identical to those of nitric oxide radical. Circ Res. 1987;61(6):866–79.

250. Patel JM, Martens JR, Li YD, Gelband CH, Raizada MK, Block ER. Angiotensin IV receptor-mediated activation of lung endothelial NOS is associated with vasorelaxation. Am J Physiol - Lung Cell Mol Physiol. 1998;275(6):L1061–8.

251. Fagan KA, Tyler RC, Sato K, Fouty BW, Morris KG, Huang PL, et al. Relative contributions of endothelial, inducible, and neuronal NOS to tone in the murine pulmonary circulation. Am J Physiol - Lung Cell Mol Physiol. 1999;277(3):L472–8.

252. Steudel W, Ichinose F, Huang PL, Hurford WE, Jones RC, Bevan JA, et al. Pulmonary vasoconstriction and hypertension in mice with targeted disruption of the endothelial nitric oxide synthase (NOS 3) gene. Circ Res. 1997;81(1):34–41.

253. Kelm M. Nitric oxide metabolism and breakdown. Biochim Biophys Acta - Bioenerg. 1999;1411(2–3):273–89.

254. Vanhoutte PM, Shimokawa H, Tang EHC, Feletou M. Endothelial dysfunction and vascular disease. Acta Physiol. 2009;196(2):193–222.

255. Fulton D, Babbitt R, Zoellner S, Fontana J, Acevedo L, McCabe TJ, et al. Targeting of endothelial nitric-oxide synthase to the cytoplasmic face of the Golgi complex or plasma membrane regulates Akt- versus calcium-dependent mechanisms for nitric oxide release. J Biol Chem. 2004;279(29):30349–57.

256. Prabhakar P, Thatte HS, Goetz RM, Cho MR, Golan DE, Michel T. Receptor-regulated translocation of endothelial nitric-oxide synthase. J Biol Chem. 1998;273(42):27383–8.

257. Michel T, Li GK, Busconi L. Phosphorylation and subcellular translocation of endothelial nitric oxide synthase. Proc Natl Acad Sci U S A. 1993;90(13):6252–6.

258. Sessa WC, Garcia-Cardena G, Liu J, Keh A, Pollock JS, Bradley J, et al. The Golgi

association of endothelial nitric oxide synthase is necessary for the efficient synthesis of nitric oxide. J Biol Chem. 1995;270(30):17641–4.

259. Shu X, Keller TCS, Begandt D, Butcher JT, Biwer L, Keller AS, et al. Endothelial nitric oxide synthase in the microcirculation. Cell Mol Life Sci. 2015;72(23):4561–75.

260. Iwakiri Y, Satoh A, Chatterjee S, Toomre DK, Chalouni CM, Fulton D, et al. Nitric oxide synthase generates nitric oxide locally to regulate compartmentalized protein S-nitrosylation and protein trafficking. Proc Natl Acad Sci U S A. 2006;103(52):19777–82.

261. Qian J, Zhang Q, Church JE, Stepp DW, Rudic RD, Fulton DJR. Role of local production of endothelium-derived nitric oxide on cGMP signaling and S-nitrosylation. Am J Physiol - Hear Circ Physiol. 2010;298(1):H112–8.

262. Feron O, Belhassen L, Kobzik L, Smith TW, Kelly RA, Michel T. Endothelial nitric oxide synthase targeting to caveolae. Specific interactions with caveolin isoforms in cardiac myocytes and endothelial cells. J Biol Chem. 1996;271(37):22810–4.

263. Busse R, Mülsch A. Calcium-dependent nitric oxide synthesis in endothelial cytosol is mediated by calmodulin. FEBS Lett. 1990;265(1–2):133–6.

264. Fleming I, Fisslthaler B, Dimmeler S, Kemp BE, Busse R. Phosphorylation of Thr(495) regulates Ca(2+)/calmodulin-dependent endothelial nitric oxide synthase activity. Circ Res. 2001;88(11):E68–75.

265. Marletta MA. Nitric oxide synthase structure and mechanism. J Biol Chem. 1993;268(17):12231–4.

266. Hu H, Xin M, Belayev LL, Zhang J, Block ER, Patel JM. Autoinhibitory domain fragment of endothelial NOS enhances pulmonary artery vasorelaxation by the NO-cGMP pathway. Am J Physiol - Lung Cell Mol Physiol. 2004;286(5):L1066–74.

267. Berka V, Wu G, Yeh HC, Palmer G, Tsai AL. Three different oxygen-induced radical species in endothelial nitric-oxide synthase oxygenase domain under regulation by L-arginine and tetrahydrobiopterin. J Biol Chem. 2004;279(31):32243–51.

268. Jerkic M, Kabir MG, Davies A, Yu LX, McIntyre BAS, Husain NW, et al. Pulmonary hypertension in adult Alk1 heterozygous mice due to oxidative stress. Cardiovasc Res.

2011;92(3):375–84.

269. Patel JM, Li YD, Zhang J, Gelband CH, Raizada MK, Block ER. Increased expression of calreticulin is linked to ANG IV-mediated activation of lung endothelial NOS. Am J Physiol - Lung Cell Mol Physiol. 1999;277(4):L794–801.

270. García-Cardeña G, Fan R, Shah V, Sorrentino R, Cirino G, Papapetropoulos A, et al. Dynamic activation of endothelial nitric oxide synthase by Hsp90. Nature. 1998;392(6678):821–4.

271. Michell BJ, Chen ZP, Tiganis T, Stapleton D, Katsis F, Power DA, et al. Coordinated Control of Endothelial Nitric-oxide Synthase Phosphorylation by Protein Kinase C and the cAMP-dependent Protein Kinase. J Biol Chem. 2001;276(21):17625–8.

272. Zhang JL, Patel JM, Li YD, Block ER. Reductase domain cysteines 1048 and 1114 are critical for catalytic activity of human endothelial cell nitric oxide synthase as probed by site-directed mutagenesis. Biochem Biophys Res Commun. 1996;226(1):293–300.

273. Francis M, Waldrup JR, Qian X, Solodushko V, Meriwether J, Taylor MS. Functional Tuning of Intrinsic Endothelial Ca2+ Dynamics in Swine Coronary Arteries. Circ Res. 2016;118(7):1078–90.

274. Lin S, Fagan KA, Li KX, Shaul PW, Cooper DMF, Rodman DM. Sustained endothelial nitric-oxide synthase activation requires capacitative Ca2+ entry. J Biol Chem. 2000;275(24):17979–85.

275. Tran QK, Leonard J, Black DJ, Nadeau OW, Boulatnikov IG, Persechini A. Effects of combined phosphorylation at Ser-617 and Ser-1179 in endothelial nitric-oxide synthase on EC50(Ca2+) values for calmodulin binding and enzyme activation. J Biol Chem. 2009;284(18):11892–9.

276. Krupp J, Boeldt DS, Yi FX, Grummer MA, Anaya HAB, Shah DM, et al. The loss of sustained Ca2+ signaling underlies suppressed endothelial nitric oxide production in preeclamptic pregnancies: Implications for new therapy. Am J Physiol - Hear Circ Physiol. 2013;305(7):H969–79.

277. García-Cardeña G, Oh P, Liu J, Schnitzer JE, Sessa WC. Targeting of nitric oxide synthase to endothelial cell caveolae via palmitoylation: Implications for nitric oxide signaling. Proc

Natl Acad Sci U S A. 1996;93(13):6448–53.

278. Liu J, Sessa WC. Identification of covalently bound amino-terminal myristic acid in endothelial nitric oxide synthase. J Biol Chem. 1994;269(16):11691–4.

279. Liu J, Hughes TE, Sessa WC. The first 35 amino acids and fatty acylation sites determine the molecular targeting of endothelial nitric oxide synthase into the Golgi region of cells: A green fluorescent protein study. J Cell Biol. 1997;137(7):1525–35.

280. Liu J, García-Cardeña G, Sessa WC. Biosynthesis and Palmitoylation of Endothelial Nitric Oxide Synthase: Mutagenesis of Palmitoylation Sites, Cysteines-15 and/or -26, Argues against Depalmitoylation-Induced Translocation of the Enzyme. Biochemistry. 1995;34(38):12333–40.

281. Erwin PA, Mitchell DA, Sartoretto J, Marletta MA, Michel T. Subcellular targeting and differential S-nitrosylation of endothelial nitric-oxide synthase. J Biol Chem. 2006;281(1):151–7.

282. Dimmeler S, Fleming I, Fisslthaler B, Hermann C, Busse R, Zeiher AM. Activation of nitric oxide synthase in endothelial cells by Akt- dependent phosphorylation. Nature. 1999;399(6736):601–5.

283. Fulton D, Gratton JP, McCabe TJ, Fontana J, Fujio Y, Walsh K, et al. Regulation of endothelium-derived nitric oxide production by the protein kinase Akt. Nature. 1999;399(6736):597–601.

284. Butt E, Bernhardt M, Smolenski A, Kotsonis P, Fröhlich LG, Sickmann A, et al. Endothelial nitric-oxide synthase (type III) is activated and becomes calcium independent upon phosphorylation by cyclic nucleotide-dependent protein kinases. J Biol Chem. 2000;275(7):5179–87.

285. Chen ZP, Mitchelhill KI, Michell BJ, Stapleton D, Rodriguez-Crespo I, Witters LA, et al. AMP-activated protein kinase phosphorylation of endothelial NO synthase. FEBS Lett. 1999;443(3):285–9.

286. Heiss E, Dirsch V. Regulation of eNOS Enzyme Activity by Posttranslational Modification. Curr Pharm Des. 2014;20(22):3503–13.

287. Ruan L, Torres CM, Qian J, Chen F, Mintz JD, Stepp DW, et al. Pin1 Prolyl isomerase regulates endothelial nitric oxide synthase. Arterioscler Thromb Vasc Biol. 2011;31(2):392–8.

288. Michell BJ, Brennan Harris M, Chen ZP, Ju H, Venema VJ, Blackstone MA, et al. Identification of regulatory sites of phosphorylation of the bovine endothelial nitric-oxide synthase at Serine 617 and Serine 635. J Biol Chem. 2002;277(44):42344–51.

289. Rafikov R, Fonseca F V., Kumar S, Pardo D, Darragh C, Elms S, et al. eNOS activation and NO function: Structural motifs responsible for the posttranslational control of endothelial nitric oxide synthase activity. J Endocrinol. 2011;210(3):271–84.

290. Tran QK, Leonard J, Black DJ, Persechini A. Phosphorylation within an autoinhibitory domain in endothelial nitric oxide synthase reduces the Ca2+ concentrations required for calmodulin to bind and activate the enzyme. Biochemistry. 2008;47(28):7557–66.

291. Fleming I. Molecular mechanisms underlying the activation of eNOS. Pflugers Arch Eur J Physiol. 2010;459(6):793–806.

292. Salerno JC, Harris DE, Irizarry K, Patelf B, Morales AJ, Smith SME, et al. An autoinhibitory control element defines calcium-regulated isoforms of nitric oxide synthase. J Biol Chem. 1997;272(47):29769–77.

293. Félétou M, Köhler R, Vanhoutte PM. Nitric oxide: Orchestrator of endothelium-dependent responses. Ann Med. 2012;44(7):694–716.

294. Adachi T, Weisbrod RM, Pimentel DR, Ying J, Sharov VS, Schöneich C, et al. S-glutathiolation by peroxynitrite activates SERCA during arterial relaxation by nitric oxide. Nat Med. 2004;10(11):1200–7.

295. Carvajal JA, Germain AM, Huidobro-Toro JP, Weiner CP. Molecular mechanism of cGMP-mediated smooth muscle relaxation. J Cell Physiol. 2000;184(3):409–20.

296. Zhang DX, Borbouse L, Gebremedhin D, Mendoza SA, Zinkevich NS, Li R, et al. H2O2-induced dilation in human coronary arterioles: role of protein kinase G dimerization and large-conductance Ca2+-activated K+ channel activation. Circ Res. 2012;110(3):471–80.

297. Vanhoutte PM, Shimokawa H, Feletou M, Tang EHC. Endothelial dysfunction and vascular

disease – a 30th anniversary update. Acta Physiol. 2017;219(1):22–96.

298. Gao Y. The multiple actions of NO. Pflugers Arch Eur J Physiol. 2010;459(6):829–39.

299. Godo S, Sawada A, Saito H, Ikeda S, Enkhjargal B, Suzuki K, et al. Disruption of Physiological Balance between Nitric Oxide and Endothelium-Dependent Hyperpolarization Impairs Cardiovascular Homeostasis in Mice. Arterioscler Thromb Vasc Biol. 2016;36(1):97–107.

300. Chen G, Suzuki H, Weston AH. Acetylcholine releases endothelium-derived hyperpolarizing factor and EDRF from rat blood vessels. Br J Pharmacol. 1988;95(4):1165–74.

301. Feletou M, Vanhoutte PM. Endothelium-dependent hyperpolarization of canine coronary smooth muscle. Br J Pharmacol. 1988;93(3):515–24.

302. Yanagisawa M, Kurihara H, Kimura S, Tomobe Y, Kobayashi M, Mitsui Y, et al. A novel potent vasoconstrictor peptide produced by vascular endothelial cells. Nature. 1988;332(6163):411–5.

303. Babaei S, Teichert-Kuliszewska K, Monge JC, Mohamed F, Bendeck MP, Stewart DJ. Role of nitric oxide in the angiogenic response in vitro to basic fibroblast growth factor. Circ Res. 1998;82(9):1007–15.

304. Murohara T, Witzenbichler B, Spyridopoulos I, Asahara T, Ding B, Sullivan A, et al. Role of endothelial nitric oxide synthase in endothelial cell migration. Arterioscler Thromb Vasc Biol. 1999;19(5):1156–61.

305. Young SL, Evans K, Eu JP. Nitric oxide modulates branching morphogenesis in fetal rat lung explants. Am J Physiol - Lung Cell Mol Physiol. 2002;282(3):L379–85.

306. Van Belle E, Rivard A, Chen D, Silver M, Bunting S, Ferrara N, et al. Hypercholesterolemia attenuates angiogenesis but does not preclude augmentation by angiogenic cytokines. Circulation. 1997;96(8):2667–74.

307. Murohara T, Asahara T, Silver M, Bauters C, Masuda H, Kalka C, et al. Nitric oxide synthase modulates angiogenesis in response to tissue ischemia. J Clin Invest. 1998;101(11):2567–78.

308. Aicher A, Heeschen C, Mildner-Rihm C, Urbich C, Ihling C, Technau-Ihling K, et al. Essential role of endothelial nitric oxide synthase for mobilization of stem and progenitor cells. Nat Med. 2003;9(11):1370–6.

309. Rössig L, Fichtlscherer B, Breitschopf K, Haendeler J, Zeiher AM, Mülsch A, et al. Nitric oxide inhibits caspase-3 by S-nitrosation in vivo. J Biol Chem. 1999;274(11):6823–6.

310. Ziche M, Morbidelli L, Masini E, Amerini S, Granger HJ, Maggi CA, et al. Nitric oxide mediates angiogenesis in vivo and endothelial cell growth and migration in vitro promoted by substance P. J Clin Invest. 1994;94(5):2036–44.

311. Ziche M, Parenti A, Ledda F, DelL'Era P, Granger HJ, Maggi CA, et al. Nitric oxide promotes proliferation and plasminogen activator production by coronary venular endothelium through endogenous bFGF. Circ Res. 1997;80(6):845–52.

312. Dulak J, Józkowicz A, Dembinska-Kiec A, Guevara I, Zdzienicka A, Zmudzinska-Grochot D, et al. Nitric oxide induces the synthesis of vascular endothelial growth factor by rat vascular smooth muscle cells. Arterioscler Thromb Vasc Biol. 2000;20(3):659–66.

313. Noiri E, Lee E, Testa J, Quigley J, Colflesh D, Keese CR, et al. Podokinesis in endothelial cell migration: Role of nitric oxide. Am J Physiol - Cell Physiol. 1998;274(1):C236–44.

314. Ziehe M, Morbidelli L, Choudhuri R, Zhang HT, Donnini S, Granger HJ, et al. Nitric oxide synthase lies downstream from vascular endothelial growth factor-induced but not basic fibroblast growth factor-induced angiogenesis. J Clin Invest. 1997;99(11):2625–34.

315. Matsunaga T, Weihrauch DW, Moniz MC, Tessmer J, Warltier DC, Chilian WM. Angiostatin inhibits coronary angiogenesis during impaired production of nitric oxide. Circulation. 2002;105(18):2185–91.

316. Han RNN, Babaei S, Robb M, Lee T, Ridsdale R, Ackerley C, et al. Defective Lung Vascular Development and Fatal Respiratory Distress in Endothelial NO Synthase-Deficient Mice: A Model of Alveolar Capillary Dysplasia? Circ Res. 2004;94(8):1115–23.

317. Schini VB, Vanhoutte PM. L-Arginine evokes both endothelium-dependent and -independent relaxations in L-arginine-depleted aortas of the rat. Circ Res. 1991;68(1):209–16.

318. Wilson AM, Harada R, Nair N, Balasubramanian N, Cooke JP. L-arginine supplementation in peripheral arterial disease: No benefit and possible harm. Circulation. 2007;116(2):188–95.

319. Ming XF, Barandier C, Viswambharan H, Kwak BR, Mach F, Mazzolai L, et al. Thrombin stimulates human endothelial arginase enzymatic activity via RhoA/ROCK pathway: Implications for atherosclerotic endothelial dysfunction. Circulation. 2004;110(24):3708–14.

320. Johnson FK, Johnson RA, Peyton KJ, Durante W. Arginase inhibition restores arteriolar endothelial function in Dahl rats with salt-induced hypertension. Am J Physiol - Regul Integr Comp Physiol. 2005;288(4):R1057–62.

321. Raman CS, Li H, Martásek P, Král V, Masters BSS, Poulos TL. Crystal structure of constitutive endothelial nitric oxide synthase: A paradigm for pterin function involving a novel metal center. Cell. 1998;95(7):939–50.

322. Ravi K, Brennan LA, Levic S, Ross PA, Black SM. S-nitrosylation of endothelial nitric oxide synthase is associated with monomerization and decreased enzyme activity. Proc Natl Acad Sci U S A. 2004;101(8):2619–24.

323. Santhanam L, Lim HK, Lim HK, Miriel V, Brown T, Patel M, et al. Inducible NO synthase-dependent S-nitrosylation and activation of arginase1 contribute to age-related endothelial dysfunction. Circ Res. 2007;101(7):692–702.

324. Pacher P, Beckman JS, Liaudet L. Nitric oxide and peroxynitrite in health and disease. Physiol Rev. 2007;87(1):315–424.

325. Tayeh MA, Marletta MA. Macrophage oxidation of L-arginine to nitric oxide, nitrite, and nitrate. Tetrahydrobiopterin is required as a cofactor. J Biol Chem. 1989;264(33):19654–8.

326. Cai S, Khoo J, Channon KM. Augmented BH4 by gene transfer restores nitric oxide synthase function in hyperglycemic human endothelial cells. Cardiovasc Res. 2005;65(4):823–31.

327. Griendling KK, Sorescu D, Lassègue B, Ushio-Fukai M. Modulation of protein kinase activity and gene expression by reactive oxygen species and their role in vascular physiology and pathophysiology. Arterioscler Thromb Vasc Biol. 2000;20(10):2175–83.

328. Miyamoto Y, Akaike T, Yoshida M, Goto S, Horie H, Maeda H. Potentiation of nitric oxide-mediated vasorelaxation by xanthine oxidase inhibitors. Proc Soc Exp Biol Med. 1996;211(4):366–73.

329. Thomas SR, Chen K, Keaney JF. Hydrogen peroxide activates endothelial nitric-oxide synthase through coordinated phosphorylation and dephosphorylation via a phosphoinositide 3-kinase-dependent signaling pathway. J Biol Chem. 2002;277(8):6017–24.

330. Aschner JL, Foster SL, Kaplowitz M, Zhang Y, Zeng H, Fike CD. Heat shock protein 90 modulates endothelial nitric oxide synthase activity and vascular reactivity in the newborn piglet pulmonary circulation. Am J Physiol - Lung Cell Mol Physiol. 2007;292(6):L1515–25.

331. Tian J, Hou Y, Lu Q, Wiseman DA, Vasconcelos Fonsesca F, Elms S, et al. A novel role for caveolin-1 in regulating endothelial nitric oxide synthase activation in response to H2O2 and shear stress. Free Radic Biol Med. 2010;49(2):159–70.

332. Hemmens B, Goessler W, Schmidt K, Mayer B. Role of bound zinc in dimer stabilization but not enzyme activity of neuronal nitric-oxide synthase. J Biol Chem. 2000;275(46):35786–91.

333. Chen W, Druhan LJ, Chen CA, Hemann C, Chen YR, Berka V, et al. Peroxynitrite induces destruction of the tetrahydrobiopterin and heme in endothelial nitric oxide synthase: Transition from reversible to irreversible enzyme inhibition. Biochemistry. 2010;49(14):3129–37.

334. Bohle DS, Hansen B, Paulson SC, Smith BD. Biomimetic Synthesis of the Putative Cytotoxin Peroxynitrite, ONOO-, and Its Characterization as a Tetramethylammonium Salt. J Am Chem Soc. 1994;116(16):7423–4.

335. Blough N V., Zafiriou OC. Reaction of Superoxide with Nitric Oxide to Form Peroxonitrite in Alkaline Aqueous Solution. Inorg Chem. 1985;24(22):3502–4.

336. Beckman JS, Beckman TW, Chen J, Marshall PA, Freeman BA. Apparent hydroxyl radical production by peroxynitrite: Implications for endothelial injury from nitric oxide and superoxide. Proc Natl Acad Sci U S A. 1990;87(4):1620–4.

337. Franco MC, Estévez AG. Tyrosine nitration as mediator of cell death. Cell Mol Life Sci.

2014;71(20):3939–50.

338. Böger RH, Sydow K, Borlak J, Thum T, Lenzen H, Schubert B, et al. LDL cholesterol upregulates synthesis of asymmetrical dimethylarginine in human endothelial cells: Involvement of S-adenosylmethionine-dependent methyltransferases. Circ Res. 2000;87(2):99–105.

339. Wilcox CS. Asymmetric dimethylarginine and reactive oxygen species: Unwelcome twin visitors to the cardiovascular and kidney disease tables. Hypertension. 2012;59(2 SUPPL. 1):375–81.

340. Scalera F, Fulge B, Martens-Lobenhoffer J, Heimburg A, Bode-Böger SM. Red wine decreases asymmetric dimethylarginine via SIRT1 induction in human endothelial cells. Biochem Biophys Res Commun. 2009;390(3):703–9.

341. Xu W, Comhair SAA, Chen R, Hu B, Hou Y, Zhou Y, et al. Integrative proteomics and phosphoproteomics in pulmonary arterial hypertension. Sci Rep. 2019;9(1):18623.

342. Zurlo G, Piquereau J, Moulin M, Pires Da Silva J, Gressette M, Ranchoux B, et al. Sirtuin 1 regulates pulmonary artery smooth muscle cell proliferation: Role in pulmonary arterial hypertension. J Hypertens. 2018;36(5):1164–77.

343. Kielstein JT, Bode-Böger SM, Hesse G, Martens-Lobenhoffer J, Takacs A, Fliser D, et al. Asymmetrical dimethylarginine in idiopathic pulmonary arterial hypertension. Arterioscler Thromb Vasc Biol. 2005;25(7):1414–8.

344. Derbyshire ER, Marletta MA. Structure and regulation of soluble guanylate cyclase. Annu Rev Biochem. 2012;81:533–59.

345. Dou D, Zheng X, Ying L, Ye L, Gao Y. Sulfhydryl-dependent dimerization and cGMP-mediated vasodilatation. J Cardiovasc Pharmacol. 2013;62(1):1–5.

346. Ye L, Liu J, Liu H, Ying L, Dou D, Chen Z, et al. Sulfhydryl-dependent dimerization of soluble guanylyl cyclase modulates the relaxation of porcine pulmonary arteries to nitric oxide. Pflugers Arch Eur J Physiol. 2013;465(2):333–41.

347. Yamamura A, Fujitomi E, Ohara N, Tsukamoto K, Sato M, Yamamura H. Tadalafil induces antiproliferation, apoptosis, and phosphodiesterase type 5 downregulation in idiopathic

pulmonary arterial hypertension in vitro. Eur J Pharmacol. 2017;810:44–50.

348. Sitbon O, Humbert M, Jagot JL, Taravella O, Fartoukh M, Parent F, et al. Inhaled nitric oxide as a screening agent for safely identifying responders to oral calcium-channel blockers in primary pulmonary hypertension. Eur Respir J. 1998;12(2):265–70.

349. Fulton DJR, Li X, Bordan Z, Haigh S, Bentley A, Chen F, et al. Reactive oxygen and nitrogen species in the development of pulmonary hypertension. Antioxidants. 2017;6(3):54.

350. Stulnig G, Frisch MT, Crnkovic S, Stiegler P, Sereinigg M, Stacher E, et al. Docosahexaenoic acid (DHA)-induced heme oxygenase-1 attenuates cytotoxic effects of DHA in vascular smooth muscle cells. Atherosclerosis. 2013;230(2):406–13.

351. Zabini D, Nagaraj C, Stacher E, Lang IM, Nierlich P, Klepetko W, et al. Angiostatic factors in the pulmonary endarterectomy material from chronic thromboembolic pulmonary hypertension patients cause endothelial dysfunction. PLoS One. 2012;7(8):e43793.

352. Grynkiewicz G, Poenie M, Tsien RY. A new generation of Ca2+ indicators with greatly improved fluorescence properties. J Biol Chem. 1985;260(6):3440–50.

353. Wang M, Yang H, Zheng LY, Zhang Z, Tang YB, Wang GL, et al. Downregulation of TMEM16A calcium-activated chloride channel contributes to cerebrovascular remodeling during hypertension by promoting basilar smooth muscle cell proliferation. Circulation. 2012;125(5):697–707.

354. Bradley E, Fedigan S, Webb T, Hollywood MA, Thornbury KD, McHale NG, et al. Pharmacological characterization of TMEM16A currents. Channels. 2014;8(4):308–20.

355. Davis AJ, Shi J, Pritchard HAT, Chadha PS, Leblanc N, Vasilikostas G, et al. Potent vasorelaxant activity of the TMEM16A inhibitor T16A inh-A01. Br J Pharmacol. 2013;168(3):773–84.

356. Centeio R, Cabrita I, Benedetto R, Talbi K, Ousingsawat J, Schreiber R, et al. Pharmacological inhibition and activation of the Ca2+activated Cl− channel TMEM16A. Int J Mol Sci. 2020;21(7):2557.

357. Seo Y, Lee HK, Park J, Jeon DK, Jo S, Jo M, et al. Ani9, a novel potent small-molecule ANO1 inhibitor with negligible effect on ANO2. PLoS One. 2016;11(5):e0155771.

358. Davis AJ, Forrest AS, Jepps TA, Valencik ML, Wiwchar M, Singer CA, et al. Expression profile and protein translation of TMEM16A in murine smooth muscle. Am J Physiol - Cell Physiol. 2010;299(5):C948–59.

359. He Q, Halm ST, Zhang J, Halm DR. Activation of the basolateral membrane Cl- conductance essential for electrogenic K+ secretion suppresses electrogenic Cl- secretion. Exp Physiol. 2011;96(3):305–16.

360. Cox DA, Matlib MA. A role for the mitochondrial Na+-Ca2+ exchanger in the regulation of oxidative phosphorylation in isolated heart mitochondria. J Biol Chem. 1993;268(2):938–47.

361. Tu H, Nelson O, Bezprozvanny A, Wang Z, Lee SF, Hao YH, et al. Presenilins Form ER Ca2+ Leak Channels, a Function Disrupted by Familial Alzheimer's Disease-Linked Mutations. Cell. 2006;126(5):981–93.

362. Graier WF, Klec C, Madreiter-Sokolowski CT, Ziomek G, Stryeck S, Sachdev V, et al. Presenilin-1 established ER-Ca2+ leak: A follow up on its importance for the initial insulin secretion in pancreatic islets and β-cells upon elevated glucose. Cell Physiol Biochem. 2019;53(3):573–86.

363. Liu Z, Zhang S, Hou F, Zhang C, Gao J, Wang KW. Inhibition of Ca 2+ -activated chloride channel ANO1 suppresses ovarian cancer through inactivating PI3K/Akt signaling. Int J Cancer. 2019;144(9):2215–26.

364. Qu Z, Yao W, Yao R, Liu X, Yu K, Hartzell C. The Ca(2+) -activated Cl(-) channel, ANO1 (TMEM16A), is a double-edged sword in cell proliferation and tumorigenesis. Cancer Med. 2014;3(3):453–61.

365. Deng L, Yang J, Chen H, Ma B, Pan K, Su C, et al. Knockdown of TMEM16A suppressed MAPK and inhibited cell proliferation and migration in hepatocellular carcinoma. Onco Targets Ther. 2016;9:325–33.

366. Lian H, Cheng Y, Wu X. TMEM16A exacerbates renal injury by activating P38/JNK signaling pathway to promote podocyte apoptosis in diabetic nephropathy mice. Biochem Biophys Res Commun. 2017;487(2):201–8.

367. Wu QQ, Liu XY, Xiong LX, Shang JY, Mai XY, Pang RP, et al. Reduction of intracellular

chloride concentration promotes foam cell formation. Circ J. 2016;80(4):1024–33.

368. Ohsawa R, Miyazaki H, Niisato N, Shiozaki A, Iwasaki Y, Otsuji E, et al. Intracellular chloride regulates cell proliferation through the activation of stress-activated protein kinases in MKN28 human gastric cancer cells. J Cell Physiol. 2010;223(3):764–70.

369. Yang T, Park JM, Arend L, Huang Y, Topaloglu R, Pasumarthy A, et al. Low chloride stimulation of prostaglandin E2 release and cyclooxygenase-2 expression in a mouse macula densa cell line. J Biol Chem. 2000;275(48):37922–9.

370. Cheng HF, Wang JL, Zhang MZ, McKanna JA, Harris RC. Role of p38 in the regulation of renal cortical cyclooxygenase-2 expression by extracellular chloride. J Clin Invest. 2000;106(5):681–8.

371. Huang L yan, Li P peng, Li Y jie, Zhao W qian, Shang W kang, Wang Y ling, et al. Decreased intracellular chloride promotes ADP induced platelet activation through inhibition of cAMP/PKA instead of activation of Lyn/PI3K/Akt pathway. Biochem Biophys Res Commun. 2018;503(3):1740–6.

372. Shiwarski DJ, Shao C, Bill A, Kim J, Xiao D, Bertrand CA, et al. To “grow” or “go”: TMEM16A expression as a switch between tumor growth and metastasis in SCCHN. Clin Cancer Res. 2014;20(17):4673–88.

373. Dixit R, Kemp C, Kulich S, Seethala R, Chiosea S, Ling S, et al. TMEM16A/ANO1 is differentially expressed in HPV-negative versus HPV-positive head and neck squamous cell carcinoma through promoter methylation. Sci Rep. 2015;5:16657.

374. Barauna VG, Mantuan PR, Magalhães FC, Campos LCG, Krieger JE. AT1 receptor blocker potentiates shear-stress induced nitric oxide production via modulation of eNOS phosphorylation of residues Thr495 and Ser1177. Biochem Biophys Res Commun. 2013;441(4):713–9.

375. Förstermann U, Sessa WC. Nitric oxide synthases: Regulation and function. Eur Heart J. 2012;33(7):829–37.

376. Eroglu E, Saeedi Saravi SS, Sorrentino A, Steinhorn B, Michel T. Discordance between eNOS phosphorylation and activation revealed by multispectral imaging and chemogenetic methods. Proc Natl Acad Sci U S A. 2019;116(40):20210–7.

377. Tuder RM, Groves B, Badesch DB, Voelkel NF. Exuberant endothelial cell growth and elements of inflammation are present in plexiform lesions of pulmonary hypertension. Am J Pathol. 1994;144(2):275–85.

378. Tu L, Dewachter L, Gore B, Fadel E, Dartevelle P, Simonneau G, et al. Autocrine fibroblast growth factor-2 signaling contributes to altered endothelial phenotype in pulmonary hypertension. Am J Respir Cell Mol Biol. 2011;45(2):311–22.

379. Merklinger SL, Jones PL, Martinez EC, Rabinovitch M. Epidermal growth factor receptor blockade mediates smooth muscle cell apoptosis and improves survival in rats with pulmonary hypertension. Circulation. 2005;112(3):423–31.

380. Izikki M, Guignabert C, Fadel E, Humbert M, Tu L, Zadigue P, et al. Endothelial-derived FGF2 contributes to the progression of pulmonary hypertension in humans and rodents. J Clin Invest. 2009;119(3):512–23.

381. Perros F, Montani D, Dorfmüller P, Durand-Gasselin I, Tcherakian C, Le Pavec J, et al. Platelet-derived growth factor expression and function in idiopathic pulmonary arterial hypertension. Am J Respir Crit Care Med. 2008;178(1):81–8.

382. Schermuly RT, Dony E, Ghofrani HA, Pullamsetti S, Savai R, Roth M, et al. Reversal of experimental pulmonary hypertension by PDGF inhibition. J Clin Invest. 2005;115(10):2811–21.

383. Tuder RM, Chacon M, Alger L, Wang J, Taraseviciene-Stewart L, Kasahara Y, et al. Expression of angiogenesis-related molecules in plexiform lesions in severe pulmonary hypertension: Evidence for a process of disordered angiogenesis. J Pathol. 2001;195(3):367–74.

384. Voelkel NF, Gomez-Arroyo J. The role of vascular endothelial growth factor in pulmonary arterial hypertension: The angiogenesis paradox. Am J Respir Cell Mol Biol. 2014;51(4):474–84.

385. Cargnello M, Roux PP. Activation and Function of the MAPKs and Their Substrates, the MAPK-Activated Protein Kinases. Microbiol Mol Biol Rev. 2011;75(1):50–83.

386. Quinlan TR, Dechun L, Laubach VE, Shesely EG, Zhou N, Johns RA. eNOS-deficient mice show reduced pulmonary vascular proliferation and remodeling to chronic hypoxia. Am J

Physiol - Lung Cell Mol Physiol. 2000;279(4 23-4).

387. Fagan KA, Fouty BW, Tyler RC, Morris KG, Hepler LK, Sato K, et al. The pulmonary circulation of homozygous or heterozygous eNOS-null mice is hyperresponsive to mild hypoxia. J Clin Invest. 1999;103(2):291–9.

388. Steudel W, Scherrer-Crosbie M, Bloch KD, Weimann J, Huang PL, Jones RC, et al. Sustained pulmonary hypertension and right ventricular hypertrophy after chronic hypoxia in mice with congenital deficiency of nitric oxide synthase. J Clin Invest. 1998;101(11):2468–77.

389. Tyler RC, Muramatsu M, Abman SH, Stelzner TJ, Rodman DM, Bloch KD, et al. Variable expression of endothelial no synthase in three forms of rat pulmonary hypertension. Am J Physiol - Lung Cell Mol Physiol. 1999;276(2 20-2).

390. Jia H, Bagherzadeh A, Bicknell R, Duchen MR, Liu D, Zachary I. Vascular endothelial growth factor (VEGF)-D and VEGF-A differentially regulate KDR-mediated signaling and biological function in vascular endothelial cells. J Biol Chem. 2004;279(34):36148–57.

8. Supplementary Tables

Table S1. Patient characteristics *

Lung ID	Age (yr)	Sex (M/F)	mPAP (Hgmm)	Material used
Donor 1	16	M		PASMCs
Donor 2	47	M		PASMCs
Donor 3	50	F		PASMC
Donor 4	22	M		PASMCs
Donor 5	22	M		PASMCs
Donor 6	42	F		LT
Donor 7	58	M		LT
Donor 8	30	M		PASMCs
Donor 9	55	F		PASMCs
Donor 10	32	M		PASMCs
Donor 11	23	M		PASMCs
Donor 12	56	F		PASMCs
Donor 13	31	F		PASMCs
Donor 14	76	F		PASMCs
Donor 15	68	F		PASMCs
Donor 16	59	F		PAs, PAECs
Donor 17	48	F		PAs
Donor 18	45	M		PAs

Donor 19	54	M		LT
IPAH 1	25	F	69	LT
IPAH 2	13	M	56	PAECs
IPAH 3	41	F	71	PAECs
IPAH 4	21	M	90	PAECs
IPAH 5	38	F	39	PAECs

*Age, sex and mean pulmonary arterial pressure (mPAP) of healthy lung transplant donors and recipient IPAH patients. The materials used from each lung (PAECs: pulmonary arterial endothelial cells; PASMCs: pulmonary arterial smooth muscle cells, LT: lung tissue) are shown. (Reproduced from (1) in accordance with the MDPI and the CC BY 4.0 license).

Table S2. Cells acquired from Lonza *

Cell ID	**Age (yr)**	**Sex (M/F)**
28032	51	M
28074	67	F
21292	21	M
21304	45	F
28343	52	F
28627	57	M
18664	63	M
15685	45	M

33756	34	F
27930	21	M
33941	48	M
35049	33	F

*Age and sex of donor PAECs acquired from Lonza. (Reproduced from (1) in accordance with the MDPI and the CC BY 4.0 license).

Table S3. Primer sequences *

Gene	Acc. Number	Forward primer	Reverse primer	Product length (bp)
ANO1	XM_011545121.1	CACGATGAGGGTCAACGAGA	ATAAGGAGTTCAGCAGCGTG	128

*Exon-exon junction spanning primer sequences multiplying all splice variants of human TMEM16A. (Reproduced from (1) in accordance with the MDPI and the CC BY 4.0 license).

Table S4. Antibodies used in western blot (WB) and immunofluorescence staining (IF) *

Antibody	Company	Catalogue number	Experiment	Dilution
Fibronectin	Abcam, UK	#ab23750	marker confirmation (isolated PAECs)	1:200
Smooth muscle myosin heavy chain		#ab53219	marker confirmation (isolated PAECs)	1:200

TMEM16A		#ab53212	WB (PAECs,, PASMCs, human lung homogenate, human pulmonary arteries)	1:1000
TMEM16A	Alomone Labs, Israel	#ACL-011	IF (PCLS, lung cuts, PAECs)	1:100
eNOS	BD Biosciences, USA	#610296	WB (PAECs)	1:1000
CD31		#550274	marker confirmation (isolated PAECs)	1:200
Cyclin D1	Cell Signaling, USA	#2978S	WB (PAECs)	1:1000
ERK1/2		#9102S	WB (PAECs)	1:1000
HRP-linked a-mouse		#7076S	WB	1:1000 – 1:5000
LC3B		#2775S	WB (PAECs)	1:1000
p38		#9212S	WB (PAECs)	1:1000
pAkt (S473)		#4058S	WB (PAECs)	1:1000
pAkt (T308)		#9275S	WB (PAECs)	1:1000
PARP		#9542S	WB (PAECs)	1:500
pERK1/2 (T202/Y204)		#9101S	WB (PAECs)	1:1000
pp38		#9211S	WB (PAECs)	1:1000
pSAPK/JNK (T183/Y185)		#9251L	WB (PAECs)	1:1000
pSer1177 eNOS		#9571S	WB (PAECs)	1:1000

pThr495 eNOS		#9574S	WB (PAECs)	1:1000
SAPK/JNK		#9252S	WB (PAECs)	1:1000
tAKT		#9272S	WB (PAECs)	1:1000
Vimentin		#3932	marker confirmation (isolated PAECs)	1:200
Von Willebrand factor	Dako, USA	M0616	IF (lung cuts, PAECs)	1:100
Von Willebrand factor		A0082	IF (PCLS); marker confirmation (isolated PAECs)	1:100 1:500
Beta-Actin	Santa Cruz, USA	SC-47778	WB (PAECs, PASMCs)	1:2000
PCNA		SC-7907	WB (PAECs)	1:1000
Vinculin		SC-25336	WB (PAECs, PASMCs, human lung homogenate, human pulmonary arteries)	1:1000
Smooth muscle actin	Sigma-Aldrich, Germany	#A2547	marker confirmation (isolated PAECs)	1:300
Alexa Fluor 555 a-rabbit	ThermoFisher Scientific, USA	#A31572	IF (Lung sections, PAECs)	1:500
Alexa Fluor 647 a-mouse		#A31571	Lung sections, PAECs	1:500

AlexaFluor 488 a-rabbit		#A21206	IF (PCLS)	1:500
HRP-linked a-rabbit		#31460	WB	1:1000

*Antibodies used for western blot and immunofluorescence staining analysis with corresponding dilutions. (Reproduced from (1) in accordance with the MDPI and the CC BY 4.0 license).

Table S5. Solutions *

Solution	Abbreviation	Ingredients (mM)		Used
Ringer´s solution	N	KCl (5.5), NaCl (119), $CaCl_2$ (1.5), $MgCl_2$ (1), Glucose (20), $NaHCO_3$ (26), HEPES (10), Na_2HPO_4 (0.5), KH_2PO_4 (0.5)	pH adjusted to 7.4; 0.2 µm-filtered; supplemented with 0,2 % penicillin/streptomycin and 0,5 or 2 % fetal bovine serum (Osmolality: ~307 mOsm/kg·H_2O)	Nitric oxide measurements, Western blot
Cl^--reduced Ringer´s solution	M	KCl (2.75), NaCl (59.5), potassium gluconate (2.75), sodium gluconate (59.5), $CaCl_2$ (1.5), $MgCl_2$ (1), Glucose (20), $NaHCO_3$ (26), HEPES (10), Na_2HPO_4 (0.5), KH_2PO_4 (0.5)	pH adjusted to 7.4 using NaOH; 0.2 µm-filtered; supplemented with 0,2 % penicillin/streptomycin and 0,5/2 % fetal bovine serum	Nitric oxide measurements, Western blot

			(Osmolality: ~302 mOsm/kg·H_2O)	
Physiological salt solution	PSS	KCl (5.5), NaCl (140.5), $CaCl_2$ (1.5), $MgCl_2$ (1), Glucose (10), HEPES (10), Na_2HPO_4 (0.5), KH_2PO_4 (0.5)	pH adjusted to 7.4 using NaOH	Wire Myography, Ca^{2+} imaging
Physiological salt solution with isotonic replacement of NaCl by KCl	KPSS	KCl (120), NaCl (120), $CaCl_2$ (1.5), $MgCl_2$ (1), Glucose (10), HEPES (10), Na_2HPO_4 (0.5), KH_2PO_4 (0.5)	pH adjusted to 7.4 using NaOH	Wire Myography
PSS without Ca^{2+}		KCl (5.5), NaCl (140.5), $MgCl_2$ (1), Glucose (10), HEPES (10), Na_2HPO_4 (0.5), KH_2PO_4 (0.5), EGTA (1)	pH adjusted to 7.4 using NaOH	Ca^{2+} imaging
Lysis buffer	CHAPS[2]	NaCl (500), Tris-Hcl pH 7.5 (50), 5 % glycerol, 2 % CHAPS, 2 % sodium deoxycholate, 1 % sodium dodecyl sulfate	Supplemented with protease- and phosphatase inhibitors	Protein collection
TBS-T	TBS-T	Tris-HCl (5), NaCl (150), 0.4 % Tween 20	pH adjusted to 7.5	Western blot
Bath solution I		NaCl (150), $CaCl_2$ (1), $MgCl_2$ (1), glucose (10), HEPES (10)	pH adjusted to 7.4 using NaOH	Patch-Clamp

Bath solution II		NaCl (140), $CaCl_2$ (1), $MgCl_2$ (1), TEA-Cl (10), glucose (10), HEPES (10)	pH adjusted to 7.4 using NaOH	Patch-Clamp
Pipette solution		CsCl (110), TEA-Cl (20), $CaCl_2$ (4.68), $MgCl_2$ (1), HEPES (10), EGTA (5), Na_2ATP (1)	pH adjusted to 7.2 using NaOH; free Ca^{2+} concentration was 2 µM (MaxChelator software)	Patch-Clamp
Cutting solution		$CaCl_2$ (1.8), $MgSO_4$ (0.8), KCl (5.4), NaCl (116.4), NaH_2PO_4 (1.2), glucose (16.7), $NaHCO_3$ (26.1), HEPES (25.2)	pH adjusted to 7.2 using NaOH	PCLS
Incubation solution		$CaCl_2$ (1.8), $MgSO_4$ (0.8), KCl (5.4), NaCl (116.4), NaH_2PO_4 (1.2), glucose (16.7), $NaHCO_3$ (26.1), HEPES (25.2), sodium pyruvate (0.5), MEM-amino acid mixture (1:50), MEM-vitamins mixture (1:100), L-glutamine (1)	pH adjusted to 7.2 using NaOH; penicillin (100 U/mL) / streptomycin (100 µg/mL)	PCLS

*Solutions developed in the course of this study. (Reproduced from (1) in accordance with the MDPI and the CC BY 4.0 license).

Table S6. Materials *

Material	Company	Catalogue number
Seahorse XFp Cell Mito Stress Test Kit	Agilent technologies	103010-100
DMSO	AppliChem	A3672,0250
Low melting agarose	Bio-Rad, USA	1613111
[^{3}H]-thymidine	BIOTREND Chemikalien, Germany	ART-0178A-1/A306756
FCS	Biowest, France	S1810-500
384 Well PCR Platte	Biozym, Germany	711225X
Blue S'Green qPCR Kit		331416XL
CaCl2	Carl-Roth, Germany	5239.2
NaCl		3957.2
HEPES		HN78.2
Bis-Acrylamid, 30 %, Rotiphorese-Gel		3029.1
Dispase	Corning, USA	354235
Adenoviruses Ctrl^{Ad} and Ano1^{Ad}	Cyagen Biosciences, USA	hAno1 acc-number: NM_018043.5
Dako Target Retrieval Solution pH 9.0	Dako, Denmark	S236784
Dako Fluorescent mounting medium		S3023
Formaldehyde	Donauchem, Austria	A191483
U-44619	Enzo Life Sciences, USA	BML-PG023-0001

Na-dodecylsulfat (SDS) 10 %	Gatt-Koller, Germany	403030722
Sodium pyruvate	GE Healthcare, USA	S8636
ECL Start Western Blotting Detection Reagent		RPN3243
ECL Prime Western Blotting Detection Reagent		RPN2232
Filter Unit 0,2µm FP30/0		B285849
L-glutamine	Gibco, USA	8051103
MEM-amino acid mixture		11140035
MEM-vitamins mixture		11120037
2-well culture-inserts	Ibidi, Germany	80209
Fura-2AM	Invitrogen	F-1221
Ethanol 70 %	Lactan, German	T9132
CellEvent™ Caspase-3/7 Green Flow Cytometry Assay Kit	Life Technologies, USA	C10427
VascuLife Basal Medium	LifeLine Cell Technology, USA	LM-0002
VascuLife SMC Medium Complete Kit		LL-0014
Trypsin-EDTA	Lonza, Switzerland	CC-5012
TNS		CC-5002
EBM-2		LONCC-3156
EGM-2		LONCC-3162
In Vitro Angiogenesis Assay Kit	Merck, Germany	ECM625
Gelatine		9000-70-8

Novagen BCA Protein Assay Kit		A270811
Methanol		8395713
HBSS	PAA Laboratories, Austria	H15-009
DPBS	Pan Biotech, Germany	P04-36500
UniFilter-96 GF/C, White 96-well Barex Microplate with 1.2 µm poresize GF/C filter	Perkin Elmer, USA	6005174
TopSeal-A PLUS, Clear adhesive seal for microplates		6050185
Collagenase A	Roche Applied Science, Germany	10103586
CsCl	Reanal Laborvegyszer, Hungary	07020-0-01-25
T25 flasks	Sarstedt, Germany	83.3910.302
DNAse	Serva, Germany	18535.01
benzbromarone	Sigma-Aldrich, Germany	B5774-1G
KCl		P9333
NaH_2PO_4		S3139-250G
D-(+)-glucose		G8270-1KG
$NaHCO_3$		S5761-1KG
Acetylcholine		A6625.25G
Bovine Serum Albumin		A6003-10G
Triton X-100		T8787-100ML

Tris-HCl		C4706-2G
Glycine		G7126-5KG
Glycerol		G5516-100ML
Sodium deoxycholate		D6750-25G
Sodium bicarbonate		S5761
Sodiumphosphate monobasic monohydrate		71507
Potassium D-gluconate		G4500-1KG
TEA-Cl		T2265
Na_2ATP		A7699
Magnesium Sulfate Heptahydrate		M5921
D-Gluconic acid sodium salt		G9005-1KG
Western blotting membranes, nitrocellulose, pore size 0.45 µm		GE10600008
TEMED		T9281
Ammonium persulfate (APS)		A3678-25G
Tween 20		P7949
EGTA		E4378-100G
Ionomycin calcium salt		I3909
L-NAME		N5751-10G
Nunc-Immuno™ MicroWell™ 96 well polystyrene plates BLACK		137101
$DiBAC_4(3)$		D8189-25MG

Cell scrapers		8536585
Mix-n-Stain™ CF™ 633 Antibody Labeling Kit		MX633S50-1KT
T75 flasks		CC7682-4875
Dynabeads® CD31 Endothelial Cell	ThermoFisher Scientific, USA	11155D
Penicillin/Streptomycin (P/S)		15140-122
Pierce protease inhibitor tablets		A32953
Pierce phosphatase inhibitor tablets		A32957
SuperSignal West Femto Chemiluminescent Substrate		34095
Restore Plus Western Blot Stripping Buffer		A323654
StemPro Accutase Cell Dissociation Reagent		11599686
DAF-DM		D23842
8-well chambered cell culture slides		10162861
CHAPS	Tocris Bioscience, UK	3172
Vectashield mounting medium with DAPI	Vector Laboratories, UK	H-1200
Thick-walled borosilicate glass (Standard Glass Capillaries, 4 in., 1.2 / 0.68 OD/ID, Filament/Fire Polished)	World Precision Instruments, USA	1B120F-4

*Information regarding all the materials used during the course of this study. (Reproduced from (1) in accordance with the MDPI and the CC BY 4.0 license).